N71-24140
NASA CR-118079

PURDUE RESEARCH FOUNDATION
Project No. 2074

TECHNICAL REPORT FMTR-71-1
January 1971

EXAMINATION OF TURBULENT SHEAR MODELS AND THE PREDICTION OF COMPRESSIBLE TURBULENT BOUNDARY LAYERS BY THE METHOD OF WEIGHTED RESIDUALS

by

Gail R. Deboy and Douglas E. Abbott

SCHOOL OF MECHANICAL ENGINEERING
FLUID MECHANICS GROUP
PURDUE UNIVERSITY

Technical Report FMTR 71-1

January 1971

NATIONAL AERONAUTICS AND SPACE ADMINISTRATION
Grant No. NGT 15-005-005

COPY NO. 40

EXAMINATION OF TURBULENT SHEAR MODELS AND THE PREDICTION OF COMPRESSIBLE TURBULENT BOUNDARY LAYERS BY THE METHOD OF WEIGHTED RESIDUALS

by

Gail R. Deboy and Douglas E. Abbott

PURDUE RESEARCH FOUNDATION
Project No. 2074

NATIONAL AERONAUTICS AND SPACE ADMINISTRATION

Grant No. NGT 15-005-005

School of Mechanical Engineering
Fluid Mechanics Group
Purdue University

Technical Report FMTR-71-1

January 1971

ACKNOWLEDGMENTS

The authors wish to acknowledge the National Aeronautics and Space Administration for providing fellowship support during the major period of this research effort. The Department of Health, Education, and Welfare is also gratefully acknowledged for their support during the final stages of the research. In addition, thanks are given to Professor R. W. Fox and Doctors S. J. Koob and V. G. Forsnes and Mr. H. T. Liu for their many helpful and stimulating discussions of this work.

TABLE OF CONTENTS

LIST OF FIGURES

LIST OF FIGURES
(Continued)

LIST OF FIGURES
(Continued)

LIST OF FIGURES
(Continued)

LIST OF FIGURES
(Continued)

Page

Appendices
Figures

NOMENCLATURE

A_{ij}	Matrix in the MWR equations, defined by equation (3.45)
B_i	Vector in the MWR equations, defined by equation (3.47)
C	Constant in Sutherland's viscosity law, equation (2.25)
C_f	Local skin-friction coefficient, $\tau_w/(1/2)\ \rho_e U_e^2$
C_j	Vector in the MWR equations, see equation (3.35)
C_p	Specific heat at constant pressure
C_v	Specific heat at constant volume
D_j	Vector in the MWR equations, see equation (3.37)
F	Approximating function, see equation (3.39)
F''_{cs}	Velocity derivative function, $Re_x^{1/2} \frac{\nu}{U_e^2} \frac{\partial u}{\partial y}$
f_i	Functions defined by equations (2.27) and (2.28) for Section 2, or weighting functions defined by equation (3.42) for Section 3
G	Approximating function, see equation (3.40)
g_i	Vector in the MWR equations, defined by equation (3.48)
H	Total enthalpy
h_i	Weighting function, defined by equation (3.41)
I_{ij}	Matrix in the MWR equations, defined by equation (3.46)
J_{ij}	Matrix in the MWR equations, defined by equation (3.49)

K	von Kármán constant, equation (2.19)
K_1	Mixing-length constant, equation (2.9)
K_2	Constant in equation (2.13)
K_3	Constant in equation (2.30)
K_{ij}	Matrix in the MWR equations, defined by equation (3.50)
k	Thermal conductivity
L	Reference length
L_i	Vector in the MWR equations, defined by equation (3.51)
ℓ	Mixing length
M	Mach number
M_i	Vector in the MWR equations, defined by equation (3.52)
N	Order of MWR approximation
P_j	Legendre polynomial, order j
Pr	Prandtl number
Pr_t	Turbulent Prandtl number
p	Time mean pressure
q_w	Heat transfer at the wall
R	Gas constant
Re_x	Reynolds number based on x, $U_e x/\nu_e$
Re_θ	Reynolds number based on θ, $U_e \theta/\nu_e$
r_i	Discrete values of the functional argument in Appendix A
S	Functional argument value in Appendix A
T	Time mean temperature
T_o	Total temperature

t	Time
U_e	Free-stream velocity
$UAIC_k$	Vector defined by equation (D.4)
u	Time mean velocity component in the x-direction
$u_1(y)$	First guess for u(y) in Section 2.5
$u_2(y)$	Second estimate for u(y) in Section 2.5
u_i	Time mean velocity in the i-direction
u_i'	Fluctuating velocity component in the i-direction
u^+	Nondimensional velocity, $u/\sqrt{\tau_w/\rho}$
V	Nondimensional velocity, defined by equation (3.25)
v	Time mean velocity component in the y-direction
W	Function specified at a discrete number of points in Appendix A
w^*	Nondimensional velocity, defined by equation (3.23)
X	Effective-viscosity variable, defined by equation (2.20)
x	Cartesian coordinate tangent to the surface
x_i	Cartesian coordinate vector, $x_1 = x$ and $x_2 = y$
y	Cartesian coordinate normal to the surface
y^+	Nondimensional y-coordinate, $\frac{y}{\nu}\sqrt{\tau_w/\rho}$
y_c	y-value defined in Figure 1
y_m^*	Match point where the eddy-viscosity values from an inner and outer expression are identical
z	Time mean component of a flow or property variable
z'	Fluctuating component of a flow or property variable
z_{in}	Instantaneous value of a flow or property variable

β	Eddy-viscosity parameter, defined by equation (3.24), $1 + \varepsilon/\nu$
γ	Ratio of specific heats, C_p/C_v
Δr_-	Increment in r, defined by equation (A.2)
Δr_+	Increment in r, defined by equation (A.1)
δ	Boundary-layer thickness
δ^*	Displacement thickness, $\int_0^\delta \left(1 - \frac{\rho}{\rho_e} \frac{u}{U_e}\right) dy$
δ^*_K	Kinematic displacement thickness defined by equation (2.15)
ε	Eddy viscosity
ε^+	Nondimensional eddy viscosity, ε/ν
η	Transformed normal coordinate, equation (3.22)
Θ	Inverse velocity slope, defined by equation (3.31)
θ	Momentum thickness, $\int_0^\delta \left(1 - \frac{u}{U_e}\right) \frac{\rho}{\rho_e} \frac{u}{U_e} dy$
λ_t	Eddy conductivity
μ	Dynamic viscosity
ν	Kinematic viscosity
ν_{ef}	Effective viscosity
ξ	Transformed tangential coordinate, equation (3.22)
ρ	Time mean density of fluid
σ	Fractional value
τ	Total shear stress
Φ	Effective-viscosity function for the defect layer, Fig. 2
ϕ	Effective-viscosity function for the wall layer, Fig. 2
ϕ_j	Approximating functions, defined by equation (3.35)
χ	Effective-viscosity variable, defined by equation (2.19)

Ω	Intermittency factor
ω_j	Approximating functions, defined by equation (3.38)

Subscripts

e	Evaluated at the outer edge of the boundary layer
i	Denotes the inner region of the boundary layer on ε, ℓ, and τ; denotes an index on all other symbols
j,k	Indices
max	Maximum
o	Denotes the outer region of the boundary layer on ε, ℓ, and τ; denotes the initial or starting value of x on all other symbols
r	Reference value
w	Evaluated at $y = 0$ (or $u = 0$)

Superscripts

———	Time averaged
'	Differentiation with respect to independent variable or time dependent portion of a local quantity
*	Denotes displacement thickness on δ; denotes non-dimensional variable, defined wherever used, on all other symbols
ξ	Differentiation with respect to ξ

ABSTRACT

There are two primary objectives of this work: first to examine the behavior of local, turbulent shear-stress models, and second to extend the method of weighted residuals (a method for solving a system of partial differential equations) to the solution of the compressible turbulent boundary-layer equations. Thus, in the first part of this work shear models are studied both as they influence a given boundary-layer prediction scheme and also as they yield shear-stress profiles independent of prediction methods. Shear-stress calculations are then examined as reported by previous workers, as calculated from the intermediate boundary-layer results of other methods, and as computed in the present investigation. It is found that the behavior of many of the shear models is qualitatively incorrect in terms of their prediction of the shear-stress distribution. The cause of the anomalous behavior of the shear-stress profiles is discussed in relation to the specific shear models, and the effects of this behavior on boundary-layer prediction programs are examined. In addition, previous efforts to correct the anomalous behavior, such as, employing a diffusion equation on the maximum eddy-viscosity or smoothing eddy-viscosity profiles, are also indicated.

Finally, it is shown possible to develop an iterative procedure to at least provide properly behaved shear-stress profiles at the initial station of a prediction program.

In the second part of this study, the computational advantages of the method of weighted residuals are compared with those of finite-difference methods and those of the conventional integral methods. Since the method of weighted residuals is found to possess many of the advantages of the other two methods, it is extended to the solution of the compressible, turbulent boundary-layer equations. Numerical solutions, for the compressible flow of air over adiabatic flat plates at free stream Mach numbers ranging from 2.54 to 4.2, are compared with both experiment and the finite-difference calculations of Cebeci, Smith, and Mosinskis [1]. The general analysis of the present investigation includes pressure-gradient and heat-transfer effects, but these effects are not incorporated into the computer program; consequently, no numerical results are presented for flows with pressure gradient or heat transfer.

1. INTRODUCTION

The prediction of the compressible, turbulent boundary layer became of critical importance with advances in the design of supersonic aircraft, guided missiles, gas turbines, and other high-speed gas flow devices. With the high velocities involved in such applications, drag and heating effects are very important design criteria; consequently, a calculation procedure for compressible, turbulent boundary layers can be a valuable design tool – particularly in the early stages of the problem analysis.

In the past twenty years considerable research effort has been focused on the understanding and prediction of turbulent boundary layers, primarily incompressible, but in the past five years a few of the incompressible analytical techniques have been extended to compressible flow applications with varying degrees of success.

In any prediction scheme for turbulent boundary layers, there are three major factors for consideration: the governing differential equations which mathematically model the physical situation; a turbulent shear-stress information model which renders the system of governing equations, with their appropriate boundary conditions, a well-posed mathematical problem; and finally the mathematical procedure to solve the well-posed problem. The goal of the present work is to advance the existing state of knowledge in two of these areas — namely, turbulent shear models and mathematical solution techniques.

An investigation is made of the predicted shear-stress distributions in turbulent flow, and the resulting calculations are analyzed for four separate investigations including the present one as well as some unpublished results of other investigators. The anomalous behavior of some of these shear-stress profiles is examined, and a plausible explanation of this behavior is set forth. Various methods of avoiding this anomalous shear-stress behavior are also postulated.

The method of weighted residuals, a powerful mathematical technique for approximately solving a system of complex partial differential equations, is described; and the computational advantages of this method are compared with those of conventional integral techniques and finite-difference procedures. Since ultimately the Method of Weighted Residuals (or MWR) is proposed as retaining many of the computational advantages of both integral and finite-difference techniques, the MWR is extended to the solution of the compressible, turbulent boundary-layer equations using both an eddy-viscosity model and various other similarity shear-stress models. A new treatment for the energy equation is developed which has distinct computational advantages over procedures previously employed for laminar flows.

Since the experimental procedure for varying Re_x differs from that of the calculation procedure, several valid techniques of comparing the experimental and analytical results are studied. A comparison technique is presented which appears to properly test the ability of a prediction method. The corresponding results of the prediction program are compared with both experiment and the finite-difference calculations of Cebeci, Smith, and Mosinskis [1] for the flow of air over an adiabatic flat plate with free stream Mach numbers ranging from 2.54 to 4.2. The accuracy, computation times, and convergence properties of these MWR predictions are examined.

In summary, the goals of this investigation are to (1) carefully examine the behavior of several local shear-stress models and (2) investigate certain computational advantages of the method of weighted residuals and extend the MWR to the analytical prediction of compressible, turbulent boundary-layer flows.

2. INVESTIGATION OF TURBULENT SHEAR STRESS

In the calculation of compressible turbulent boundary layers there are three major factors for consideration; these are the governing differential equations of motion, the mathematical method to solve these differential equations, and the physical model to yield the required turbulent shear-stress information. The task of studying and selecting a turbulent shear information model is considered in this section.

2.1 Review of Turbulent Shear Information Models

The two basic types of turbulent shear information models are global descriptions, which depend only on the streamwise x-coordinate, the local descriptions, which depend on both the x-coordinate and the normal y-coordinate. A global shear model is an algebraic or differential equation which relates an integral of the shear stress, for example,

$$\int_0^\infty f(x,y)\tau \, dy \qquad (2.1)$$

to the boundary-layer integral parameters ($f(x,y)$ is an arbitrary function and the integration eliminates the y-variation). A local shear model is an algebraic or differential equation relating shear stress, eddy viscosity, or mixing length to the boundary-layer parameters and/or the velocity field.

Boussinesq [2] first introduced the eddy-viscosity concept in the form

$$-\overline{u_i'u_j'} = \varepsilon\left(\frac{\partial u_i}{\partial x_j} + \frac{\partial u_j}{\partial x_i}\right) \tag{2.2}$$

where the eddy viscosity has a scalar value with directional constancy. Hinze [3] has shown that a constant eddy viscosity will yield satisfactory velocity profiles for the free turbulent wake far behind a cylinder. In general, however, eddy viscosity has a spacial variation, e.g. in boundary-layer shear flows. It must also be recognized that the form of equation (2.2) cannot be mathematically correct if ε is considered to be a scalar because a contraction of this equation yields

$$-\overline{u_i'u_i'} = 2\varepsilon\,\frac{\partial u_i}{\partial x_i} \tag{2.3}$$

The right side of this equation is always zero for incompressible flow (from the continuity equation) while the left side can only be zero if there is no turbulence. Similar arguments utilizing properties of symmetric tensors show that tensors of second and third order are also unsatisfactory representations for eddy viscosity; whereas, a fourth-order tensor can satisfy all contraction and symmetricity relations. Despite these objections the Boussinesq formulation with a scalar eddy viscosity is often adopted in calculation procedures for turbulent flow. The major justification for its use is the successful agreement often shown between the calculated and measured values of the gross, mean properties of the flow.

For turbulent boundary-layer calculations the Clauser [4] eddy-viscosity model is generally used in the outer or law-of-the-wake region, while various other models are employed in the inner or law-of-the-wall region. The inner and outer models are then patched together in a variety of ways. The resulting predictions of mean velocity and temperature profiles, integral thickness parameters, and skin friction have been quite adequate for engineering purposes except in flows with very sudden changes in pressure gradient or flows near separation.

Some interesting differences in opinion can be found over the last decade. In considering eddy-viscosity models, Laufer [5] states that he is doubtful that a "correct" formulation exists in the inner or wall region. Conversely, Clauser [4] said ten years earlier that the inner region could essentially be considered as solved with a logarithmic velocity profile and an eddy viscosity proportional to y. Clauser then proceeded to consider what he called the much more difficult problem of predicting the behavior of the outer portion of the boundary layer. It should certainly be noted that Clauser's comments were made in 1956 and Laufer's in 1968, and that in 1956 much more was known about the inner region than the outer region. It now appears that with the results of Clauser's work, the outer region can essentially be considered as solved, and attention should be focused on the more difficult problem of predicting the behavior of the inner layer; some consideration of this point will be given later in this section.

Forsnes and Abbott [6] reported an extensive study of over thirty global and local turbulent shear-stress models for two-dimensional, incompressible, turbulent boundary layers. Only a few of these models have been extended to compressible flow: for example, Alber and Coats [7] extended their dissipation integral formulation; Cebeci, Smith and Mosinskis [1] modified their eddy-viscosity expression; and Herring and Mellor [8] reworked their effective-viscosity hypothesis for the compressible regime. Forsnes and Abbott [6] evaluated the incompressible versions of these three turbulent shear models independently of any boundary-layer prediction scheme by directly substituting experimental data into the shear models and comparing the outputs from the various models. The main items of concern in Forsnes and Abbott's [6] results are that the dissipation-integral values calculated from Alber and Coats' [7] formulation are always much larger than the values calculated by five other dissipation-integral correlations and that the shear-stress profiles calculated by both the Herring-Mellor model and the Cebeci-Smith-Mosinskis model have grossly unrealistic behavior in the inner region of the boundary layer where y/δ is less than about two-tenths. Forsnes and Abbott [6] then employed these three models in a two-dimensional, incompressible, turbulent, boundary-layer prediction program, but the predictions of C_f, δ^*, and θ were very inaccurate. These inaccurate predictions were certainly expected considering the grossly unrealistic behavior of the input shear profiles.

In the light of Forsnes and Abbott's [6] earlier comparison of the dissipation-integral values and shear-stress profiles calculated by the above three shear models, considerably more work and understanding must be accomplished before these models can be successfully incorporated into an arbitrary boundary-layer prediction scheme. The rationale for continuing this approach of understanding is: (1) the Cebeci-Smith-Mosinskis and the Herring-Mellor eddy-viscosity models are among the best known and regarded shear models in the turbulent boundary-layer community; and (2) the calculations for two-dimensional, incompressible, turbulent boundary layers by these two groups ranked in the best third of the prediction methods as determined by the evaluation committee of the 1968 AFOSR-IFP Stanford Conference entitled, "Computation of Turbulent Boundary Layers" [9]. These two eddy-viscosity models are presented and studied in Sections 2.2 and 2.3, but first a policy of evaluation needs to be clarified.

In evaluating turbulent shear models in the past, the popular approach has appeared to be — the better the calculated values of δ^*, θ, and C_f agree with the experimental data, then the better the shear model used in the prediction procedure must be. This implied evaluation is often made without any regard to the behavior of the calculated shear-stress profiles. Of course, there is always the implicit assumption that the shear-stress profiles are correct if the integral parameters are adequately predicted. This applied point of view has its chief defense in the fact that the industrial user is generally only interested in the prediction of δ^*, C_f, and the separation point, and he has little interest in the predicted behavior of the velocity and shear-stress profiles. Further justification for the applied evaluation approach may be that very little measured shear-stress data are available for comparison by any means.

There is an element of risk with this applied evaluation, however. While the applied user is mostly concerned with computational results, he nevertheless would like to see existing turbulence formulations pushed to newer and often more complex applications, such as, for example, compressibility, boundary-layer control, low Reynolds number effects, wall-roughness effects, etc. Typically such extensions by the originators of the earlier shear-stress models (see, for example, [10] and [11]) assume that the new and more complicated phenomenon can be accounted for by deducing appropriate modifications of the details of the previously successful turbulent shear-stress model in some intuitively logical manner. The continued success of such a line of research, measured in terms of integral parameters, would thus imply the soundness of the original assumption for the shear stress. Presumably, only when a failure is encountered with this chain of deduction would it be necessary to examine the details of the assumed shear stress.

A different philosophy presents itself to the investigator who desires to accept the merits of one of the earlier shear models and perform his own extensions or modifications to suit some specific need. For the sake of saving time or at least optimizing the effort, such an investigator would like to select the "best" of the shear models available. This is the philosophy adopted in this report and in keeping with this approach, the eddy-viscosity models proposed by Cebeci, Smith, and Mosinskis [1] and Herring and Mellor [8, 12] will be reviewed in some detail, including an examination of the resulting shear-stress profiles.

2.2 Eddy-Viscosity Models

The defining equations for eddy viscosity are

$$\frac{\tau}{\rho} = (\nu+\varepsilon)\ \frac{\partial u}{\partial y} \tag{2.4}$$

and

$$\varepsilon\,\frac{\partial u}{\partial y} = -\ \overline{u'v'} \tag{2.5}$$

where ε is the eddy viscosity. The defining equations for the Prandtl mixing length are

$$\frac{\tau}{\rho} = \left(\nu+\ell^2 \left|\frac{\partial u}{\partial y}\right|\right) \frac{\partial u}{\partial y} \qquad (2.6)$$

and

$$-\overline{u'v'} = \ell^2 \frac{\partial u}{\partial y} \left|\frac{\partial u}{\partial y}\right| \qquad (2.7)$$

where ℓ is the mixing length. Combining equations (2.5) and (2.7) yields a relation between eddy viscosity and mixing length

$$\varepsilon = \ell^2 \left|\frac{\partial u}{\partial y}\right| \qquad (2.8)$$

Prandtl originally argued that for the inner region of the boundary layer (denoted by subscript i)

$$\ell_i = K_1 y \qquad (2.9)$$

where K_1 is a constant for fully-developed turbulent flow. Van Driest [13] modified Prandtl's argument for mixing length to account for the viscous sublayer by consideration of a Stokesian flow over an oscillating flat plate. Van Driest made the analogy between the Stokesian flow and the fluctuating turbulent fluid over a stationary flat plate, resulting in the introduction of a damping factor into equation (2.9) which becomes

$$\ell_i = K_1 y[1-\exp(-y/A)] \qquad (2.10)$$

where A is a constant for a given streamwise location. Combining equations (2.8) and (2.10) results in

$$\varepsilon_i = K_1^2 y^2[1-\exp(-y/A)]^2 \left|\frac{\partial u}{\partial y}\right| \qquad (2.11)$$

Equation (2.11) was developed by Van Driest for incompressible flow over a flat plate with zero pressure gradient. Cebeci, Smith, and Mosinskis [1] have extended Van Driest's development to encompass compressible flows with pressure gradients. Their final result is

$$\varepsilon_i = K_1^2 \, y^2 \left(1 - \exp\left[- \frac{y}{26\nu} \left(\frac{\tau_w}{\rho} + \frac{dp}{dx} \frac{y}{\rho} \right)^{\frac{1}{2}} \right] \right)^2 \left| \frac{\partial u}{\partial y} \right| \tag{2.12}$$

In the outer region of the boundary layer (denoted by subscript o), Clauser [4] heuristically derived the result

$$\varepsilon_o = K_2 \, U_e \, \delta^* \tag{2.13}$$

for incompressible, equilibrium turbulent boundary layers where K_2 is a constant. Equation (2.13) has been modified by the intermittency factor given by Klebanoff [14] as

$$\Omega = \frac{1}{2} \{1 - \mathrm{erf}[5(y/\delta - 0.78)]\} \tag{2.14}$$

where Ω is the intermittency factor. Clauser's model has been further modified by Herring and Mellor [8] by replacing δ^* with δ_K^* for compressible flows, where the kinematic displacement thickness

$$\delta_K^* = \int_0^\infty (1 - u/U_e) \, dy \tag{2.15}$$

is used to account for the kinematic character of the eddy viscosity. Cebeci, Smith and Mosinskis [1] also have approximated equation (2.14) by

$$\Omega = [1 + 5.5(y/\delta)^6]^{-1}$$

The complete, composite eddy-viscosity model used by Cebeci, Smith, and Mosinskis [1] is given in the inner region by

$$\varepsilon_i = K_1^2\, y^2 \left(1 - \exp\left[-\frac{y}{26\nu}\left(\frac{\tau_w}{\rho} + \frac{dp}{dx}\frac{y}{\rho}\right)^{\frac{1}{2}}\right]\right)^2 \left|\frac{\partial u}{\partial y}\right| \qquad (2.12)$$

and in the outer region by

$$\varepsilon_o = K_2\, U_e\, \delta_K^* \,[1 + 5.5(y/\delta)^6]^{-1} \qquad (2.16)$$

where $K_1 = 0.40$, $K_2 = 0.0168$, and δ is defined as the distance from the wall to the point where $u/U_e = 0.995$. The dividing point between the inner and outer region of the boundary layer is defined by requiring the eddy-viscosity function to be continuous. Thus, equation (2.12) is used for $0 \le y < y_c$, and equation (2.16) is used for $y_c \le y \le \delta$ where y_c is defined as the value of y where $\varepsilon_i = \varepsilon_o$. Figure 1 graphically depicts the joining of the two regions.

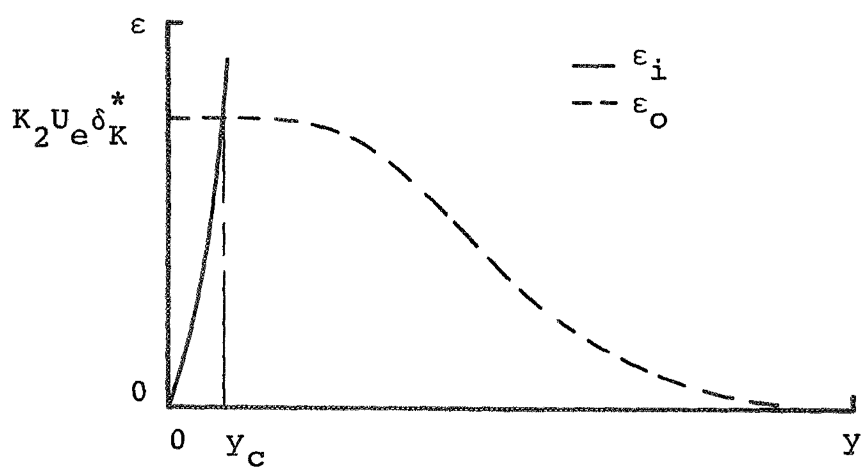

Figure 1: Eddy-Viscosity Model of Reference 1

Herring and Mellor develop their effective-viscosity model in References 8 and 12. The defining equations are

$$\frac{\tau}{\rho} = \nu \frac{\partial u}{\partial y} - \overline{u'v'} \tag{2.17}$$

and

$$\frac{\tau}{\rho} = \nu_{ef} \frac{\partial u}{\partial y} \tag{2.18}$$

where ν_{ef} is the effective viscosity. Utilizing physical and dimensional arguments they obtain

$$\frac{\nu_{ef}}{\nu} = \phi(\chi) \quad , \quad \chi = \frac{Ky}{\nu} \sqrt{\tau/\rho} \quad \text{in the wall layer} \tag{2.19}$$

and

$$\frac{\nu_{ef}}{U_e \delta_K^*} = \Phi(X) \quad , \quad X = \frac{Ky}{U_e \delta_K^*} \sqrt{\tau/\rho} \quad \text{in the defect layer} \tag{2.20}$$

where ϕ and Φ are, as yet, undetermined functions and $K = 0.41$ is the von Karman constant. With the assumption that an overlap region occurs between the wall and defect layers and Clauser's [4] assumption that ν_{ef} is constant in the defect layer, Herring and Mellor obtain the functional form for Φ. Once again using the overlap region assumption with the law of the wall and some of Laufer's [15] data (to specify an empirical constant), they determine the ϕ function. Figure 2 displays these functions. Herring and Mellor then unite their composite model into a single equation by the matched asymptotic expansions (Van Dyke [16]); this is

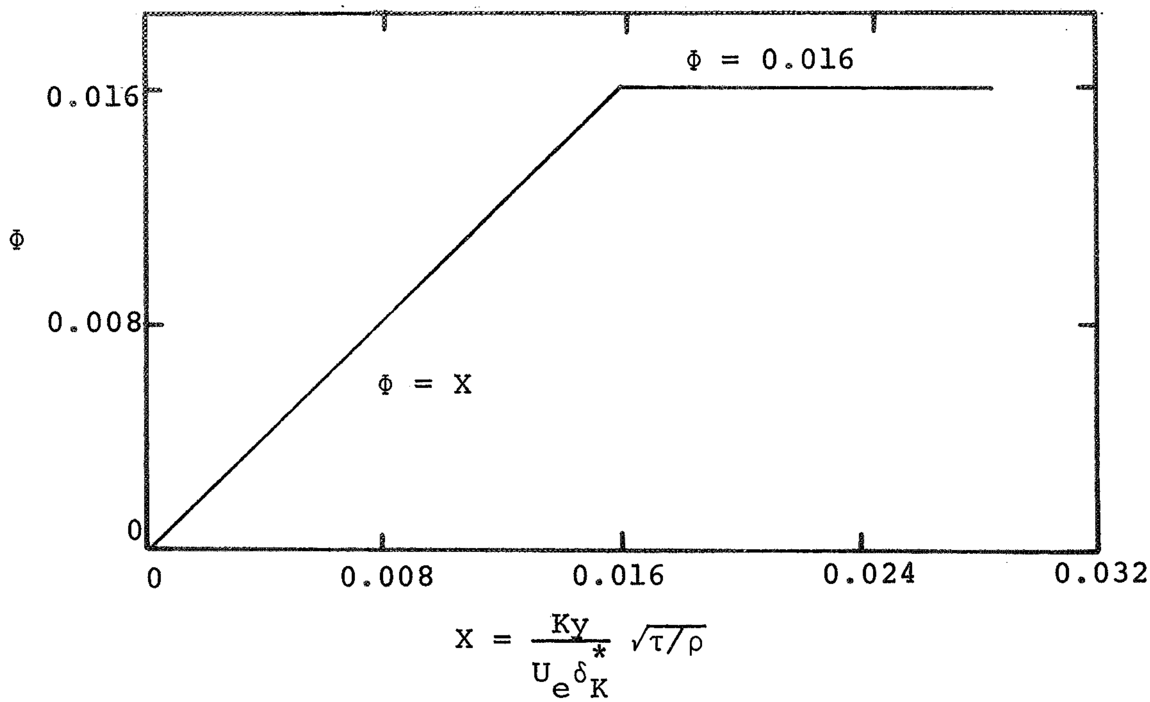

(a) Defect Layer

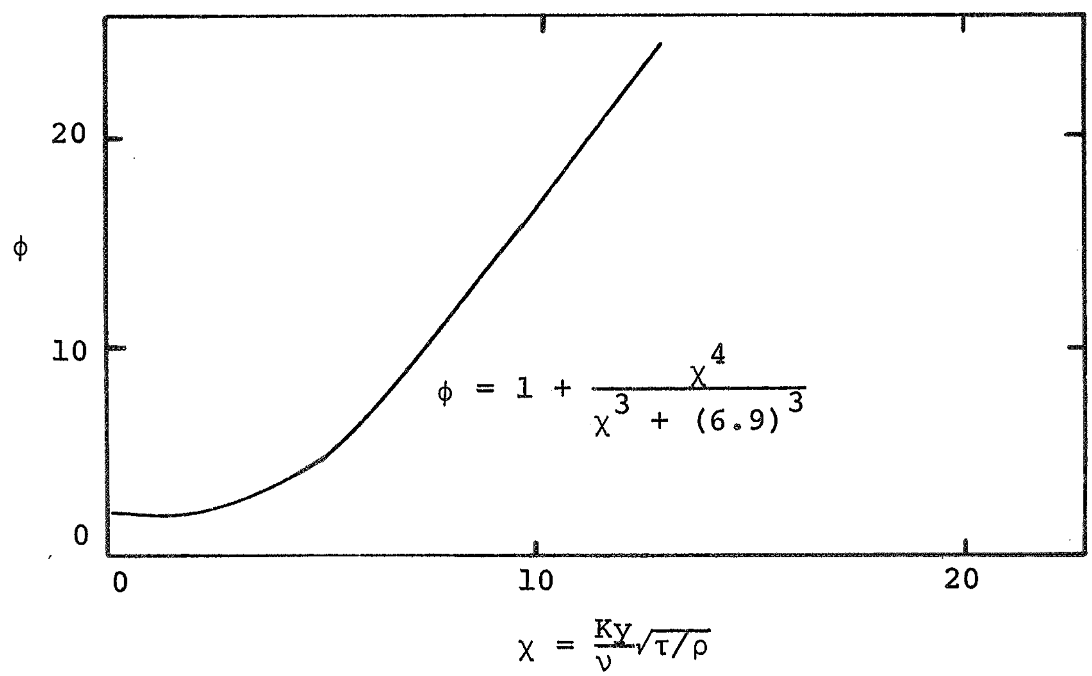

(b) Wall Layer

Figure 2: The Effective-Viscosity Functions of Herring and Mellor [8]

achieved by adding the inner model to the outer model and subtracting the common asymptote to obtain their final, resultant effective-viscosity model,

$$\frac{\nu_{ef}}{U_e \delta_K^*} = \frac{\nu}{U_e \delta_K^*} \phi(\chi) + \Phi(X) - X \tag{2.21}$$

Hereafter, equation (2.21) will be referred to as the HM effective- or eddy-viscosity model for Herring and Mellor, and equations (2.12) and (2.16) will be referred to as the CSM eddy-viscosity model for Cebeci, Smith and Mosinskis. There is a decided difference in the application of these two models. If values for $u(y)$, $\frac{\partial u(y)}{\partial y}$, and $T(y)$ are known from experimental measurements or from the calculations of a prediction scheme, then the CSM model is an explicit equation for the eddy viscosity; while the HM model is an implicit equation for effective viscosity which must be solved by iteration, since the terms on the right-hand side of equation (2.21) contain X and χ which are functions of the shear stress. In a boundary-layer calculation program where the shear-stress profile must be calculated at many streamwise locations, the iterative procedure required by the HM model could cause a considerable increase in computer time.

2.3 Shear-Stress Calculations in the Literature

Before shear-stress profiles are calculated by the CSM and HM models, it will be instructive to examine the calculated shear-stress profiles of previous investigators.

Predicted shear-stress distributions are rare in the literature, but shear profiles have been obtained from three separate investigations. Perhaps some insight on the behavior to expect of calculated shear profiles can be gained from these three investigations.

Dvorac [17] calculated the shear-stress profile on an incompressible flat plate at x = 0.937 meters for flow case number 1400 of the Stanford data [18]. By using an eddy-viscosity model, which is briefly presented in Reference 9, he obtained the result shown in Figure 3; the interesting feature of this graph is the anomalous behavior near the wall. The shear-stress curve should approach its maximum value at the wall with a slope normal to the wall (as seen by evaluating the momentum boundary-layer equation at the wall). Dvorac used a diffusion equation on the maximum eddy viscosity in the outer region to obtain the results of Figure 3, but when he did not use this diffusion equation, he predicted an even larger $(\tau/\rho)_{max}$ of 2.14. The use of the diffusion equation was mentioned to emphasize that Dvorac has already attempted to improve his shear-stress calculations.

Forsnes and Abbott [6] also calculated the shear-stress profile for flow 1400 of the Stanford data [18] at x = 0.937 meters. They used the experimental velocity profile and derivatives obtained from it (by an averaged linear-slope scheme) to calculate the shear-stress profiles with several

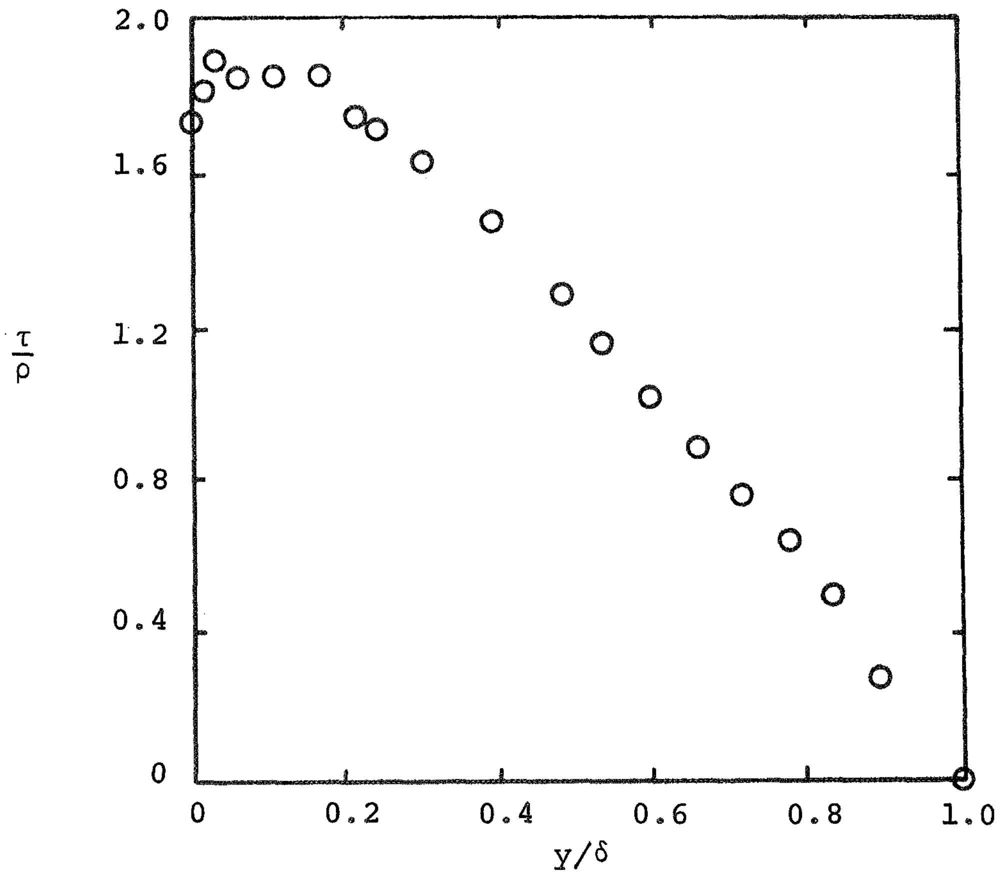

Figure 3: Dvorac's [17] Calculation of Shear Stress at x = 0.937 Meters for the Zero Pressure-Gradient Flow 1400

different eddy-viscosity and mixing-length models. Some of their results are shown in Figure 4; it is important to realize that they did not use the boundary-layer equations or any prediction program to obtain the results in Figure 4. They simply substituted experimental data and their derivatives into shear models which were reported by the several authors. Figure 4 shows that the shear-stress distributions are very poorly behaved near the wall for all four shear models, while the shear-stress curves for two of the models are unacceptably high in the outer region of the boundary layer*. It is not the intent of Figure 4 to imply that it is impossible to predict correct shear-stress profiles with these four shear models; instead, it might imply that the shear models are unusually sensitive to their input velocity and derivative profiles. The sensitivity of a particular model, the CSM model, will be discussed later in Section 2.6.

Another investigation for which shear-stress profiles are available is that of Cebeci and Smith [23]. Although Reference 23 does not explicitly contain the shear-stress values, it does contain tabular values of the variables ε^+ and F''_{cs} for the Stanford [18] data case 4400. When these

*Admittedly, the magnitude of these curves depends on the method of obtaining the velocity profile derivative; however, since the velocity profile slope is the same for each curve, relative variations are most significant.

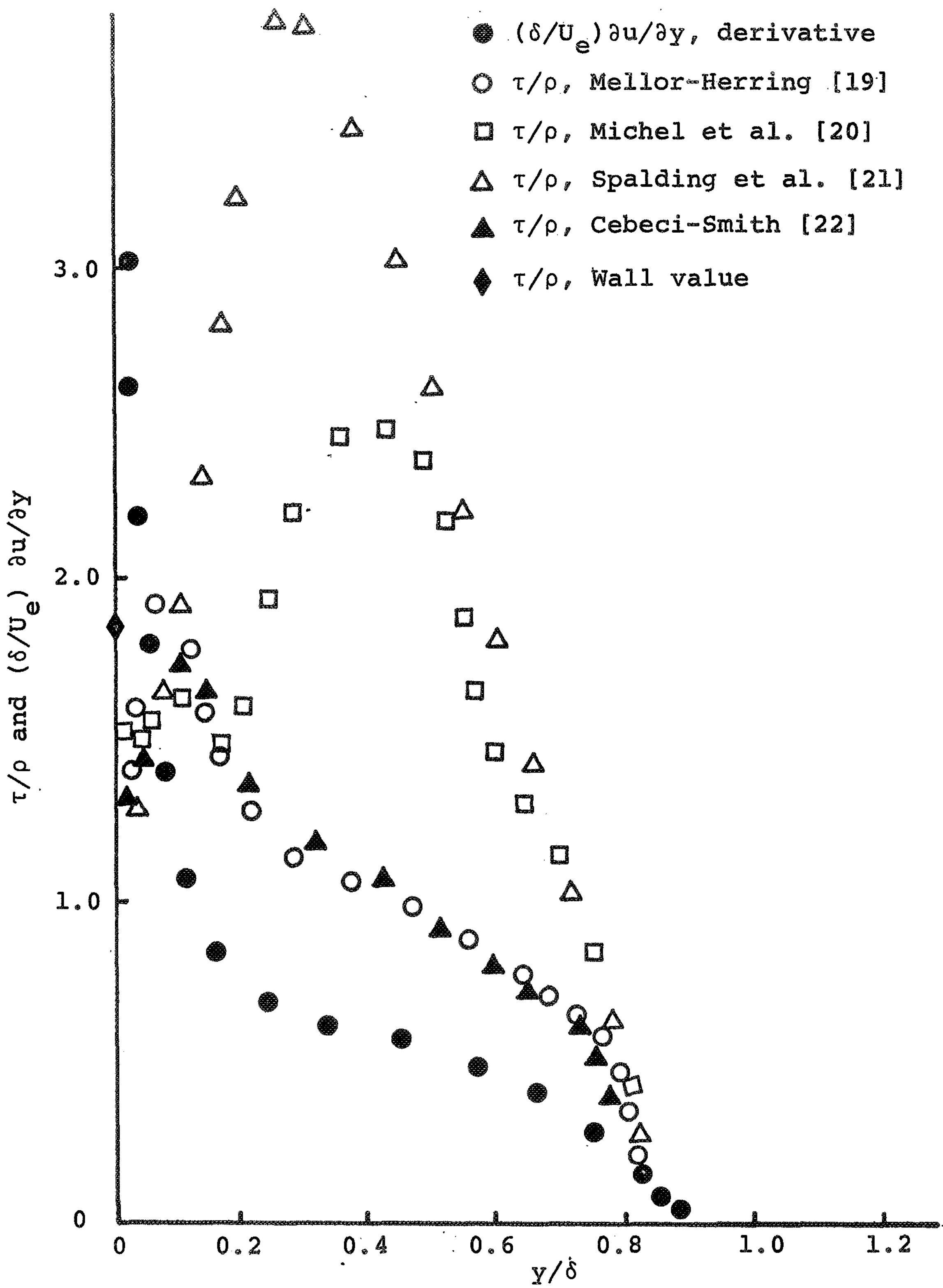

Figure 4: Velocity-Derivative and Shear-Stress Calculations of Forsnes and Abbott [6] Using Several Turbulent Shear Models, Zero Pressure Gradient Flow 1400, $x = 0.937$ meters

variables are combined properly, the shear-stress values are obtained, since

$$(1 + \varepsilon^{+})\ F''_{cs} = Re_x^{\ 1/2}\ \frac{\tau}{\rho U_e^2} \qquad (2.22)$$

Calculations of ε^{+} and F''_{cs} were also cooperatively supplied by Cebeci and Smith for several other incompressible, turbulent boundary-layer flows. However, Cebeci and Smith do not directly use the CSM eddy-viscosity model in their predictions, since the direct use of their model led to oscillations in the calculated values of δ^* and C_f and caused their iterative procedure to diverge; consequently, they use an averaging or smoothing technique on their eddy-viscosity profiles to prevent the oscillations and divergence. Figure 5 depicts the calculated shear-stress profiles at three different streamwise locations for flow case 2100 of the Stanford data [18]. This case is a boundary layer on a large airfoil-like body. The profile at $x = 2.84$ feet is in a mild favorable pressure gradient; the one at $x = 19.84$ feet is in a strong adverse pressure gradient; and the profile at $x = 26.11$ feet is within a few inches of separation. All three shear-stress profiles are smooth and properly behaved. A comparison of the calculations of the global, boundary-layer parameters in Reference [9] shows that the predictions of δ^*, θ, and C_f by Cebeci and Smith are quite good for this flow case. As one would expect, well-behaved shear-stress profiles generated good

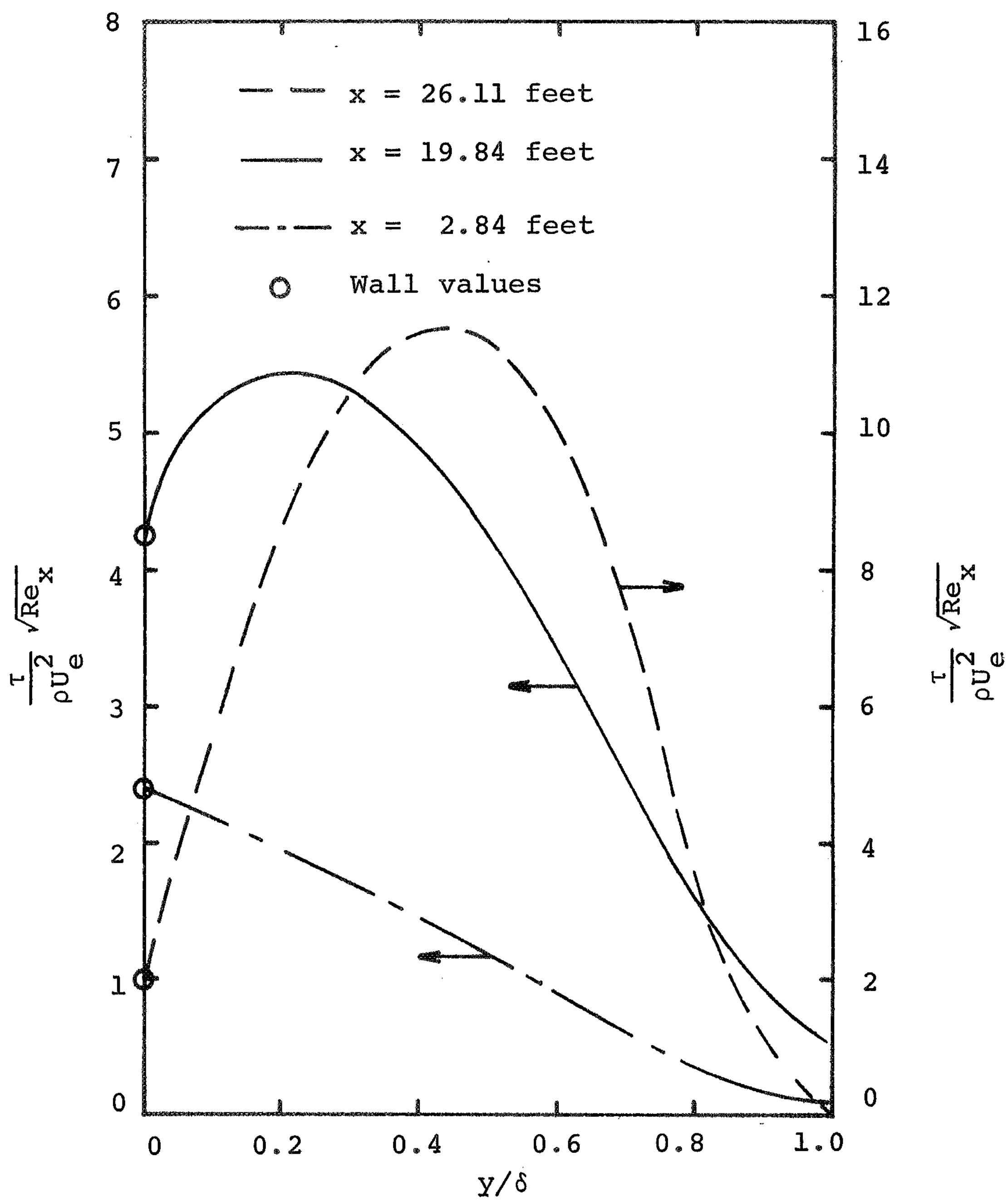

Figure 5: Shear-Stress Calculations from Cebeci and Smith [23] for Flow Case 2100

predictions for the global parameters.

Figure 6 displays the shear-stress profiles from the Cebeci-Smith boundary-layer calculation program for flow case 2400 [18]. This is a flow with a moderate, adverse, equilibrium pressure gradient which is abruptly decreased to zero and then allowed to relax to this new equilibrium pressure gradient of zero. The profile at x = 4.917 feet is near the end of the adverse pressure-gradient region while the one at x = 7.2 feet is well into the zero pressure-gradient region. Thus, the profile at x = 7.2 feet should have a slope of zero at the wall, but the calculated profile does not. Another anomally exhibited by both of the calculated profiles is a sudden jump very near the wall so that in general the calculated shear-stress profiles for this flow case are rather ill-behaved. An examination of the calculations in Reference 9 reveals that for this flow case Cebeci and Smith predict δ^* and θ very well but do rather poorly on C_f. As one would expect, the unrealistic shear distributions led to inaccurate skin-friction calculations, while the boundary-layer thickness parameters are apparently less sensitive to the shear-stress inaccuracies.

Figure 7 shows two shear-stress distributions calculated from Cebeci and Smith's results for flow 4400 [18], which is a boundary layer in a strong adverse pressure gradient. Both of these profiles have a large unrealistic jump at $y/\delta \approx 0.035$ which is undoubtedly in the zone of

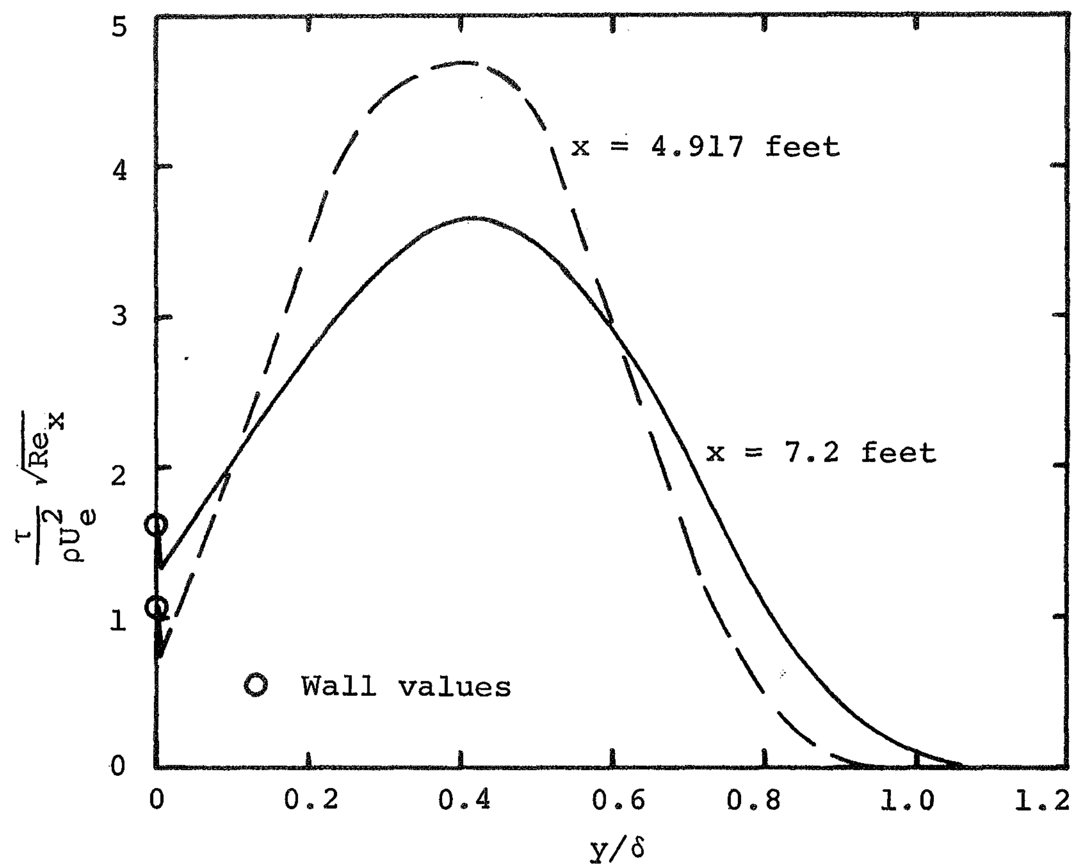

Figure 6: Shear-Stress Calculations from Cebeci and Smith [23] for Flow Case 2400

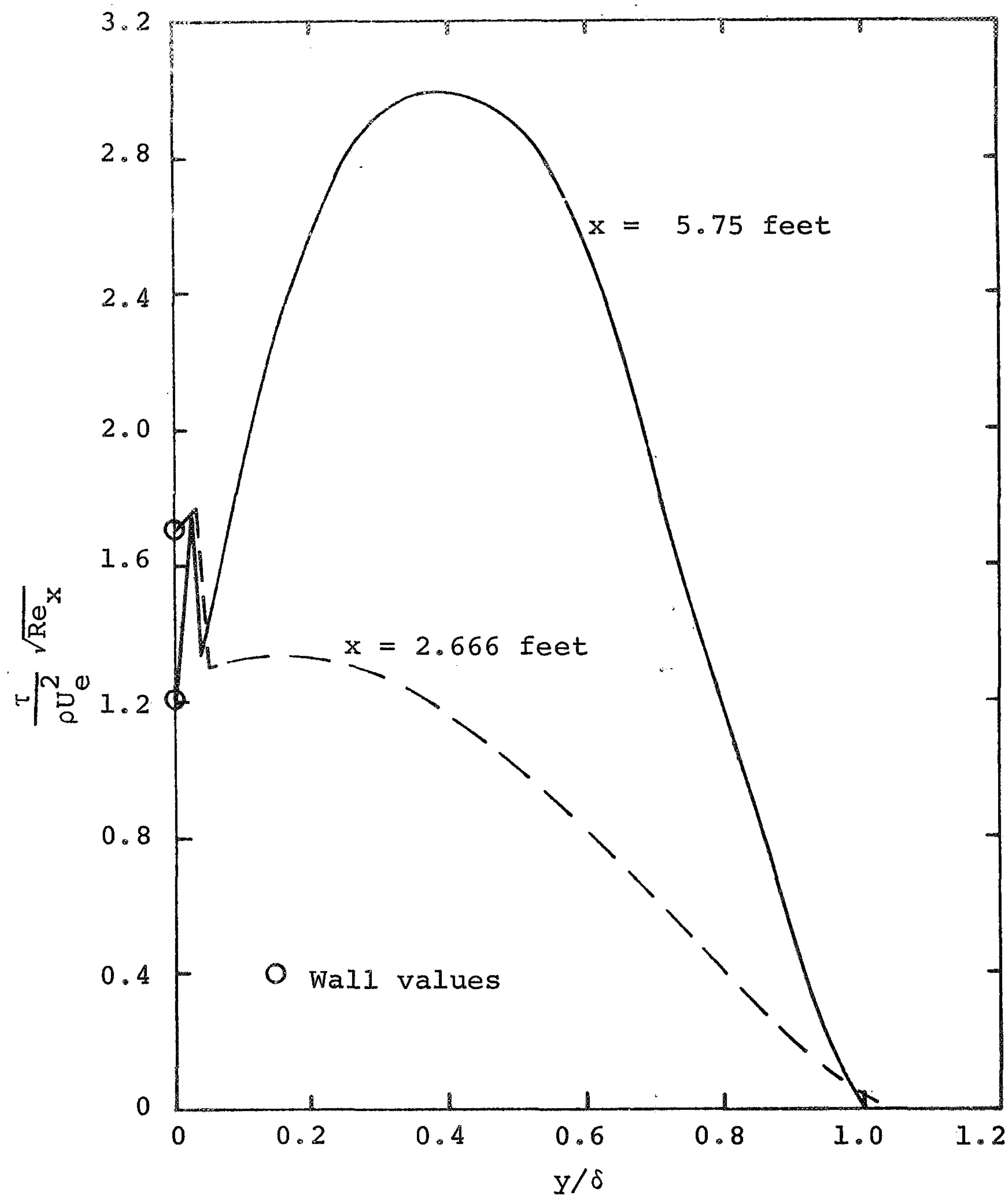

Figure 7: Shear-Stress Calculations from Cebeci and Smith [23] for Flow Case 4400

application of the inner-region model. In view of these shear-stress profiles, one might expect very inaccurate calculations of the global parameters, but Reference 9 shows that the Cebeci-Smith calculations of δ^*, θ, and C_f are nearly perfect — passing through almost every experimental data point. In fact all seventeen investigators who predicted flow 4400 in Reference 9 did extremely well. The reason Cebeci and Smith were able to correctly predict the global parameters with such poor shear-stress profiles is probably because the turbulent shear information terms in the governing equations are of only secondary importance for this flow case. Further substantiation of this claim is seen in the work of Forsnes and Abbott [6]. They developed a first approximation to the solution of the governing equations using the method of weighted residuals. This first approximation contains no turbulent shear information, since all terms containing τ are identically zero. Forsnes and Abbott's first approximation calculations for flow 4400 are given in Figure 8 and show remarkably good agreement with experiment. Additional first-approximation or "zero-physics" predictions are given in Reference 6 which shows comparable success for several of the flow cases in Reference 18. These "zero-physics" results indicate that the turbulent shear information terms may be of secondary importance for certain classes of flows.

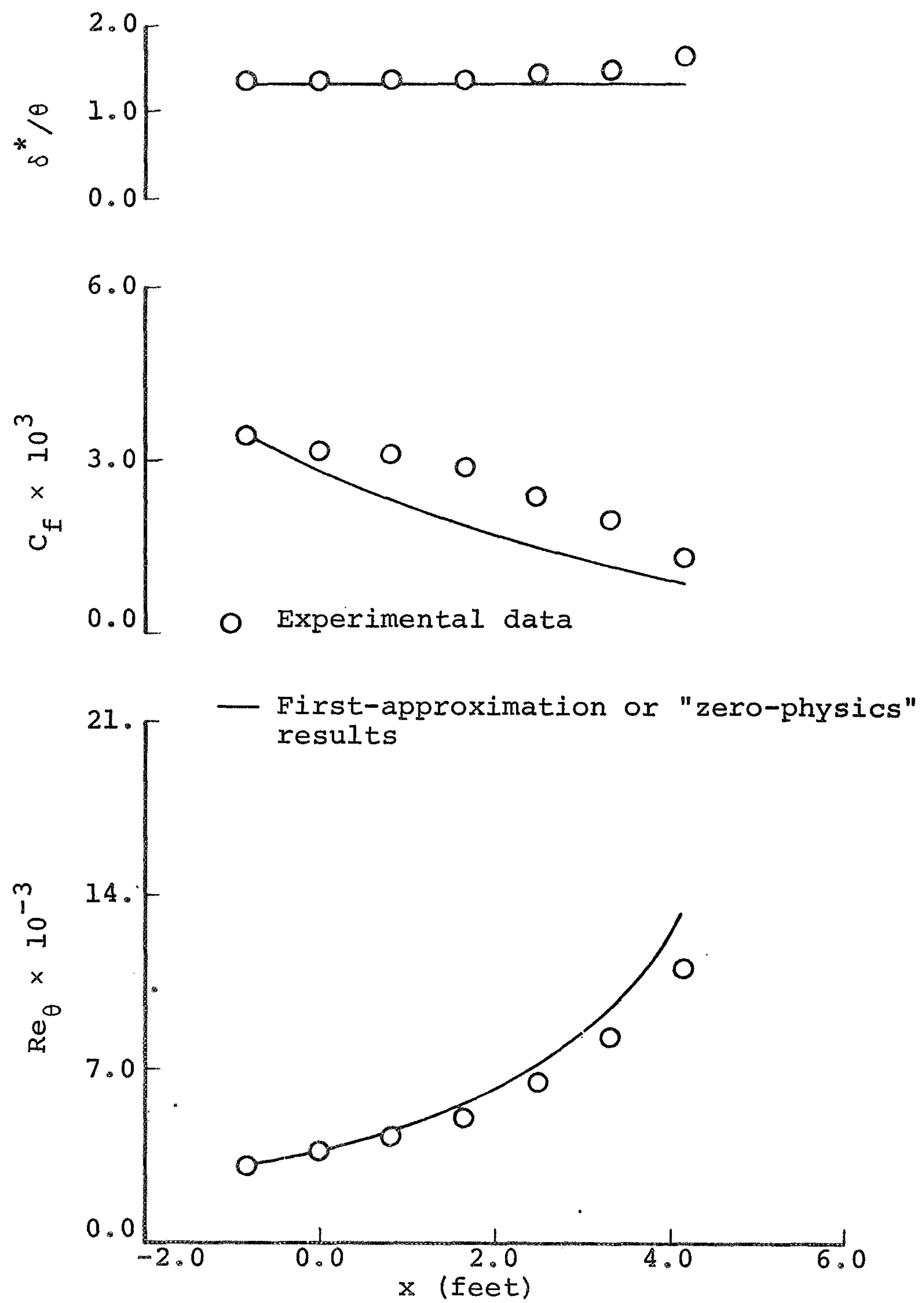

Figure 8: First-Approximation Prediction of Forsnes and Abbott [6] Compared with Experimental Data of Flow Case 4400

2.4 Shear-Stress Calculations in the Present Investigation

Now that the shear-stress calculations from several previous investigations have been examined, the present investigation can proceed with some calculations of its own for compressible, turbulent boundary layers — the task which was originally proposed in Section 2.2 where the CSM and HM eddy-viscosity models were presented in detail. These two models will be examined by calculating the shear-stress profiles for adiabatic, turbulent, compressible data cases. The inputs to the eddy-viscosity models are the experimental velocity and Mach-number profiles and the velocity-profile derivative calculated by the weighted central finite-difference scheme derived in Appendix A. Other equations necessary to calculate all the variables occurring in the eddy-viscosity models are: the perfect gas law

$$p = \rho RT \tag{2.23}$$

Mach number for a perfect gas

$$M = u/\sqrt{\gamma RT} \tag{2.24}$$

Sutherland's viscosity law

$$\frac{\mu}{\mu_r} = \left(\frac{T}{T_r}\right)^{3/2} \frac{T_r + C}{T + C} \tag{2.25}$$

where $C = 192°R$, $T_r = 492°R$, and $\mu_r = 3.59 \times 10^{-7}$ slug/ft-sec. The present calculations for the shear-stress profiles using the CSM and HM eddy-viscosity models are shown in Figures 9, 10, and 11. The calculated velocity derivatives

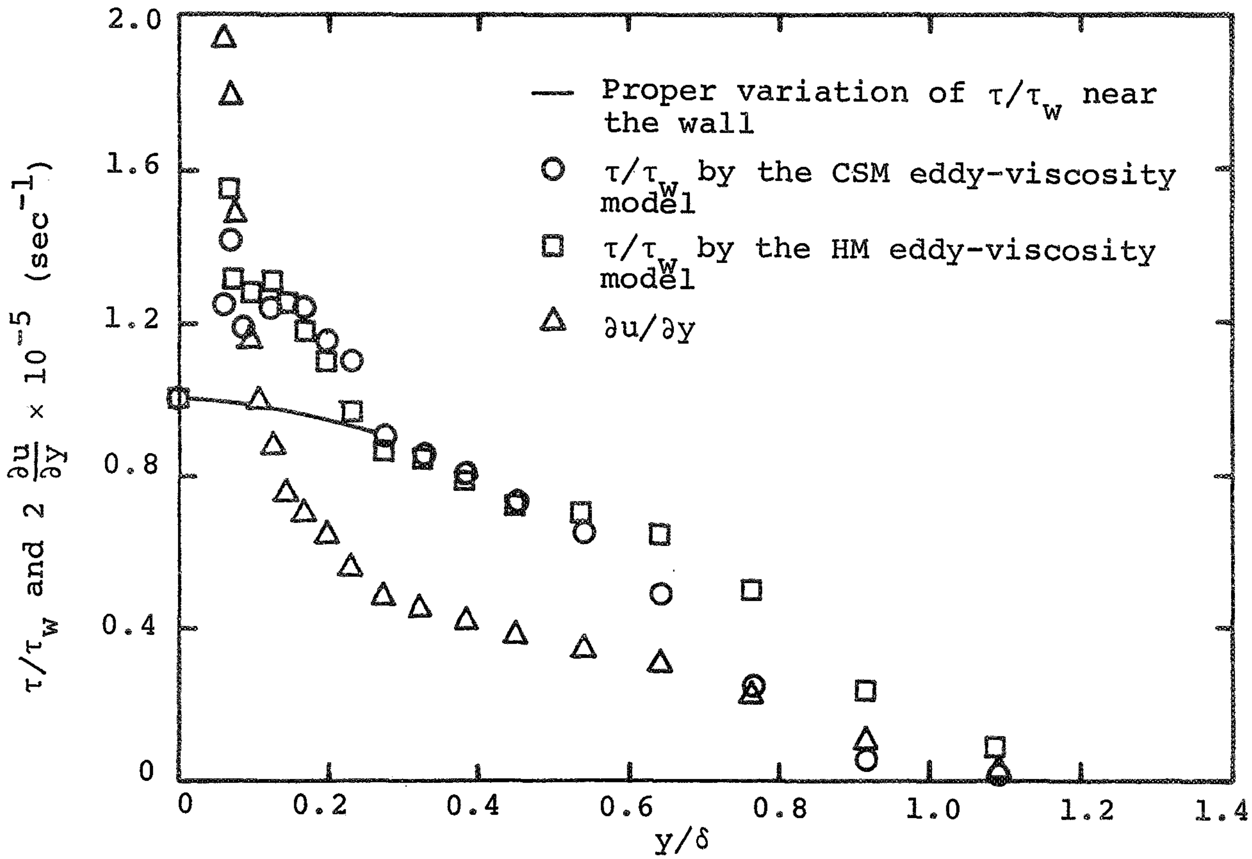

Figure 9: Calculation of Velocity Derivative and Shear Stress for the Experimental Data of Coles [24] on an Adiabatic Flat Plate at $M_e = 1.978$ and $Re_x = 4.33 \times 10^6$

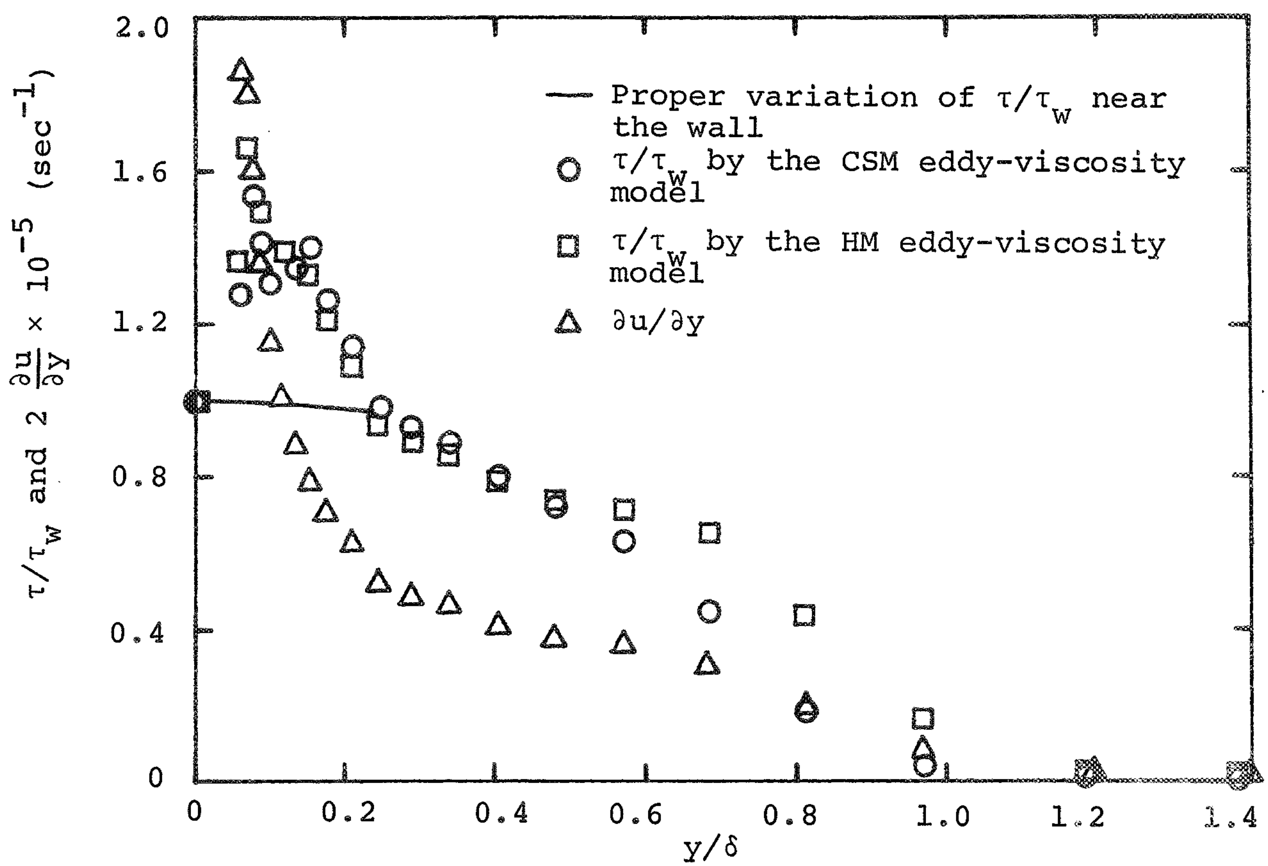

Figure 10: Calculation of Velocity Derivative and Shear Stress for the Experimental Data of Coles [24] on an Adiabatic Flat Plate at $M_e = 1.982$ and $Re_x = 6.18 \times 10^6$

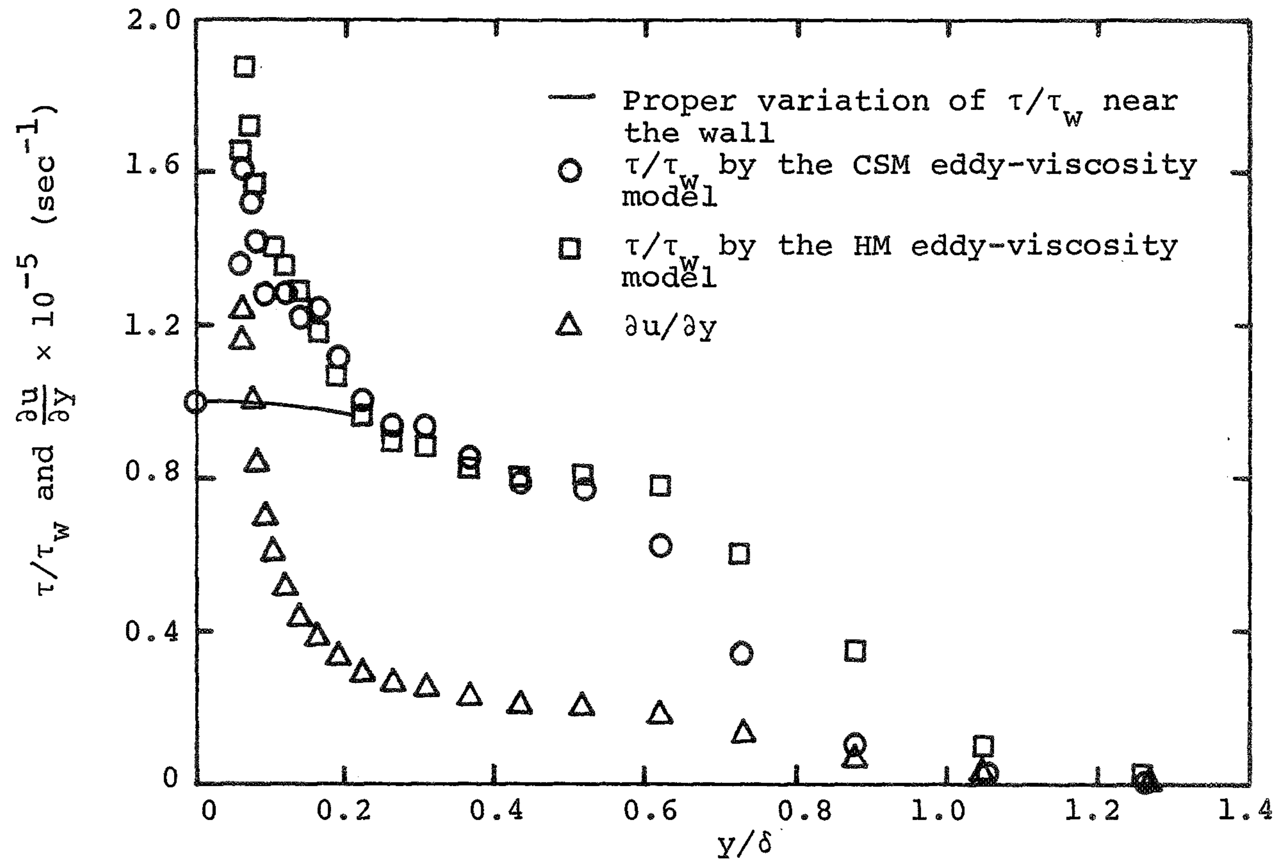

Figure 11: Calculation of Velocity Derivative and Shear Stress for the Experimental Data of Coles [24] on an Adiabatic Flat Plate at $M_e = 2.568$ and $Re_x = 4.84 \times 10^6$

are also plotted to show their smooth nature near the wall where the shear-stress profiles are erratic. For a comparison with these calculations, the correct qualitative behavior of the τ/τ_w function near the wall is sketched in with a solid line. Figures 9 and 10 exhibit the calculations at two different Reynolds numbers for approximately the same Mach number while Figure 11 shows the calculations at another Mach number. It is seen that the results in all three figures are quite similar. Both the CSM and HM models generate erratic behavior in the shear-stress profiles near the wall, and the CSM shear-stress profile decreases to zero faster than the HM profile in the outer region of the boundary layer. The faster descent of the shear-stress profile calculated by the CSM model can be explained in the following manner. An intermittency factor is built into the CSM eddy-viscosity model to account for the intermittent character of the turbulent boundary layer. The intermittency factor is employed to decrease the outer eddy-viscosity values as y increases. The HM model does not use an intermittency factor; it employs Clauser's [4] theory of a constant eddy viscosity in the outer region of the boundary layer. Although Mellor [12] noticed the shortcoming of the Clauser theory, Mellor felt that this shortcoming would not appreciably affect the boundary-layer calculations.

Before an attempt is made to use either the CSM or the HM eddy-viscosity model to predict compressible, turbulent boundary layers, it is considered desirable to improve the shear-stress profile in the inner or wall region of the boundary layer. There seems little to choose from, between these two eddy-viscosity models, since both have proven to yield accurate predictions of the global boundary-layer parameters in Reference 9. However, two analytical factors warrant a preference for the CSM eddy-viscosity model: (1) it contains an intermittency factor which creates the qualitatively correct reduction of eddy viscosity in the outer region, and (2) it is an explicit equation for eddy viscosity which can thus be solved without iteration. Two other reports lend credence to the preference of the CSM model. Bankston and McEligot [25] made numerical predictions of heat-transfer rates in the entry region of circular ducts using several different eddy-viscosity and mixing-length models. They found the best agreement between calculations and experimental measurements with a version of the Van Driest mixing length, which is included in the CSM model. Martellucci, Rie, and Santowskii [26] calculated total-temperature and pressure profiles over a cone at Mach eight using three different eddy-viscosity models. In general the calculations using the CSM model agreed slightly better with the data than the calculations using either the Santowskii model or the Patankar-Spalding model. Consequently, further consideration in this report will be restricted to the CSM eddy-viscosity model. A major effort of the present investigation will be directed toward improving the inner-region behavior of the CSM shear-stress profile.

2.5 Analysis of the Anomalous Shear-Stress Behavior

For a first attempt at understanding the shear-stress problem in the wall region, it is considered desirable to find out what velocity profile will give the physically correct shear-stress distribution when that velocity profile is substituted into the CSM eddy-viscosity model. The method devised to answer this question will now be described. The correct shear-stress profile is assumed to be the solid line (Figures 9, 10, and 11) in the inner region plus a faired curve through the points marked with open circles in the outer region. The equations required for the property variations are (2.23), (2.24), (2.25), and the Crocco relation relating the temperature profile to the velocity profile,

$$T/T_w = 1 + (T_o/T_w - 1)\, u/U_e + (T_e/T_o - 1)\, T_o/T_w (u/U_e)^2 \tag{2.26}$$

Equivalent forms of equation (2.26) have been derived by Crocco [27] and Van Driest [28]. The Crocco relation has proven to agree quite well with experimental data for the flow of air over a flat plate; e.g. see Bushnell, Johnson, Harvey, and Feller [29]. To make the description of the calculation procedure more easily understandable, the working equations will be represented in functional form. The

CSM eddy-viscosity model becomes

$$\varepsilon = f_1 \ (u, \frac{\partial u}{\partial y} , K_1) \tag{2.27}$$

where f_1 is a two layer function given by equations (2.12) and (2.16). Rearrangement of equation (2.4) yields

$$\frac{\partial u}{\partial Y} = f_2(\varepsilon, u, \tau) \tag{2.28}$$

where

$$f_2(\varepsilon, u, \tau) = \frac{\tau}{\rho(\nu + \varepsilon)} \tag{2.29}$$

Admittedly f_1 and f_2 are functions of many other variables, but they will be taken as parameters, and the three arguments shown for each function are taken to be the only dependent variables once the equations for the property variations have been employed. The constant K_1 in equation (2.27) has been included as an argument for reasons that will become apparent later, but for the present $K_1 = 0.40$ will be used. Equations (2.27) and (2.28) are readily solved. The physically correct shear-stress distribution, $\tau(y)$, is substituted into equation (2.28); then equations (2.27) and (2.28) become two equations in the two unknowns, $u(y)$ and $\varepsilon(y)$. At a given x-location these equations are first-order ordinary differential equations for u and algebraic equations for ε. These equations are solvable by Picard's method. A first guess, say $u_1(y)$, is made for the solution of $u(y)$; when $u_1(y)$ is inserted into the right-hand side of equations (2.27) and (2.28), these equations become two algebraic equations in two unknowns, $\frac{\partial u(y)}{\partial y}$ and $\varepsilon(y)$ which are readily solvable. The $\frac{\partial u(y)}{\partial y}$ profile is integrated to yield a second approximation, $u_2(y)$; then $u_2(y)$ takes the previous role of $u_1(y)$, and the process is continued until convergence is obtained. Approximately twenty iterations were generally required to obtain convergence to six significant figures of u when $u_1(y)$ was taken to be the experimental velocity profile. Upon convergence the $u(y)$ profile is the desired one. When this profile is substituted into the CSM eddy-viscosity model, a physically correct shear-stress distribution is obtained.

This iterative procedure has been applied to several sets of experimental data measured by Coles [24] and Matting, Chapman, Nyholm, and Thomas [30] for the compressible flow of air over an adiabatic flat plate. The solid line curves in Figures 12 and 13 show the results of these calculations which are compared with experimental data. Figure 12 shows one of the best agreements between calculation and experiment while Figure 13 shows the worst. The best agreement occurs at the lowest Mach number, and this trend in general occurred for all the data that was examined; this trend with Mach number will be examined later in this section.

In the application of the CSM model, poor behavior of the shear-stress profile occurs only in the inner region of the boundary layer where equation (2.12) is utilized;

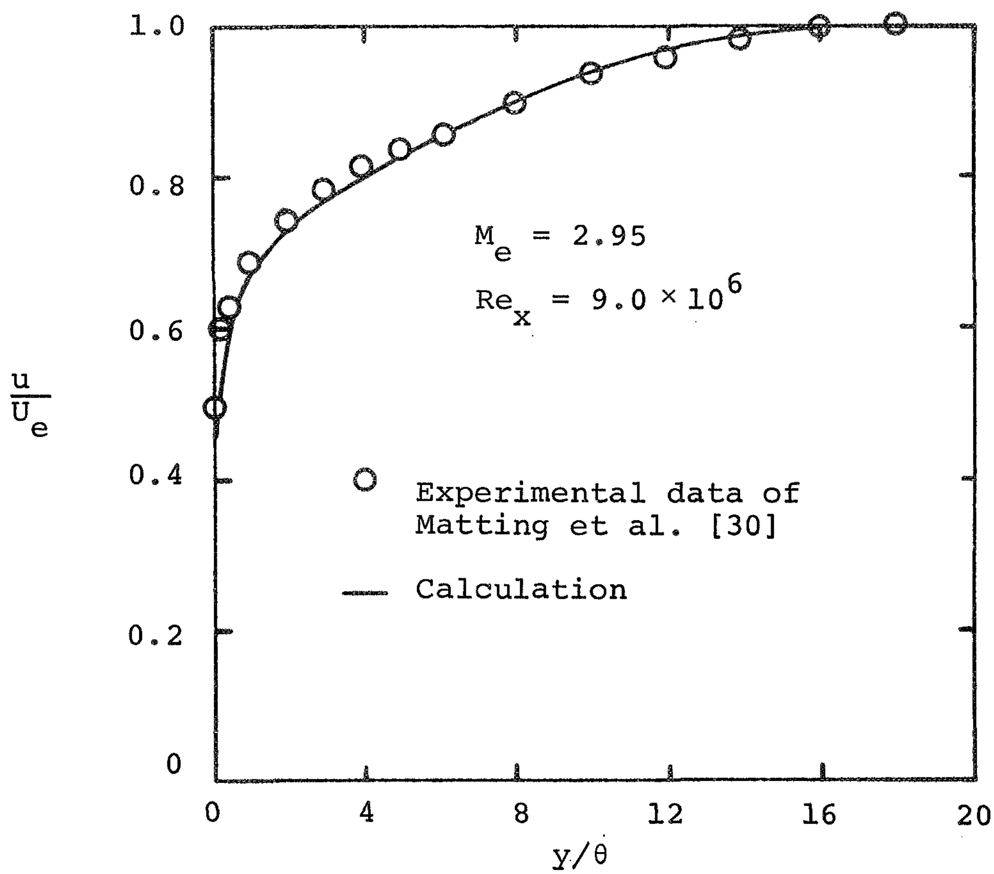

Figure 12: Velocity Profile Calculated by the Iterative Procedure on Eddy Viscosity with $K_1 = 0.40$

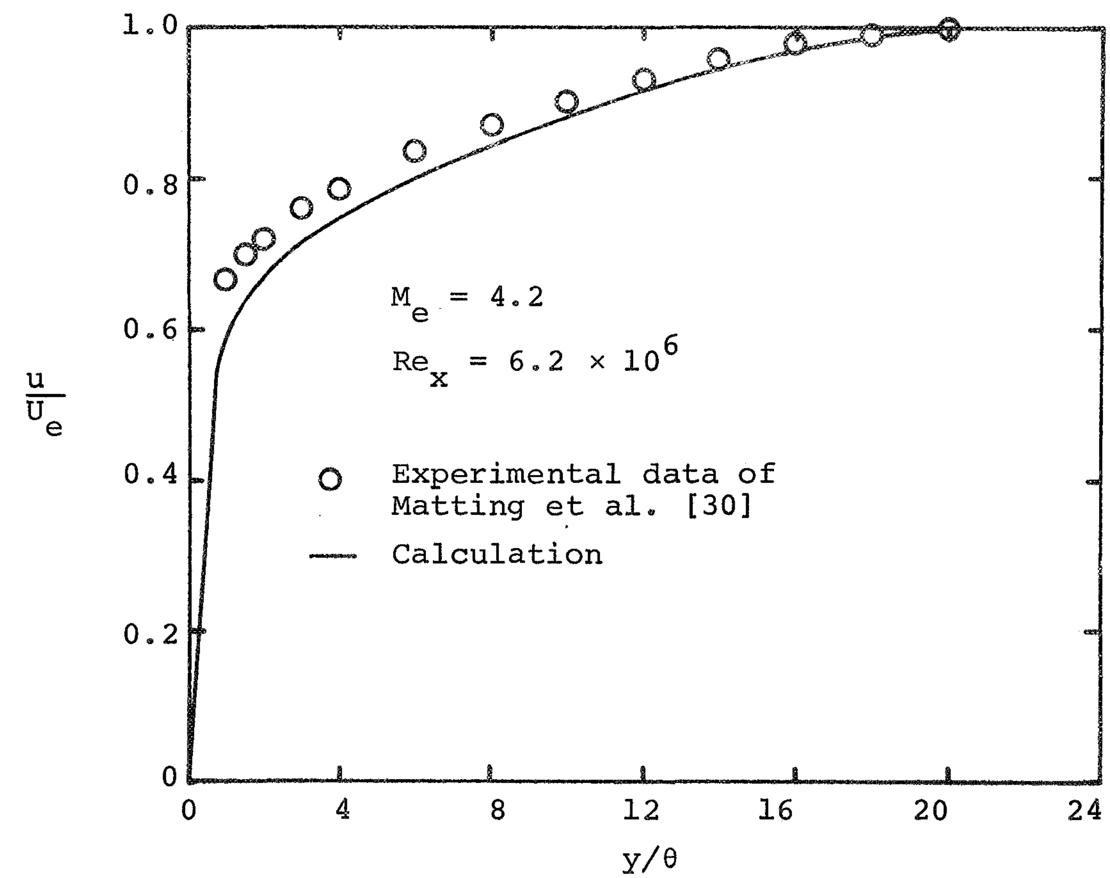

Figure 13: Velocity Profile Calculated by the Iterative Procedure on Eddy Viscosity with $K_1 = 0.40$

therefore, this equation will be examined in detail. In the derivation of equation (2.10), Van Driest [13] showed that the constant K_1 corresponds exactly to the constant K_1 in the universal logarithmic velocity distribution in the fully turbulent region of the boundary layer

$$u^+ = \frac{1}{K_1} \ell n\ y^+ + K_3 \tag{2.30}$$

Equation (2.30) has been found to agree very well with experimental data for incompressible flow using $K_1 = 0.4$, but Coles [24] and Van Driest [28] have shown that equation (2.30) does not agree with compressible flow data nearly as well as it does for incompressible data. Consequently, the constant value of $K_1 = 0.4$ in the mixing-length expression is questionable for compressible flow. The same calculations as before were made to determine what velocity profile will give a correct shear-stress profile using the CSM model; only this time the value of K_1 was optimally adjusted until the velocity profile which agreed best with the experimental data was calculated. These calculated velocity profiles with an optimum value of K_1 are shown in Figures 14 and 15 by the broken lines where they are compared with two sets of experimental data and the corresponding calculations using $K_1 = 0.4$ (solid lines). These same calculations were performed to find the optimal values of K_1 for several other data sets measured by Coles [24] and Matting, et al. [30], and these results are plotted for K_1 versus Mach number in Figure 16. Although possibilities of

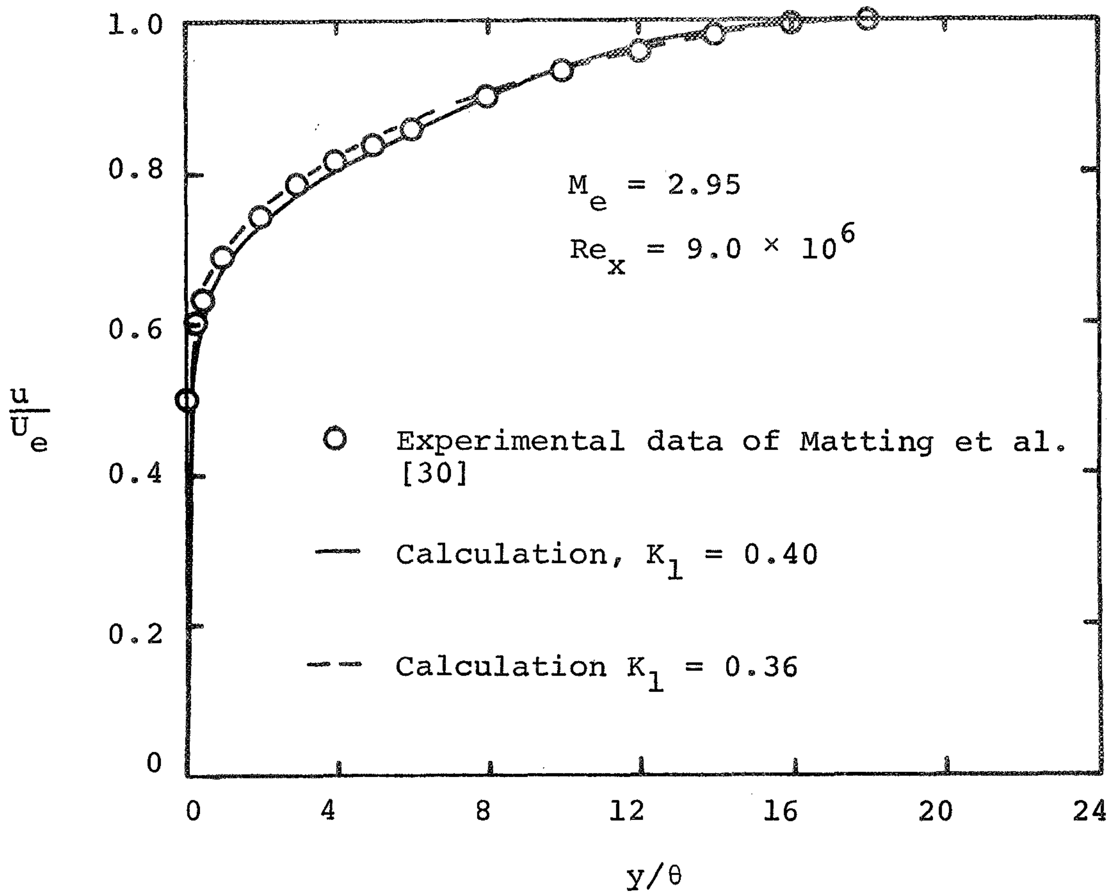

Figure 14: Velocity Profile Calculated by the Iterative Procedure on Eddy Viscosity for $K_1 = 0.40$ and the Optimum Value of $K_1 = 0.36$

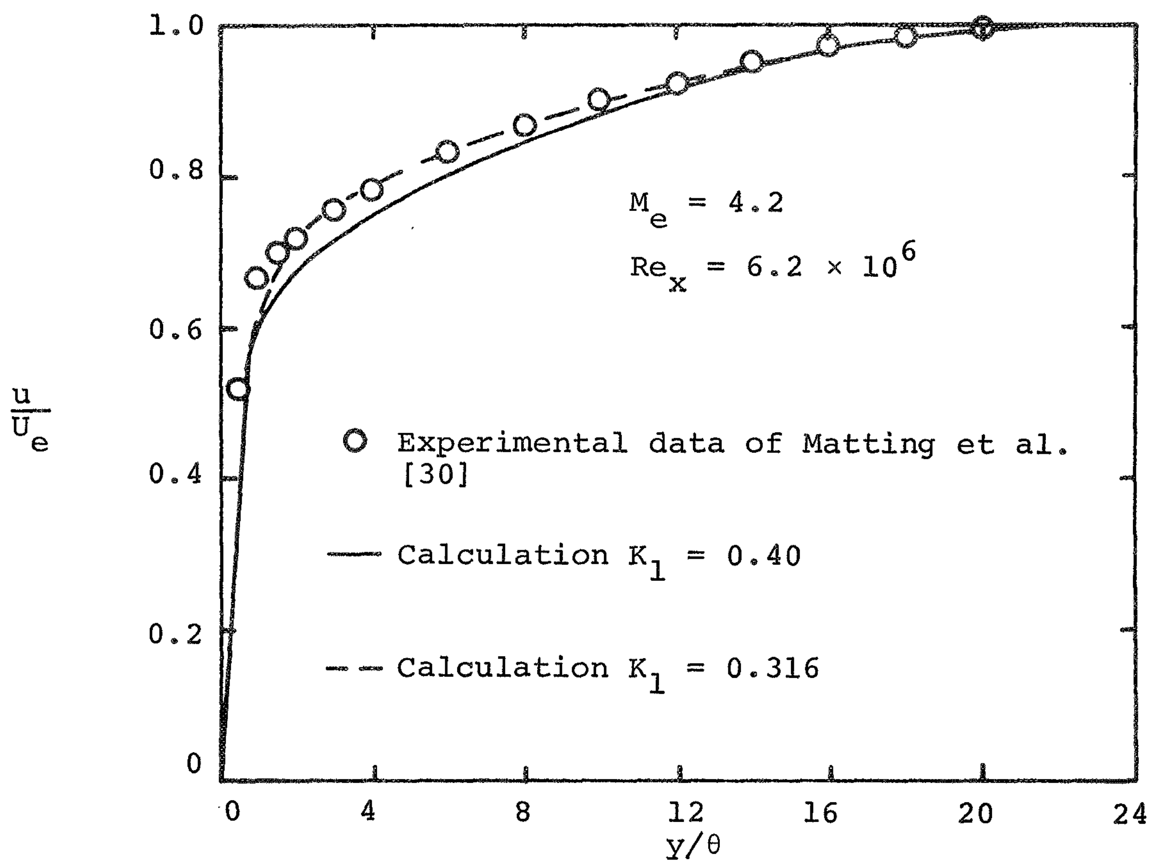

Figure 15: Velocity Profile Calculated by the Iterative Procedure on Eddy Viscosity for $K_1 = 0.40$ and the Optimum Value of $K_1 = 0.316$

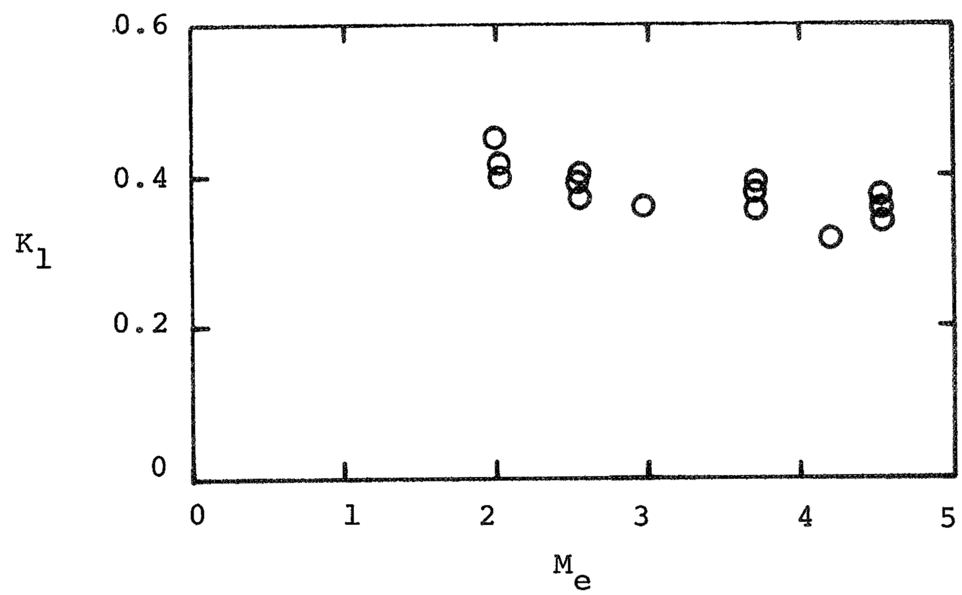

Figure 16: Variation of the Optimal Values of K_1 with Mach Number

trends for K_1 in the parameters C_f, Re_x, Re_θ, etc. were explored, none appeared except the one shown in Figure 16. Although a definite trend of decreasing K_1 with increasing Mach number exists, the large degree of scatter in the calculated points prohibits the discovery of an accurate correlation function for K_1 in compressible flow. Still a least-squares parabolic or linear fit to the calculated points should make a significant improvement over the $K_1 = 0.40$ constant value.

2.6 Sensitivity of the CSM Eddy-Viscosity Model

Shear-stress profiles have been calculated by the CSM eddy-viscosity model, and the erratic behavior of these profiles in the inner region has been noted. An iterative procedure has been developed to remove the erratic behavior by generating velocity profiles which are physically compatible with the CSM model. Physically realistic shear-stress profiles resulted, but little light was shed on the actual cause of the erratic behavior. That is the purpose of this section.

Recall the significance of Figure 12. The data points are the experimentally measured velocity profile, which, when substituted into the CSM model, generates a very poorly behaved shear-stress profile in the inner region. The solid line in Figure 12 is the iterated velocity profile with $K_1 = 0.40$, which, when substituted into the CSM model, generates a physically correct shear-stress distribution. The fact that two velocity profiles so nearly the same yield shear-stress profiles so different implies that the CSM eddy-viscosity model is very sensitive to its input velocity profile. This sensitivity in the inner region can be easily analyzed with a simple example. Suppose there is a (σy) error in the value of y to be substituted into the inner region eddy-viscosity model, equation (2.12), where σ is the fractional error. Then the fractional error in the y^2 factor in equation (2.12) is $2\sigma + \sigma^2$, so a 10 percent error in y causes a 21 percent error in the y^2 term. If in addition there is a positive 10 percent error in the $\frac{\partial u}{\partial y}$ value, then this error enters as a multiplicative factor with the 21 percent error in y^2, and the total contribution is an error of 33.1 percent in the eddy viscosity ε. For the data case of Figure 12 the edge of the inner region occurs where $u/U_e = 0.75$; at this point $\varepsilon_i/\nu = 90.6$; thus, from equation (2.4) it is seen that $\varepsilon \frac{\partial u}{\partial y}$ is about 99 percent of the value of τ/ρ so that a percentage error in ε causes approximately the same percentage error in τ. With this error analysis in mind, it is seen in Figure 12 for $u/U_e < 0.75$ that there are differences of the order of 10 to 50 percent in the y values of the two velocity profiles at a given value of u/U_e. This error is then compounded when these y values are substituted into the equations for ε_i and τ, and drastically different shear-stress profiles are the result.

2.7 Summary

In this section a brief review of some pertinent literature on turbulent shear information modeling is presented, and some available shear-stress calculations are examined. An anomalous behavior of the shear-stress profile is noted, and avenues of emphasis and approach are outlined and followed. Calculations of shear stress are made by two of the best known and regarded eddy-viscosity expressions, and these calculations displayed a very unrealistic behavior in the inner region of the boundary layer. The cause of this is explained by an error analysis which points out the sensitivity of an inner region eddy-viscosity expression to the velocity profile. A method is devised to correct this unrealistic behavior, and, furthermore, a correction of an inner region eddy-viscosity model is recommended.

3. BOUNDARY-LAYER PREDICTION ANALYSIS

3.1 Introduction

One of the purposes of this work is the development of a prediction procedure for two-dimensional, compressible, turbulent boundary layers. In Section 2 physical shear-stress models were examined, and a particular model was developed so that it would yield well-behaved shear-stress distributions. This analysis was done entirely independent of any mathematical technique for solving the boundary-layer equations. In this section the governing equations are presented and a mathematical solution technique is formulated which will be completely independent of any physical shear model. The distinct separation of the analyses for the solution technique and for the physical shear model allows a clearer understanding of the difficulties caused by each phase of the overall prediction program. Finally in Section 4 the shear model and the solution technique will be combined into a prediction program.

3.2 Boundary-Layer Equations

The derivation of the appropriate equations has been documented in a number of references. For example, Schubauer and Tchen [31] start with the two-dimensional, compressible, Navier-Stokes equations and substitute the sum of a time mean and a fluctuating quantity for all the instantaneous variables, for example,

$$z_{in} = z + z' \tag{3.1}$$

where z_{in} is the instantaneous value of a physical variable, z' is the fluctuating component of z_{in}, and z is the time mean component of z_{in}. They then take the time average of the resulting equations and perform an order of magnitude analysis which results in the following governing equations for the mean properties of a two-dimensional, compressible, turbulent boundary layer:

Continuity:

$$\frac{\partial \rho}{\partial t} + \frac{\partial}{\partial x} (\rho u) + \frac{\partial}{\partial y} (\rho v + \overline{\rho' v'}) = 0 \tag{3.2}$$

x-momentum:

$$\frac{\partial}{\partial t} (\rho u) + \frac{\partial}{\partial x} (\rho u^2) + \frac{\partial}{\partial y} (\rho u v) = - \frac{\partial p}{\partial x} + \frac{\partial}{\partial y} \left(\mu \frac{\partial u}{\partial y} - \rho \overline{u' v'} - u \overline{\rho' v'} \right) \tag{3.3}$$

y-momentum:

$$- \frac{\partial p}{\partial y} - \frac{\partial}{\partial y} (\rho \overline{v'^2}) = 0 \tag{3.4}$$

Energy:

$$\frac{\partial}{\partial t} (\rho H) + \frac{\partial}{\partial x} (\rho H u) + \frac{\partial}{\partial y} (\rho H v) = \frac{\partial}{\partial y} \left(\mu \frac{\partial H}{\partial y} - \rho \overline{v' H'} - \overline{\rho' v'} H \right) + \frac{\partial}{\partial y} \left[\left(\frac{1}{Pr} - 1 \right) \mu \frac{\partial (C_p T)}{\partial y} \right] + \rho \overline{u' v'} \frac{\partial u}{\partial y} \tag{3.5}$$

Integration of equation (3.4) yields

$$p = p_e - \rho\overline{v'^2} \tag{3.6}$$

or

$$p = p_e \left(1 - \gamma M_e^2 \frac{\rho\overline{v'^2}}{\rho_e U_e^2}\right) \tag{3.7}$$

since

$$M_e^2 = \frac{\rho_e U_e^2}{\gamma p_e} \tag{3.8}$$

For small turbulence level $(\overline{v'^2}/u^2 << 1)$ and for M_e of the order of one,

$$p = p_e \tag{3.9}$$

Equations (3.2), (3.3), (3.5), and (3.9) can be combined to yield the usual boundary-layer equations for the steady mean flow of a two-dimensional, compressible, turbulent boundary layer:

Continuity:

$$\frac{\partial}{\partial x}(\rho u) + \frac{\partial}{\partial y}(\rho v + \overline{\rho' v'}) = 0 \tag{3.10}$$

Momentum:

$$\rho u \frac{\partial u}{\partial x} + (\rho v + \overline{\rho' v'}) \frac{\partial u}{\partial y} = - \frac{dp}{dx} + \frac{\partial \tau}{\partial y} \tag{3.11}$$

Energy:

$$\rho u \frac{\partial H}{\partial x} + (\rho v + \overline{\rho' v'}) \frac{\partial H}{\partial y} = \frac{\partial}{\partial y}\left[\frac{\mu}{Pr}\left(1 + \frac{\varepsilon}{\nu}\frac{Pr}{Pr_t}\right)\frac{\partial H}{\partial y} + \mu\left(1 - \frac{1}{Pr}\right) u \frac{\partial u}{\partial y}\right] \tag{3.12}$$

where

$$\varepsilon \frac{\partial u}{\partial y} = -\overline{u'v'} \tag{3.13}$$

$$\frac{\lambda_t}{C_p} \frac{\partial H}{\partial y} = -\rho\overline{v'H'} \tag{3.14}$$

$$Pr_t = \frac{C_p \varepsilon}{\lambda_t} \tag{3.15}$$

$$\tau = \rho(\nu + \varepsilon) \frac{\partial u}{\partial y} \tag{3.16}$$

These equations may also be found derived in equivalent forms by Cebeci and Smith [32], Herring and Mellor [8], and Schlichting [33].

At this point, the streamwise gradient of the apparent normal stresses $\frac{\partial}{\partial x} (\rho\overline{u'^2} - \rho\overline{v'^2})$ have been assumed negligible as is usually done; there has been considerable discussion on the validity of this assumption for a flow near separation. For example, Goldberg [34] shows that the apparent normal stresses may not be negligible compared to the apparent shear stress for flows approaching separation; furthermore, in the discussion at the Stanford conference on turbulent boundary layers [9], V. A. Sandborn states that the apparent shear-stress term in the equation of motion was found to be negligible but that the $\frac{\partial p}{\partial y}$ was not negligible for his experimental investigations of turbulent separation. Consequently, since it appears that the governing equations presented here are not completely valid for flows near separation, this analysis may not apply to the investigation of turbulent separation.

The appropriate boundary conditions for equations (3.10), (3.11), and (3.12) are

$$u(x_o,y) = u_o(y) \tag{3.17a}$$

$$u(x,0) = 0 \tag{3.17b}$$

$$\lim_{y\to\infty} u(x,y) = U_e(x) \tag{3.17c}$$

$$v(x,0) = 0 \tag{3.17d}$$

$$H(x_o,y) = H_o(y) \tag{3.17e}$$

$$H(x,0) = H_w \text{ or } \frac{\partial H}{\partial y}(x,0) = \left(\frac{\partial H}{\partial y}\right)_w \tag{3.17f}$$

and

$$\lim_{y\to\infty} H(x,y) = H_e(x) \tag{3.17g}$$

Additional equations are needed for the property variations. The relations used in this investigation are the perfect gas equation of state

$$p = \rho RT \tag{2.23}$$

and Sutherland's viscosity law

$$\frac{\mu}{\mu_r} = \left(\frac{T}{T_r}\right)^{3/2} \frac{T_r + C}{T + C} \tag{2.25}$$

where

$$C = 192°R$$

$$T_r = 492°R$$

$$\mu_r = 3.59 \times 10^{-7} \text{ slug/ft-sec}$$

Also, the following values of the Prandtl number and the turbulent Prandtl number are assumed (for air):

$$Pr = 0.72 \tag{3.18}$$

$$Pr_t = 1.0 \tag{3.19}$$

Although these property variation equations have been used in this work, any available equations for the equation of state, viscosity, Prandtl number, or turbulent Prandtl number could be easily incorporated into the ensuing analysis. Perhaps some discussion is in order at this point on the selection of a turbulent Prandtl number of unity.

Figures 17 and 18, taken from Cebeci [35], are offered as justification for the use of $Pr_t = 1.0$. Due to the large extent of the experimental scatter in these figures, $Pr_t = 1$ was thought to be a suitable approximation until further experimental investigations of the turbulent Prandtl number have been undertaken. Cebeci is currently seeking a correlation equation for the turbulent Prandtl number; and, as mentioned previously, such a correlation could be easily utilized in the present analysis.

3.3 Mathematical Solution Technique

Mathematical methods for the solution of boundary-layer problems have historically been classified into two major divisions; integral methods and finite-difference methods. W. C. Reynolds [39] states, "The chief virtue of integral

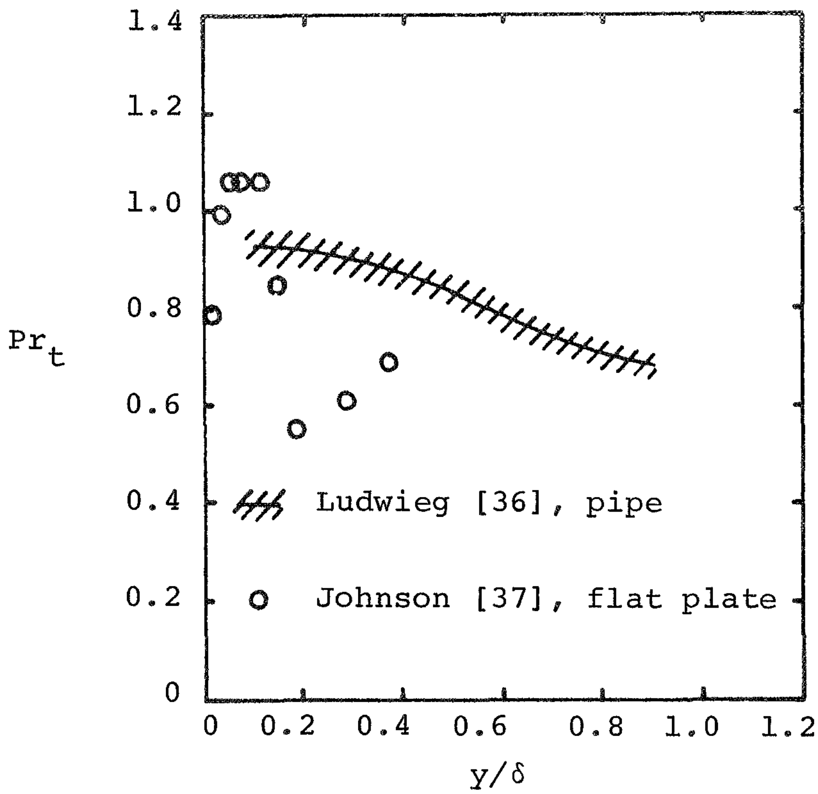

Figure 17: Experimental Measurements of Turbulent Prandtl Number

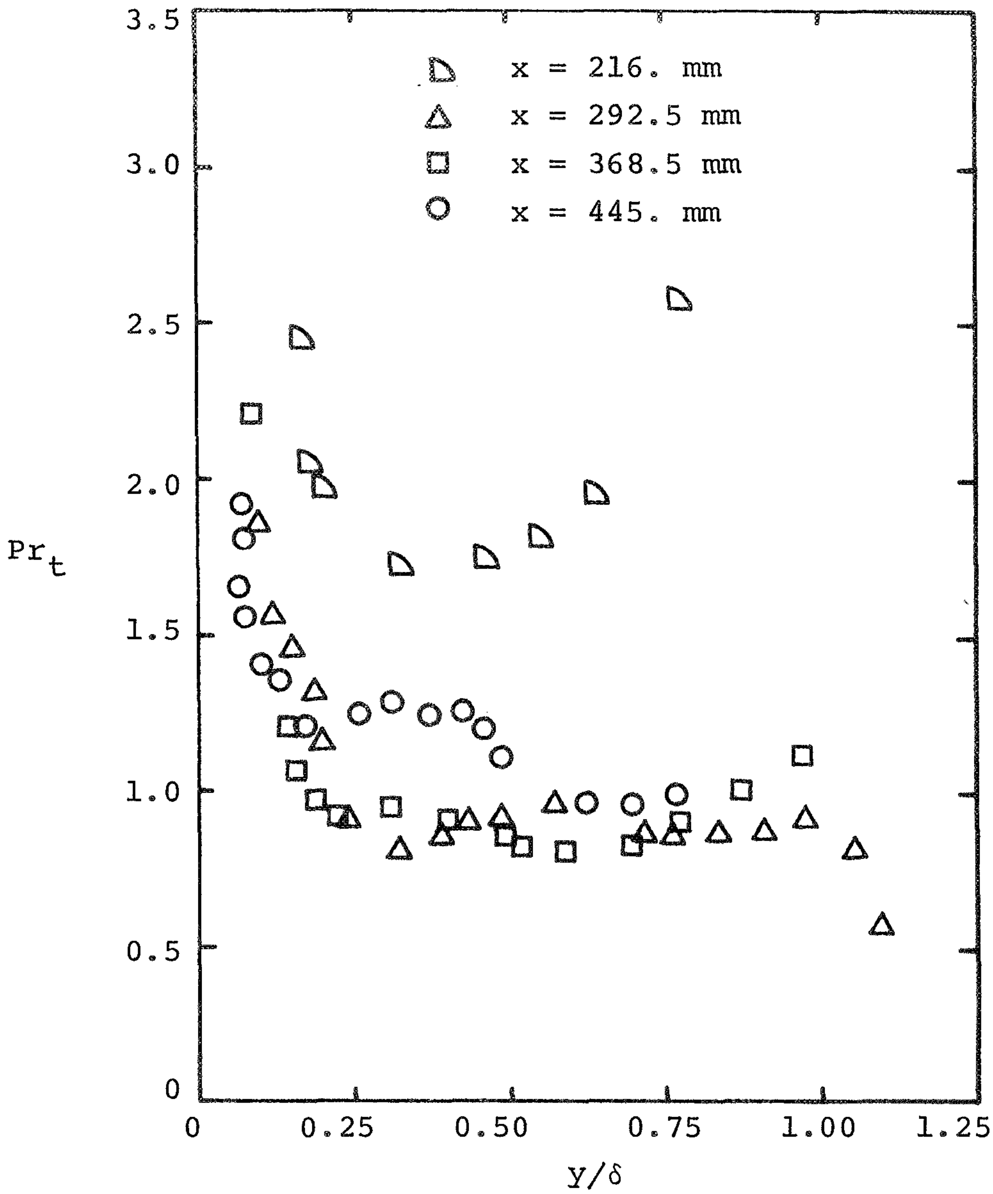

Figure 18: Experimental Measurements from Rotta [38] for the Turbulent Prandtl Number Across the Boundary Layer of a Cooled Flat Plate, $M_e = 5.1$

methods for turbulent boundary layers lies in the implicit and global manner in which the effects of turbulence can be incorporated. A disadvantage of integral methods often cited by users of differential methods is the difficulty of extension to wider classes of flows. The avoidance of local turbulence assumptions offsets this disadvantage in the view of many users of integral methods." The primary objections usually raised against finite-difference solutions are long calculation times and difficulty in obtaining mesh restrictions to assure stable solutions, but to the users of finite-difference methods, these disadvantages are offset by more exact solutions of the governing partial differential equations and by the extendability to a more general, wider, or more complicated class of flows.

In this report the Method of Weighted Residuals (hereinafter abbreviated as MWR)* is advocated as retaining many of the advantages of both the integral and finite-difference methods while eliminating many of their disadvantages. The MWR solution technique is presented in detail in Section 3.4 as related to the solution of the compressible, turbulent boundary-layer problem.

---

*The MWR is an N-parameter approximate solution technique for solving a set of partial differential equations, where N is the order of the approximation. For a detailed discussion of the basic MWR solution technique, see Bethel and Abbott [40] and Koob and Abbott [41].

For the past several years considerable differences of opinion have occurred in the literature in attempts to categorize the MWR as either an integral or finite-difference method; for example, Spalding [42] combines the MWR with finite-difference methods into a category he calls complete theories. However, Reynolds [39] calls the MWR an integral method while Abbott, Deiwert, Forsnes, and Deboy [43] point out many similarities between the MWR and finite-difference methods. Perhaps the MWR has sufficient unique characteristics that it is in a class of its own and consequently defies the usual methods of categorization.

Two complaints which have often been brought against the MWR are: (1) the MWR cannot be easily extended to calculate complex flow situations and (2) the MWR requires a multitude of matrix inversions which can ultimately lead to the inversion of a singular matrix, implying a hidden singularity in the mathematical formulation. However, in the past decade many successful applications of the MWR have made the validity of these complaints doubtful. The following list is a sample of the applications of the MWR over a wide range of flow conditions: Bethel and Abbott [40] calculated laminar flows with pressure gradient and predicted separation points; Ero [44] calculated the shock-induced, laminar, compressible flow over a flat plate; Koob and Abbott [41] calculated the laminar time dependent flow over a suddenly accelerated flat plate; Forsnes and Abbott [6] calculated the two-dimensional, incompressible, turbulent boundary layer with pressure gradient; Nielson, Goodwin, and Kuhn [45] calculated the laminar and turbulent shock-wave interaction problem in two-dimensional, axisymmetric flow; and Bossel [46] calculated incompressible, laminar boundary layers with suction. While the number of matrix inversions can create difficulties in a specific analysis, in the formulation of the MWR for the flow problems that have been examined by Professor D. E. Abbott and his students at Purdue University, it is necessary to perform only one matrix inversion for the entire calculation of a flow case; thus, this inversion is achieved, once and for all, at the start of the flow calculations, and no further matrix inversions are required as the calculations proceed downstream. It is theoretically possible that the matrix to be inverted could be singular for a specific problem formulation, but no such difficulty has been encountered in the work at Purdue University.

In the application to turbulent boundary layers for low orders of approximation, $N < 4$, the MWR has the advantage of the integral methods in that it can use global inputs, such as semi-empirical equations for the dissipation integral and other weighted integrals of the shear stress (for the turbulent information terms), but an eddy-viscosity formulation can also be used for all orders of approximations ($0 < N < \infty$). Thus, the MWR has the added flexibility of allowing the user to apply either global or local turbulent shear inputs. Still another advantage is short machine calculation times; for example, in the work of Forsnes and Abbott [6] and Deiwert and Abbott [47] it was found that a second approximation gave good results while requiring only about one-third of the computer time used by finite-difference methods. Nevertheless, the MWR has the advantage of being able to obtain a more exact solution of the governing equations for larger N; of course, the required computer time would increase considerably. With the selection of a solution technique having been made, the next step is the application of the MWR to the governing equations of Section 3.2.

3.4 Application of the MWR Solution Technique

Strictly for computational convenience the Dorodnitsyn transformation was modified to apply to the compressible form of the equations. The transformation as modified is given by:

Dependent variables:

$$u^* = \frac{u}{U_e} \qquad v^* = \frac{V}{U_e}\sqrt{\frac{U_r L}{\nu_r}} \qquad H^* = \frac{H}{H_e} \tag{3.20}$$

Property variables:

$$\rho^* = \rho/\rho_e \qquad \mu^* = \mu/\mu_e \tag{3.21}$$

Independent variables:

$$\xi = \frac{1}{L} \int_{o}^{x} \frac{\rho_e U_e}{\rho_r U_r} dx \qquad \eta = y \frac{\rho_e U_e}{\rho_r U_r L} \sqrt{\frac{U_r L}{\nu_r}} \tag{3.22}$$

Other variables, defined for convenience, are

$$w^* = v^* + u^* \frac{\eta (\rho_e U_e)_\xi}{\rho_e U_e} \tag{3.23}$$

$$\beta = 1 + \frac{\varepsilon}{\nu} \tag{3.24}$$

and

$$\rho V = \rho v + \overline{\rho' v'} \tag{3.25}$$

The transformation of equations (3.10), (3.11), and (3.12) yields

Continuity:

$$\frac{\partial}{\partial \xi} (\rho^* u^*) + \frac{\partial}{\partial \eta} (\rho^* w^*) = 0 \tag{3.26}$$

Momentum:

$$\rho^* u^* \frac{\partial u^*}{\partial \xi} + \rho^* w^* \frac{\partial u^*}{\partial \eta} = \frac{U_{e_\xi}}{U_e} (1 - \rho^* u^{*2}) + \frac{\mu_e}{\mu_r} \frac{\partial}{\partial \eta} \left(\mu^* \beta \frac{\partial u^*}{\partial \eta} \right) \tag{3.27}$$

Energy:

$$\rho^* u^* \frac{\partial H^*}{\partial \xi} + \rho^* w^* \frac{\partial H^*}{\partial \eta} = - \rho^* u^* H^* \frac{H_{e_\xi}}{H_e} + \frac{\partial}{\partial \eta} \left[\frac{\mu_e}{\mu_r} \frac{\mu^*}{Pr} \left(1 + \frac{\varepsilon}{\nu} \frac{Pr}{Pr_t} \right) \frac{\partial H^*}{\partial \eta} + \frac{\mu_e}{\mu_r} \mu^* \left(1 - \frac{1}{Pr} \right) \frac{U_e^2}{H_e} u^* \frac{\partial u^*}{\partial \eta} \right] \tag{3.28}$$

To solve the above equations an historically proven

MWR formulation is used for the momentum equation. For the treatment of the energy equation, the method developed by Ero [44] for shock-induced laminar flow over a flat plate was considered. Although this method generated a simplified system of equations solvable with short computer run-times for Ero's problem, it created a complicated formulation requiring long computer times for the present problem which involves pressure gradient and turbulence terms. Consequently, an entirely new treatment of the energy equation has been developed. This new treatment is quite analogous to that of the momentum equation and is therefore easily understood in concept and application once the handling of the momentum equation has been mastered. Thus, directly parallel analyses for the momentum and energy equations are developed below.

In following the historically proven formulation, the continuity equation (3.26) is multiplied by a weighting function $h_i(u^*)$, to be specified later, and the momentum equation (3.27) is multiplied by $\frac{dh_i}{du^*}$, and the resulting two equations are added, yielding

$$\frac{\partial}{\partial \xi}(h_i \rho^* u^*) + \frac{\partial}{\partial \eta}(h_i \rho^* w^*) = h_i'(u^*) \frac{U_{e_\xi}}{U_e}(1 - \rho^* u^{*2})$$

$$+ \frac{\mu_e}{\mu_r} \frac{\partial}{\partial \eta}\left[\mu^* \beta \frac{\partial u^*}{\partial \eta}\right] h_i'(u^*) \tag{3.29}$$

Similarly, the continuity equation (3.26) is multiplied by a weighting function $f_i(H^*)$, to be specified later, and the energy equation (3.28) is multiplied by $\frac{df_i}{dH^*}$, and the resulting equations are added, yielding

$$\frac{\partial}{\partial \xi}(\rho^* u^* f_i) + \frac{\partial}{\partial \eta}(\rho^* w^* f_i) = - f_i \rho^* u^* H^* \frac{H_{e_\xi}}{H_e}$$

$$+ f_i' \frac{\partial}{\partial \eta}\left[\frac{\mu_e}{\mu_r}\frac{\mu^*}{Pr}\left(1 + \frac{\varepsilon}{\nu}\frac{Pr}{Pr_t}\right)\frac{\partial H^*}{\partial \eta}\right.$$

$$\left. + \frac{\mu_e}{\mu_r}\mu^*\left(1 - \frac{1}{Pr}\right)\frac{U_e^2}{H_e} u^* \frac{\partial u^*}{\partial \eta}\right] \qquad (3.30)$$

Equation (3.29) is integrated over the domain of interest $(0,\infty)$ of the variable η, and the independent variables (ξ,η) are transformed to (ξ,u^*) so that in reality all integrations are taken over the interval (0,1) in u^*, thus eliminating the problem of integration over a semi-infinite interval. For details of this transformation, see Appendix C of Koob and Abbott [41]. For convenience a new variable is defined

$$\Theta = \left(\frac{\partial u^*}{\partial \eta}\right)^{-1} \qquad (3.31)$$

The integrated form of equation (3.29) becomes

$$\frac{d}{d\xi}\int_0^1 h_i \rho^* u^* \Theta du^* - \frac{U_{e_\xi}}{U_e}\int_0^1 h_i' (1 - \rho^* u^{*2}) \Theta du^*$$

$$+ \frac{\mu_e}{\mu_r}\frac{h_i'(0)\rho_w^* \mu_w^*}{\rho_w^* \Theta(\xi,0)} + \frac{\mu_e}{\mu_r}\int_0^1 \frac{\rho^* \mu^* \beta h_i'' du^*}{\rho^* \Theta} = 0 \qquad (3.32)$$

by requiring $h_i(1) = 0$.

Equation (3.30) is now handled in a very similar manner; it is integrated with respect to η, and the independent variables (ξ,η) are transformed to (ξ,H^*) so that in reality all integrations are taken over the finite interval $(H_w^*, 1)$ in the variable H^*. For convenience another new variable is defined

$$\chi = \left(\frac{\partial H^*}{\partial \eta}\right)^{-1} \tag{3.33}$$

and the final resulting equation is

$$\frac{d}{d\xi} \int_{H_w^*}^{1} \rho^* u^* f_i \chi dH^* = - \frac{H_{e_\xi}}{H_e} \int_{H_w^*}^{1} f_i' \rho^* u^* H^* \chi dH^*$$
$$- f_i'(H_w^*) \frac{\mu_e}{\mu_r} \frac{\mu_w^*}{Pr} \frac{1}{\chi_w} - \int_{H_w^*}^{1} \left[\frac{\mu_e}{\mu_r} \frac{\mu^*}{Pr} \left(1 + \frac{\varepsilon}{\nu} \frac{Pr}{Pr_t}\right) \frac{1}{\chi}\right.$$
$$\left. + \frac{\mu_e}{\mu_r} \mu^* \left(1 - \frac{1}{Pr}\right) \frac{U_e^2}{H_e} u^* \frac{1}{\Theta}\right] f_i'' \, dH^* \tag{3.34}$$

with the restriction that $f_i(1) = 0$. The resulting equations to be solved for Θ and χ are equations (3.32) and (3.34), which are integro-differential equations that have been integrated out of their u^* and H^* variations until only ordinary differential equations in ξ remain.

3.5 Approximating and Weighting Functions

Approximating functions for groupings of variables involving χ and Θ must be chosen. These groupings should be chosen to simplify algebraic manipulation as well as to reduce computer calculation time. In Reference 44, $\rho^*\Theta$ was found to be a computationally convenient group, and it is seen to naturally arise many times in equation (3.32), while in the present work $\rho^* u^* \chi$ was discovered to be another computationally convenient group. In selecting the form of the approximating functions, the perturbation procedure developed in Koob and Abbott [41] was followed where the initial distribution of a group in one variable is perturbed by a polynomial in the same variable which has coefficients that are a function of the other variable, for example

$$\rho^*\Theta\ (u^*,\xi) = C_j(\xi)\phi_j(u^*) \tag{3.35}$$

where $$\phi_j(u^*) = P_{j-1}(2u^* - 1)\ \frac{F(u^*)}{1-u^*} \tag{3.36}$$

$$\rho^* u^*\chi\ (H^*,\xi) = D_j(\xi)\omega_j(H^*) \tag{3.37}$$

where $$\omega_j(H^*) = P_{j-1}(2H^* - 1)\ \frac{G(H^*)}{1-H^*} \tag{3.38}$$

$$\frac{F(u^*)}{1-u^*} = \rho^*\Theta(u^*,\xi_o) \tag{3.39}$$

and

$$\frac{G(H^*)}{1-u^*} = \rho^* u^*\chi(H^*,\xi_o) \tag{3.40}$$

$P_{j-1}(2u^*-1)$ is the Legendre polynomial of (j-1) order with argument $(2u^*-1)$. Repeated subscripts imply summation from $j=1$ to N, where N is the order of the approximation.

The prime considerations in selecting the form of the weighting functions are that the weighting functions should be an orderly successive subset of a complete set of functions to obtain solutions that converge most rapidly for successive approximations (see Bethel and Abbott [40]) and that the weighting functions should simplify the evaluation of the integrals in equations (3.32) and (3.34) as much as possible. The weighting functions chosen for this work are

$$h_i(u^*) = (1-u^*)\ P_{i-1}\ (2u^*-1) \tag{3.41}$$

$$f_i(H^*) = (1-H^*)\ P_{i-1}\ (2H^*-1) \tag{3.42}$$

The form of the weighting function $h_i(u^*)$ was selected because it has proven to work well in the incompressible work of Deiwert and Abbott [47], and its computational advantages carry over to the compressible regime. No precedent has been set for the selection of $f_i(H^*)$; due to the analogous manner in which the momentum and energy equations were treated, the selection of $f_i(H^*)$ was taken to have the same functional form as $h_i(u^*)$. This achieved the same computational advantages for the energy equation treatment as were obtained for the momentum equation*.

Upon substitution of equations (3.35) and (3.37) into equations (3.32) and (3.34) one obtains

*Credit should be extended here to the work of J. D. Murphy at NASA-Ames Research Center for the development of the Legendre polynomial formulation in the weighting and approximating functions and for the discovery that this formulation generates matrices whose terms are of the same order of magnitude; consequently, round-off errors are reduced in the ordinary differential equation solution and the matrix inversion process.

$$\frac{dC_j}{d\xi}\int_o^1 h_i u^*\phi_j \, du^* - \frac{U_{e_\xi}}{U_e} C_j \int_o^1 h_i' \frac{(1-\rho^* u^{*2})}{\rho^*} \phi_j du^*$$

$$+ \frac{\mu_e}{\mu_r} \frac{h_i'(0)\rho_w^*\mu_w^*}{C_j \ \phi_j(0)} + \frac{\mu_e}{\mu_r}\int_o^1 \frac{\rho^*\mu^*\beta h_i''}{\rho^*\Theta} du^* = 0 \qquad (3.43)$$

and

$$\frac{dD_j}{d\xi}\int_{H_w^*}^1 f_i\omega_j dH^* = -\frac{H_{e_\xi}}{H_e} D_j \int_{H_w^*}^1 f_i' \ H^*\omega_j dH^*$$

$$- f_i'(H_w^*) \frac{\mu_e}{\mu_r}\frac{\mu_w^*}{Pr}\frac{1}{\chi_w} - \int_{H_w^*}^1 \left[\frac{\mu_e}{\mu_r}\frac{\mu^*}{Pr}\left(1 + \frac{\varepsilon}{\nu}\frac{Pr}{Pr_t}\right)\frac{\rho^* u^*}{D_j\omega_j}\right.$$

$$\left. + \frac{\mu_e}{\mu_r}\mu^*\left(1 - \frac{1}{Pr}\right)\frac{U_e^2}{H_e}\frac{u^*\rho^*}{C_j\phi_j}\right] f_i'' \quad dH^* \qquad (3.44)$$

To simplify the notation in equations (3.43) and (3.44), some matrices will be defined as follows:

$$A_{ij} = \int_o^1 h_i u^*\phi_j du^* \qquad (3.45)$$

$$I_{ij} = \int_o^1 h_i' \frac{(1-\rho^* u^{*2})}{\rho^*} \phi_j du^* \qquad (3.46)$$

$$B_i = \frac{\mu_e}{\mu_r}\frac{h_i'(0)\rho_w^*\mu_w^*}{C_j \ \phi_j(0)} \qquad (3.47)$$

$$g_i = \int_o^1 \frac{\rho^*\mu^*\beta h_i''}{\rho^*\Theta} du^* \qquad (3.48)$$

$$J_{ij} = \int_{H_w^*}^1 f_i\omega_j dH^* \qquad (3.49)$$

$$K_{ij} = \int_{H_w^*}^1 f_i' H^*\omega_j dH^* \qquad (3.50)$$

$$L_i = f_i'(H_w^*) \frac{\mu_e}{\mu_r} \frac{\mu_w^*}{Pr} \frac{1}{\chi_w} \tag{3.51}$$

$$M_i = \int_{H_w^*}^{1} \left[\frac{\mu_e}{\mu_r} \frac{\mu^*}{Pr} \left(1 + \frac{\varepsilon}{\nu} \frac{Pr}{Pr_t}\right) \frac{\rho^* u^*}{D_j \omega_j} + \frac{\mu_e}{\mu_r} \mu^* \left(1 - \frac{1}{Pr}\right) \frac{U_e^2}{H_e} \frac{u^* \rho^*}{C_j \phi_j} \right] f_i'' dH^* \tag{3.52}$$

Using the above definitions, equations (3.43) and (3.44) in matrix notation become

$$A_{ij} \frac{dC_j}{d\xi} - \frac{U_{e_\xi}}{U_e} I_{ij} C_j + B_i + \frac{\mu_e}{\mu_r} g_i = 0 \tag{3.53}$$

and

$$J_{ij} \frac{dD_j}{d\xi} = - \frac{H_{e_\xi}}{H_e} K_{ij} D_j - L_i - M_i \tag{3.54}$$

Multiplication of equation (3.53) by the inverse matrix of A_{ij} and equation (3.54) by the inverse of J_{ij} yields

$$\frac{dC_k}{d\xi} = \frac{U_{e_\xi}}{U_e} A_{ki}^{-1} I_{ij} C_j - A_{ki}^{-1} B_i - \frac{\mu_e}{\mu_r} A_{ki}^{-1} g_i \tag{3.55}$$

and

$$\frac{dD_k}{d\xi} = - \frac{H_{e_\xi}}{H_e} J_{ki}^{-1} K_{ij} D_j - J_{ki}^{-1} L_i - J_{ki}^{-1} M_i \tag{3.56}$$

It should be noted here that A_{ij} and J_{ij} are constant matrices for a given flow case and consequently only have to be inverted once for any particular flow calculation as was previously mentioned. Further examination reveals that K_{ij} is also a constant matrix while I_{ij}, B_i, g_i, L_i and M_i are variable matrices and must be evaluated at each

ξ-location. Equations (3.55) and (3.56) are the nonlinear ordinary differential equations to be solved for C_k and D_k which completely specify the desired solution variables as shown in Section 3.7.

3.6 Initial Conditions

Initial conditions must be obtained for the C_k and D_k coefficients before the solution of equations (3.55) and (3.56) can be found. These initial conditions can be obtained quickly and simply by combining equations (3.35), (3.36), and (3.39) into

$$\rho^*\Theta(u^*,\xi) = C_j(\xi)P_{j-1}(2u^*-1)\rho^*\Theta(u^*,\xi_o) \tag{3.57}$$

Evaluation of equation (3.57) at ξ_o yields

$$1 = C_j(\xi_o)P_{j-1}(2u^*-1) \tag{3.58}$$

Recalling that $P_o(2u^*-1) = 1$ and that $P_{j-1}(2u^*-1)$ is a linearly independent set of functions, it is seen that

$$C_1(\xi_o) = 1 \tag{3.59}$$

and

$$C_j(\xi_o) = 0 \quad \text{for} \quad j \neq 1 \tag{3.60}$$

In the same manner it is noted that

$$\rho^*u^*\chi(H^*,\xi) = D_j(\xi)P_{j-1}(2H^*-1)\rho^*u^*\chi(H^*,\xi_o) \tag{3.61}$$

and

$$1 = D_j(\xi_o)P_{j-1}(2H^*-1) \tag{3.62}$$

thus

$$D_1(\xi_o) = 1 \tag{3.63}$$

and

$$D_j(\xi_o) = 0 \quad \text{for} \quad j \neq 1 \tag{3.64}$$

Quite simply the coefficients have been specified at the initial location ξ_o without any dependence on the physical initial conditions (velocity and temperature profile), since the initial velocity and temperature profiles are the basis for the approximating functions.

3.7 Calculation of the Desired Solution Variables from the Coefficients $C_k(\xi)$ and $D_k(\xi)$

Some of the desired outputs of a boundary-layer prediction technique are skin-friction coefficient C_f, displacement thickness δ^*, momentum thickness θ, velocity profile $u(y)$, temperature profile $T(y)$, heat transfer at the wall q_w, and various other thickness and shape parameters. The derivation of these desired outputs is shown below. First, from the solutions of equations (3.55) and (3.56) the $C_k(\xi)$ and $D_k(\xi)$ coefficients are known; thus, from equations (3.35) and (3.37), $\rho^*\theta(u^*,\xi)$ and $\rho^*u^*\chi(H^*,\xi)$ are known. Using the identity

$$\frac{\Theta}{u^*\chi} = \frac{\rho^*\Theta(u^*,\xi)}{\rho^*u^*\chi(H^*,\xi)} \tag{3.65}$$

and after some algebraic manipulation and integration over η, equation (3.66) is obtained.

$$\int_0^\eta \rho^* u^* \chi(H^*,\xi)\ \frac{\partial H^*}{\partial \eta}\ d\eta = \int_0^\eta u^* \rho^* \Theta(u^*,\xi)\ \frac{\partial u^*}{\partial \eta}\ d\eta \tag{3.66}$$

Upon change of the variable of integration, equation (3.66) becomes

$$\int_{H_w^*}^{H^*} \rho^* u^* \chi(H^*,\xi)\ dH^* = \int_0^{u^*} \rho^* \Theta(u^*,\xi)\ u^* du^* \tag{3.67}$$

which yields $H^*(u^*)$ at a specified value of ξ. From this $H^*(u^*)$ function, $\rho^*(u^*)$ is immediately obtained by use of the definition

$$H^* = (C_p T + u^2/2)/H_e \tag{3.68}$$

and the perfect gas law

$$\rho^* = \frac{\rho_e p_e}{RT} \tag{3.69}$$

Now using the identity

$$\Theta = \frac{\rho^* \Theta(u^*,\xi)}{\rho^*(u^*)} \tag{3.70}$$

with some algebraic manipulation and integration, one obtains

$$\eta = \int_0^{u^*} \frac{\rho^* \Theta(u^*,\xi)}{\rho^*(u^*)}\ du^* \tag{3.71}$$

which gives the velocity profile at a given ξ location in the form of $\eta(u^*)$ instead of the usual form $u^*(\eta)$. The total-enthalpy profile is obtained by incorporating the $\eta(u^*)$ function of equation (3.71) into the $H^*(u^*)$ function given by equation (3.67). Using

$$C_f = \frac{\tau_w}{\frac{1}{2}\rho_e U_e^2} \tag{3.72}$$

$$\tau_w = \mu_w \left.\frac{\partial u}{\partial y}\right|_w \tag{3.73}$$

$$\Theta = \left(\frac{\partial u^*}{\partial \eta}\right)^{-1} \tag{3.31}$$

and the approximation function for Θ, equation (3.35), one obtains

$$C_f = \frac{2\mu_w \rho_w^*}{\rho_r U_r L} \quad \frac{\sqrt{Re_r}}{(-1)^{j-1} C_j F(0)} \tag{3.74}$$

From the definitions of displacement thickness and momentum thickness,

$$\delta^* = \int_o^{\delta} (1 - \rho^* u^*)\ dy \tag{3.75}$$

and

$$\theta = \int_o^{\delta} \rho^* u^* (1-u^*)\ dy \tag{3.76}$$

one obtains

$$\delta^* = \frac{L}{\sqrt{Re_r}} \int_o^1 (1 - \rho^* u^*)\Theta du^* \tag{3.77}$$

and

$$\theta = \frac{L}{\sqrt{Re_r}} \int_o^1 u^*(1-u^*)\ \rho^*\Theta du^* \tag{3.78}$$

For the heat transfer at the wall

$$q_w = -\ k \left.\frac{\partial T}{\partial y}\right|_w \tag{3.79}$$

one obtains

$$q_w = -\ k\ \frac{\rho_e U_e}{\rho_r U_r L}\ \frac{\sqrt{Re_r}\ H_e}{C_p \chi(H_w^*, \xi)} \tag{3.80}$$

Further derivations for shape parameters and higher order thickness parameters can be performed easily.

3.8 Analysis of Experimental Data

In the search for sets of experimental data on supersonic, compressible, turbulent boundary layers with which to compare theoretical calculations, the task is more in the line of discovery than selection. Add the further restriction of moderate Mach numbers, say $M_e < 6$, which is required for the validity of the governing equations and the eddy-viscosity model used in this investigation, and the available experimental data shrinks to a few isolated data sets for flat-plate type flows — flow over a flat-plate model, flow along hollow cylinders, and flow on wind tunnel walls — and only a handful of data for pressure-gradient flows. Johnson and Bushnell [48] have made a rather exhaustive tabulation of experimental data for the flat-plate type flows while a couple of the pressure-gradient data cases for moderate Mach numbers are available in the reports by Pasiuk, Hastings, and Chatham [49] and by Winter, Smith, and Rotta [50].

An additional complication arises in comparing calculated results with experimental data in that the majority of the experimental data is for the adiabatic flat-plate case and as reported by any given author was taken by holding the streamwise measuring station and the free-stream Mach number fixed while the Re_x parameter was varied by changing the pressure level, and consequently the free-stream density, in the wind tunnel. The measurements were made in this manner due to the complications arising from the reflection of shock waves inside the wind tunnel. Consequently, when such data is presented as a plot of C_f versus Re_x at a constant value of M_e, it represents the variation of C_f with a change in pressure level instead of with a change in x - the normal case for incompressible data. Since prediction schemes are designed to calculate the development of a boundary layer with increasing x, some method must be devised to compare the calculated results with this type of experiment.

Cebeci, Smith, and Mosinskis [1] devised a method which consists of starting their calculations at the leading edge of the adiabatic flat plate where the flow is assumed to be laminar and then arbitrarily specifying the flow to be turbulent at the next x-station which is arbitrarily assumed to be at x = 0.001 ft. The calculations are then carried out downstream until the calculated value of Re_θ reaches the experimental value, and at that point the calculated boundary-layer parameters are compared with the experimental measurements. Despite their rather harsh assumptions that the laminar region is 0.001 ft. long for all flow cases and that there is no transition region, their calculations of boundary-layer parameters agree very well with experiment. Herring and Mellor [8] have devised a scheme whereby they carry out calculations by assuming U_e

and δ^* to be linear in x and the ($\rho^* u^*$) and H profiles to be independent of x; after performing calculations in this manner up to within two or three x-steps of the point where the experimental data is given, they relax their above assumptions and continue the calculations through the final two or three x-steps up to the data point and at that x-location compare their calculations with the experimental data for the boundary-layer parameters and profiles. Herring and Mellor's method of comparing their calculations with experimental data that has been obtained at one x-location can thus be characterized as an elaborate initialization procedure; indeed, they use an iteration on this procedure to get the initial conditions for their calculations when they are computing a flow which has been measured at various x-locations.

There is another possible approach by which calculations can be compared with the experimental data measured at one x-location, and this approach is a better indication of the ability of a calculation technique to predict the behavior of a turbulent, compressible boundary layer. This method will be explained after a brief introduction of some experimentally observed trends which underlie the basis for this new approach. The chief experimental observation noted by Matting et al. [30] is the one shown by Figure 19 which is a comparison of faired curves through experimental data for adiabatic flat plates. All of the data for $M_e \geq 2.54$ was obtained by holding the streamwise measuring station and the

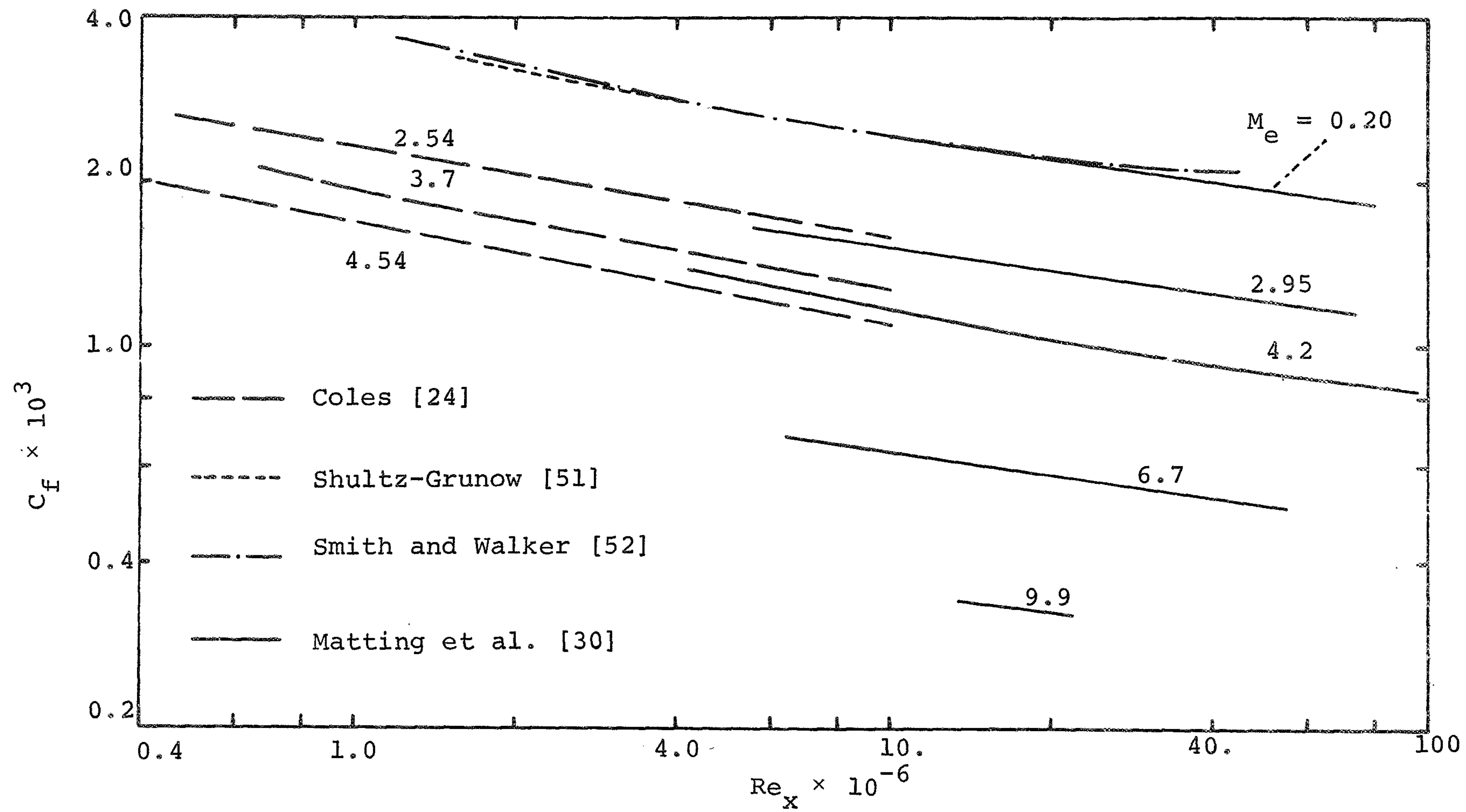

Figure 19: Comparison of Direct Force Measurements of Turbulent Skin Friction

free-stream Mach number fixed while Re_x was varied by changing the pressure level in the wind tunnel. In Figure 19, x is the distance between the transition point and the location of the measuring station; the transition point is assumed to be the point of maximum C_f. The parameter x was used because, to obtain some type of universal relationship involving Reynolds number, it is necessary to obtain a virtual origin for the turbulent boundary layer so that the length parameter in the Reynolds number is independent of the length of the laminar region. Figure 19 implies that the resulting C_f - Re_x relationship is a universal one, and this fact can now be used in comparing analytical and empirical results. The calculations are started for a given data Mach number by generating initial conditions at the lowest experimental value of Re_x, then the calculations are continued downstream and the calculated values of C_f are compared with the empirical values at the experimental points where Re_x is known.

Further examination of the experimental data shows that there is no possibility for a direct comparison between the measured and predicted values of the boundary-layer thickness parameters (δ, δ^*, and θ); the measured values of the thickness parameters generally decrease with increasing Re_x, while the predicted values increase. The reason for the discrepancy between the predicted and experimental results is easily understood if we revert to the incompressible turbulent boundary-layer case where a simple analytical computation can be performed. The one-seventh power velocity law and the momentum integral equation combine to give an ordinary differential equation for δ which upon integration yields

$$\frac{\delta(x)}{x} = 0.37 \left(\frac{U_e x}{\nu}\right)^{-1/5} \tag{3.81}$$

for the boundary-layer thickness on a flat plate. This result shows that if Re_x is caused to increase by increasing x, then δ also increases, as is the case for the predicted results; but if Re_x is made to increase by increasing the value of U_e/ν, then δ decreases, as in the case of the experimental data. While this analysis is not directly applicable to compressible flow, it suggests a possible rationale for the aforementioned discrepancy which is consistant with evidence for compressible flow.

Although it is not possible to directly compare the boundary-layer thickness parameters, the velocity profiles (in the form of u/U_e versus y/θ) and the Mach-number profiles (in the form of M/M_e versus y/θ) may be compared, since these profiles form nearly universal functions (see Schlichting [33]*). These functions are not exactly universal in that all data points do not fall on exactly the same curve; in particular, there is considerable deviation near the wall; however, such a deviation might also be caused by probe

*Schlichting's argument is based upon the velocity profile. The universality of the Mach-number function is then directly implied by the universality of the Crocco relationship for T(u) which is valid for the adiabatic, flat-plate flow case.

interference close to the wall. In any event, for lack of a more reliable comparison, the u/U_e versus y/θ and M/M_e versus y/θ profiles are utilized in this work for a comparison between theory and experiment. The measured value of θ is used in the experimental profiles and the calculated value of θ is used in the predicted profiles. It will be shown in Section 4 that the present MWR calculations agree not only with the experimental data but also with the finite-difference calculations of Cebeci, Smith and Mosinskis [1].

3.9 Summary

In Section 3 the mathematical modeling of the physical problem — compressible, turbulent boundary layers — is presented, and solution techniques for the governing equations are discussed. The selection of the MWR solution procedure is discussed, and the details of its application to the governing equations are presented. Upon the introduction of a shear model into the resulting equations, the prediction analysis for compressible, turbulent boundary layers is completed. A search for experimental results to compare with the analytical predictions is undertaken, and the available data is found to be taken in a manner different than that assumed in developing the prediction program. Two procedures, developed by other investigators for comparing the data with predictions, are examined while a somewhat different procedure is developed and suggested as a proper indication of the ability of a prediction scheme.

4. COMPARISON OF CALCULATED AND EXPERIMENTAL RESULTS

4.1 The Numerical Solution Procedure

The appropriate MWR equations governing the flow over an adiabatic flat plate have been programmed for a CDC 6500 computer. The Crocco equation relating temperature to velocity has been used instead of the complete energy equation, since, as explained in Section 2.5*, the Crocco equation is quite adequate for the adiabatic flat-plate case. A numerical solution was obtained for equations (3.55), which are a system of N first-order ordinary differential equations where N is the order of the desired approximation. Equations (2.23) to (2.26) were used for the property variations while several different turbulent shear models were employed to evaluate the turbulent shear terms in the governing equations. This MWR formulation was used to predict the flows over adiabatic flat plates at four different free-stream Mach numbers. Skin friction variation, velocity profiles and Mach-number profiles were computed and compared with experimentally measured values. In programming the solution for the MWR equations, two methods were used to solve the first-order system of

*This adequacy is further substantiated by the fact that Herring and Mellor [8] calculated adiabatic flat-plate flow cases two ways, once using the Crocco relation, and once using the complete energy equation. The results were identical within the accuracy of their graphs.

ordinary differential equations, equations (3.55); they are Hamming's modified predictor-corrector method and the fourth-order Runge-Kutta method (see Ralston and Wilf [53] for details of these methods). Both methods worked quite well; however, Hamming's method was slightly faster; and, therefore, it was used in obtaining the results presented in this paper. The resultant computer program used to solve the system of equations is presented in Appendix B. The calculation time on a CDC 6500 computer for an entire flow case was generally about 20, 150, and 350 seconds for the first, second, and third approximations respectively. The time for a second approximation was the same order as the time required by the CSM [1] finite-difference methods. Usually the MWR takes considerably less calculation time than does a finite-difference method; however, in the present work the calculation times of the two techniques were comparable because an eddy-viscosity model was used which required calculation of velocity and eddy-viscosity profiles at every ξ-location and because the sensitivity of the eddy-viscosity model necessitated a very small $\Delta\xi$ step size (as will be explained in Section 4.4). Nevertheless, a potential reduction of the MWR calculation time by an order of magnitude is indicated in Section 4.4

4.2 The MWR Results Using the CSM Eddy-Viscosity Model

The results of this section are obtained using the CSM eddy-viscosity model in the third approximation formulation of the MWR*. To obtain starting velocity and shear-stress distributions, the iteration procedure described in Section 2.4 and Section 2.5 is used. However, no smoothing or iteration (of any variable) is employed downstream.

The first comparison is for the flow over an adiabatic flat plate with the following values of the parameters:

$$M_e = 2.54$$

$$U_e = 1931 \text{ ft/sec}$$

$$T_w = 519.3°R$$

$$L = 8.194 \text{ ft}$$

The MWR predicted results are compared with the experimental measurements of Coles [24] and with some analytical results of Cebeci, Smith, and Mosinskis [1]. The starting velocity and shear-stress profiles, obtained by the iterative procedure of Section 2.4 and Section 2.5, are given in Figures 20 to 23. Figure 20 displays the shear-stress and

*Solutions from the first, second and third approximations are displayed in Appendix C where the convergence properties of the MWR are discussed.

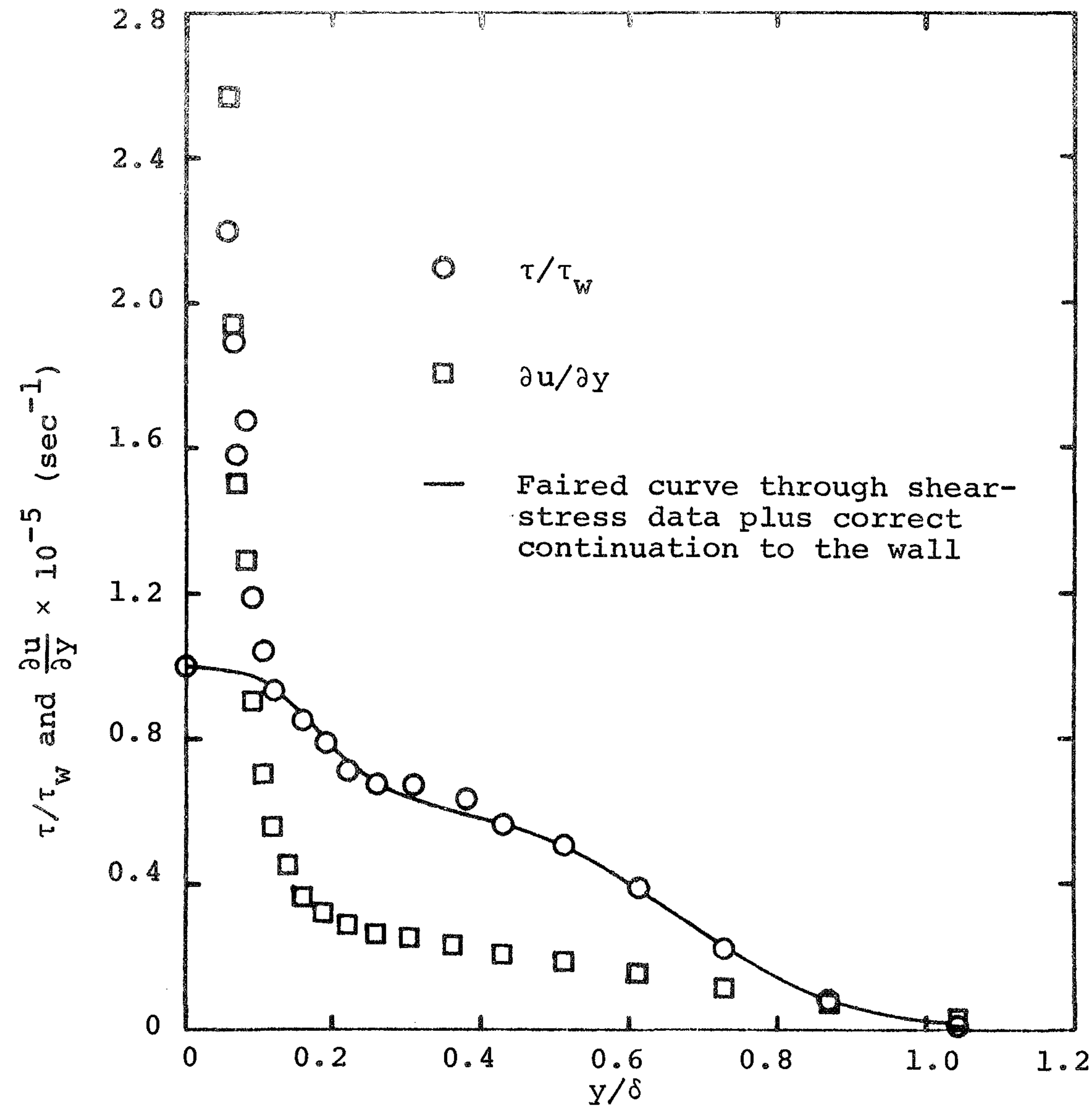

Figure 20: Calculations of Velocity Derivative and Shear Stress by the CSM Eddy-Viscosity Model Without Iteration for the Experimental Data of Coles [24], $M_e = 2.54$, $Re_x = 0.63 \times 10^6$

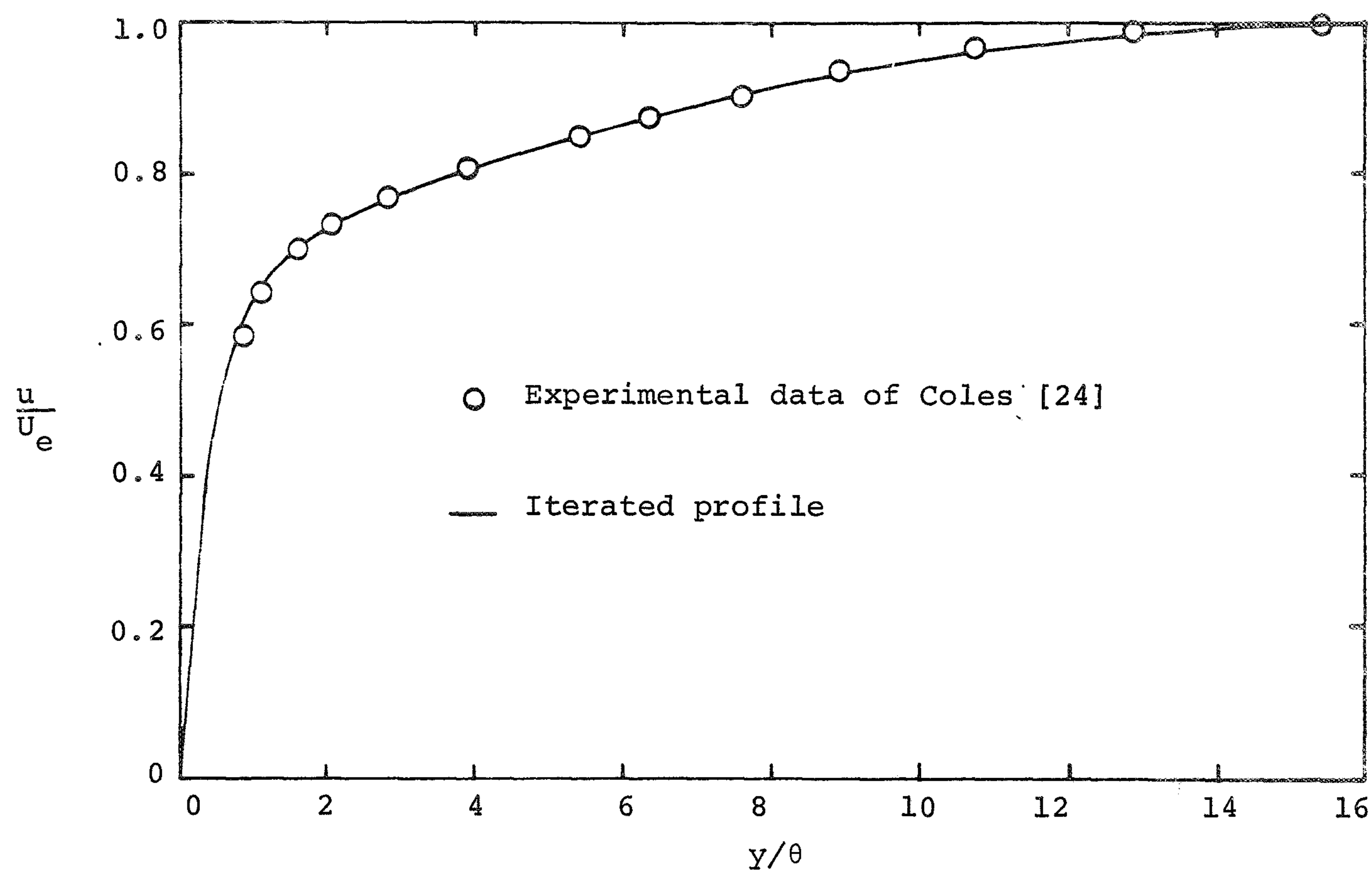

Figure 21: Comparison of the Iterated Starting Profile with Experimental Data, $M_e = 2.54$, $Re_x = 0.63 \times 10^6$

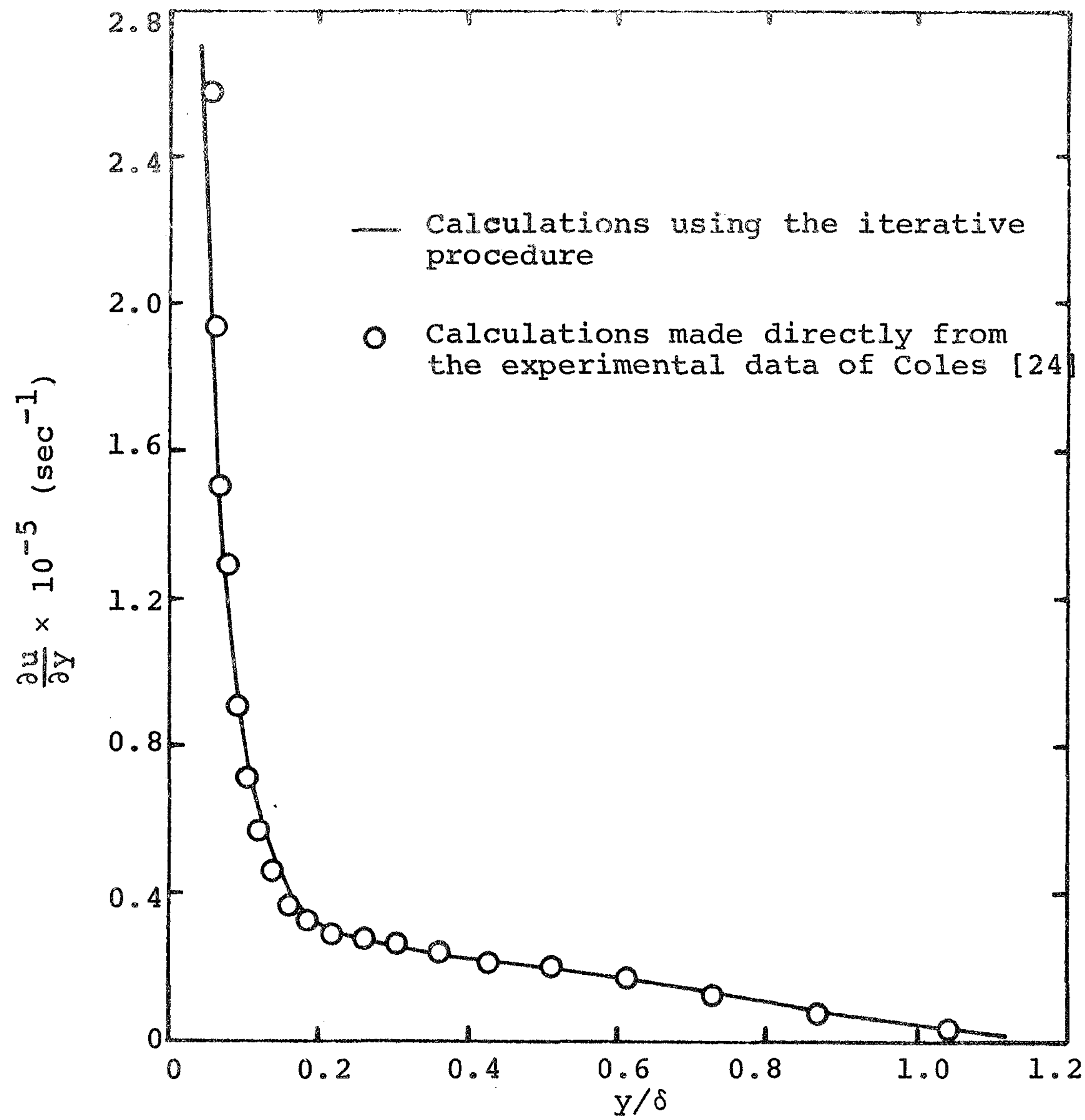

Figure 22: Comparison of the Velocity-Derivative Profile Calculated with and without Iteration, $M_e = 2.54$, $Re_x = 0.63 \times 10^6$

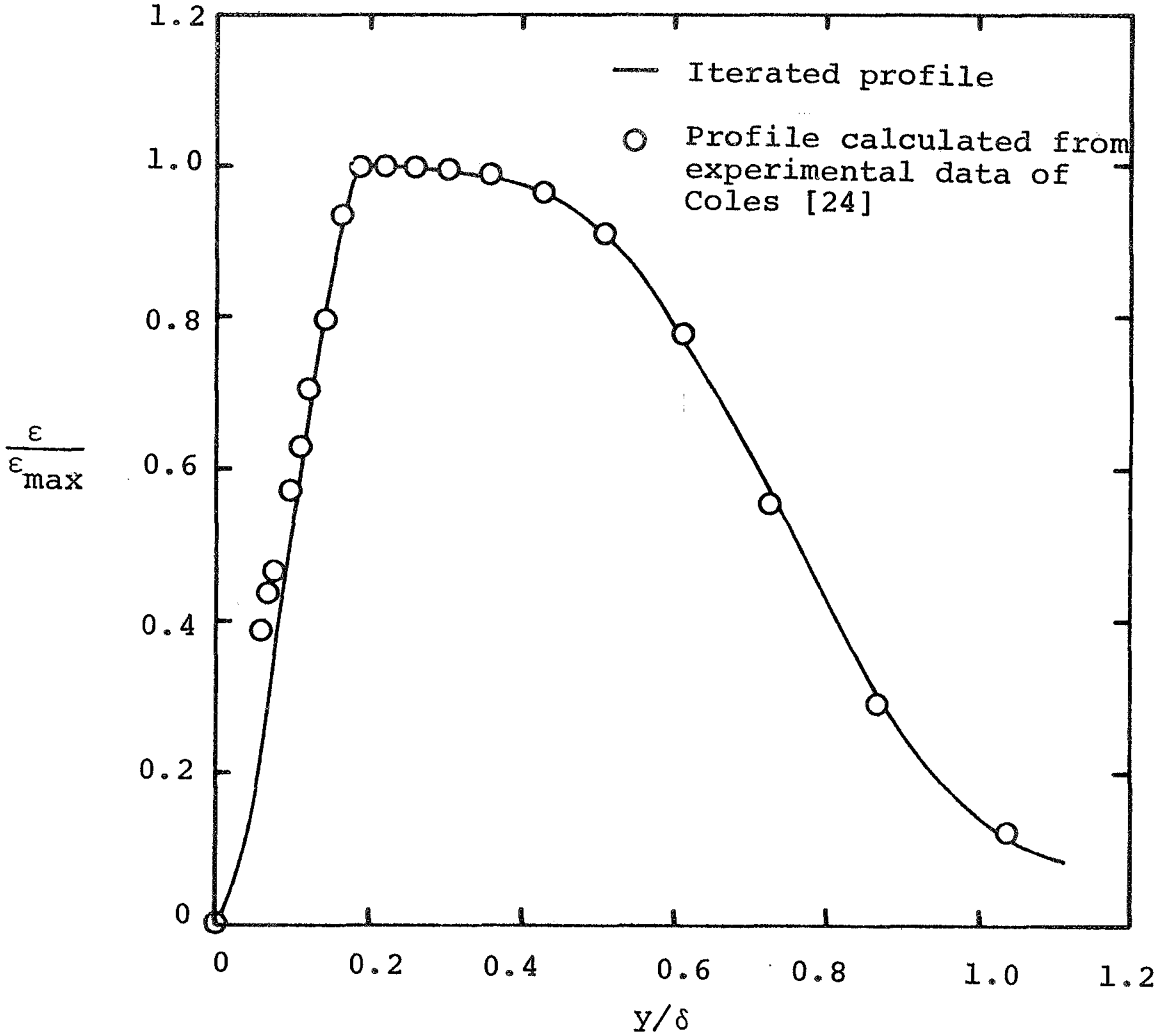

Figure 23: Comparison of the Eddy-Viscosity Profile with and without Iteration, $M_e = 2.54$, $Re_x = 0.63 \times 10^6$

velocity-derivative distributions which were calculated from the experimental data by the procedure of Section 2.4. Figure 21 shows the velocity profile after iteration compared with the experimental profile. Figure 22 compares the velocity-derivative profiles before and after iteration while the eddy-viscosity profiles before and after iteration are shown in Figure 23. The profiles after iteration are the input, starting profiles for the MWR solution technique. Figure 24 displays the MWR skin-friction variation, the experimental values, and one result of the CSM calculations. The one CSM calculated value is in error 3.31 percent. (For the purpose of calculating errors the experimental values are assumed to be correct.) The maximum error in the MWR solution is 3.5 percent at $Re_x = 4.21 \times 10^6$. Figures 25 and 26 present the velocity and Mach-number profiles at the initial x-station and two downstream stations. The MWR calculated profiles agree fairly well with the experimental data while the CSM profiles at $Re_x = 4.21 \times 10^6$ are slightly better than the MWR calculations.

A second case was considered for an adiabatic flat plate with

$$M_e = 2.95$$

$$U_e = 2140 \text{ ft/sec}$$

$$T_w = 551°R$$

$$L = 13.5 \text{ ft}$$

The predicted results were then compared with the experimental

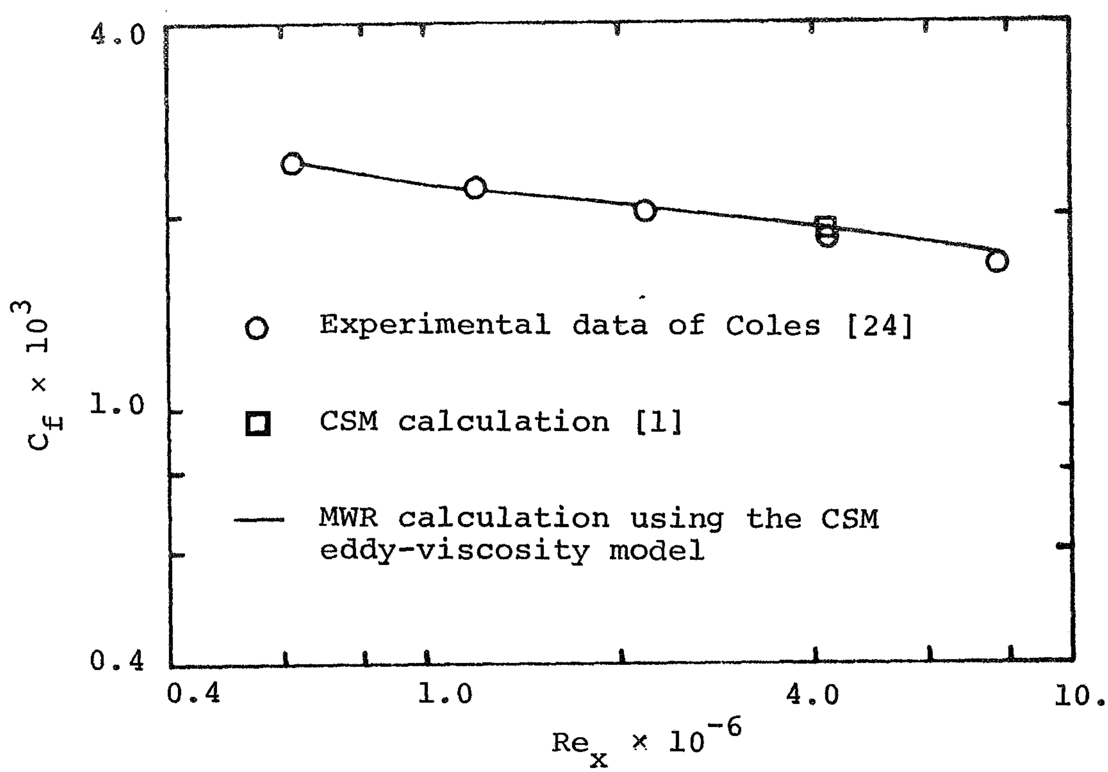

Figure 24: Comparison of Skin-Friction Calculations with Experiment, $M_e = 2.54$

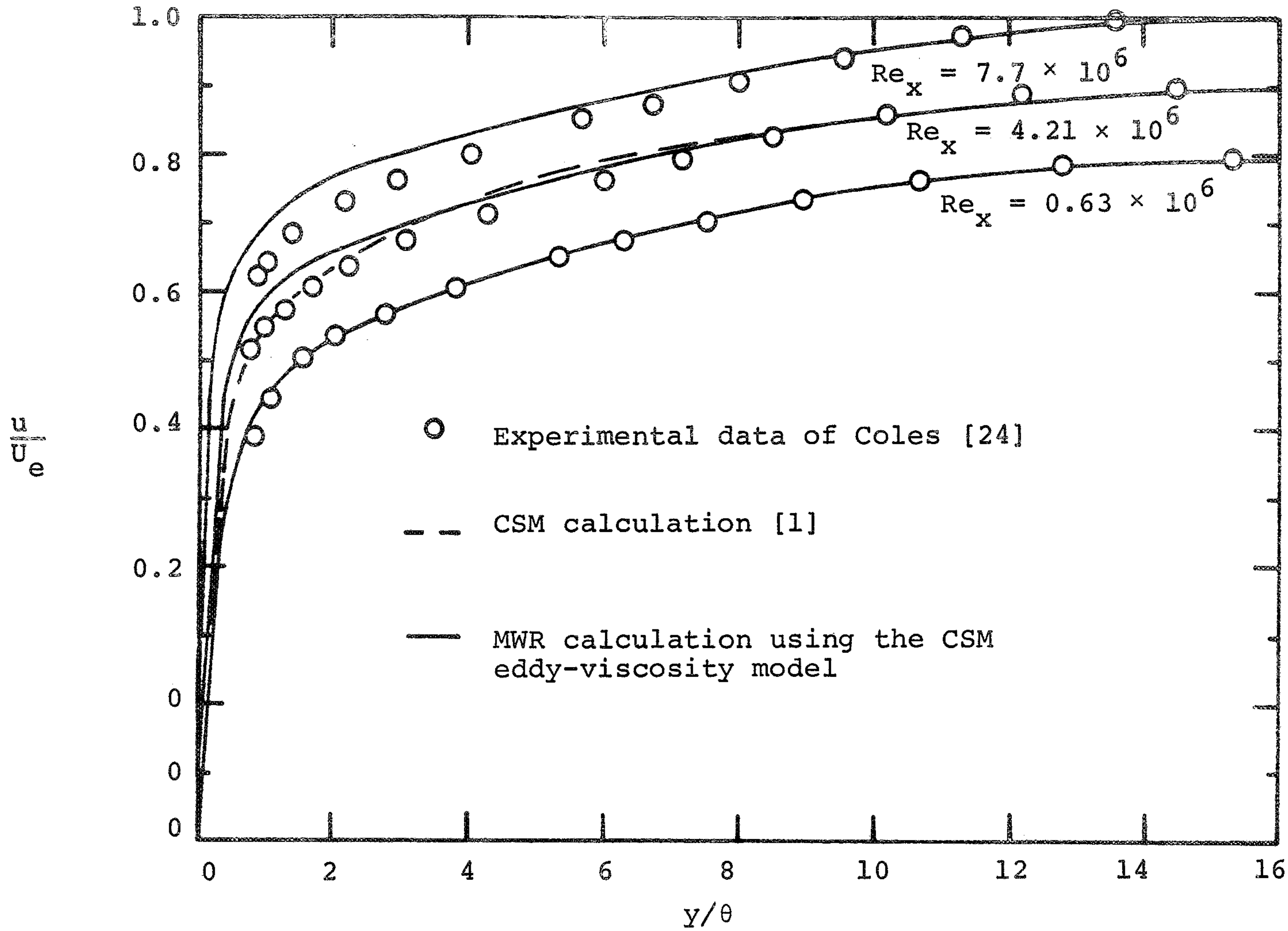

Figure 25: Comparison of Velocity-Profile Calculations with Experiment, $M_e = 2.54$

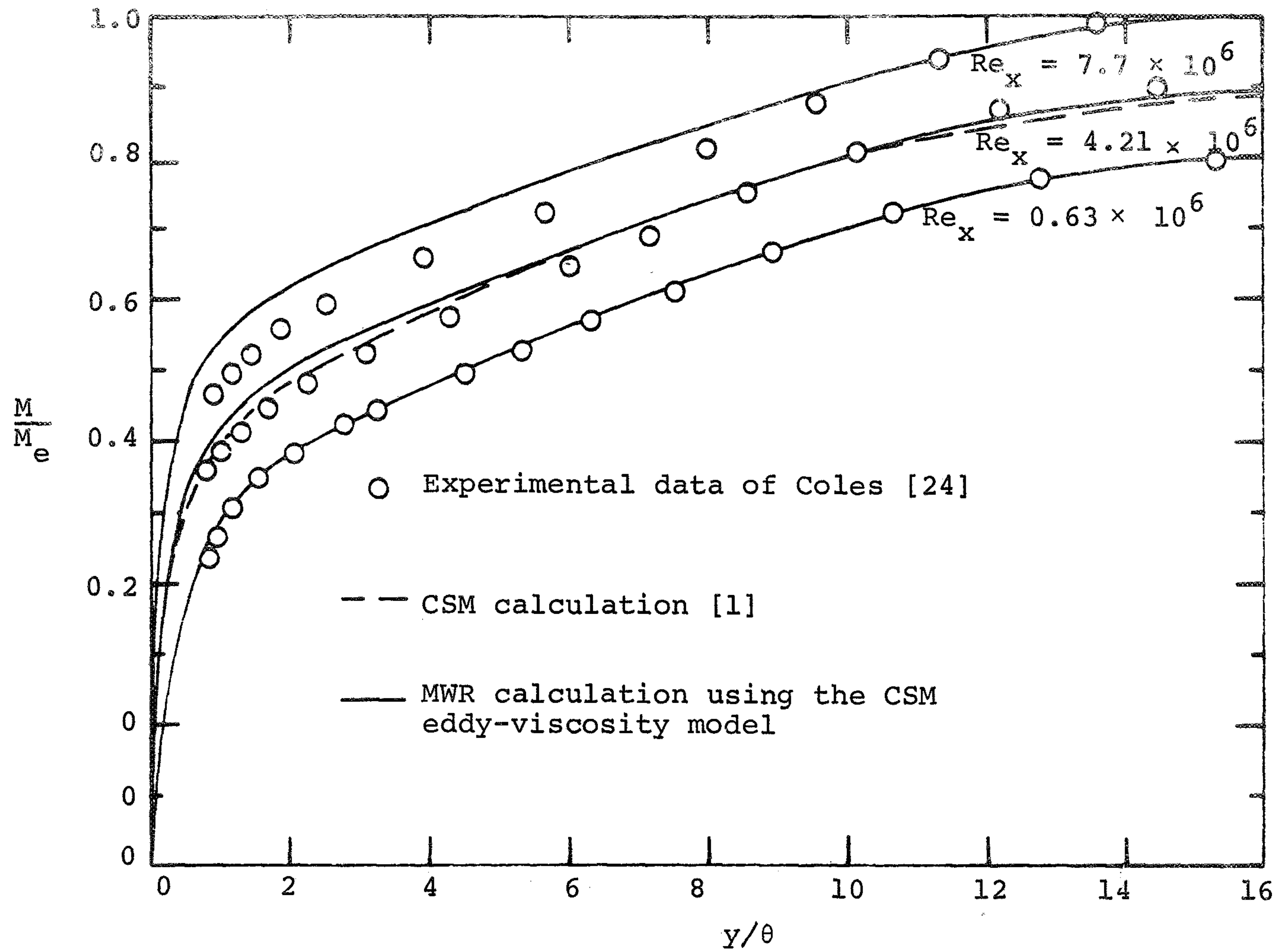

Figure 26: Comparison of Mach-Number Profile Calculations with Experiment, $M_e = 2.54$

measurements of Matting, Chapman, Nyholm, and Thomas [30] and with some analytical calculations of Cebeci, Smith, and Mosinskis [1]. Figure 27 shows the comparisons for the variation of the skin-friction coefficient. The CSM calculations and the MWR predictions agree very well with the experimental data. The maximum error in the MWR solution is 2.23 percent at $Re_x = 20 \times 10^6$ while the maximum error of the CSM calculations is 2.6 percent at $Re_x = 9 \times 10^6$. Figures 28 and 29 show comparisons of the velocity and Mach-number profiles at the initial x-location and a downstream location. The calculated profiles agree quite well with the experimental data. The MWR predictions are slightly better than the CSM calculations at the lower Reynolds number and at the outer edge of the thermal boundary layer.

A third case was considered for an adiabatic flat plate with

$$M_e = 3.69$$
$$U_e = 2202 \text{ ft/sec}$$
$$T_w = 516°R$$
$$L = 8.647 \text{ ft}$$

Figure 30 shows the MWR calculations for skin-friction variation compared with the experimental data of Coles [24] and with the one calculated value of Cebeci, Smith, and Mosinskis [1]. The one value from the CSM results was essentially identical to the experimentally measured value. The maximum error in the MWR results is 7.25 percent at $Re_x = 6.35 \times 10^6$.

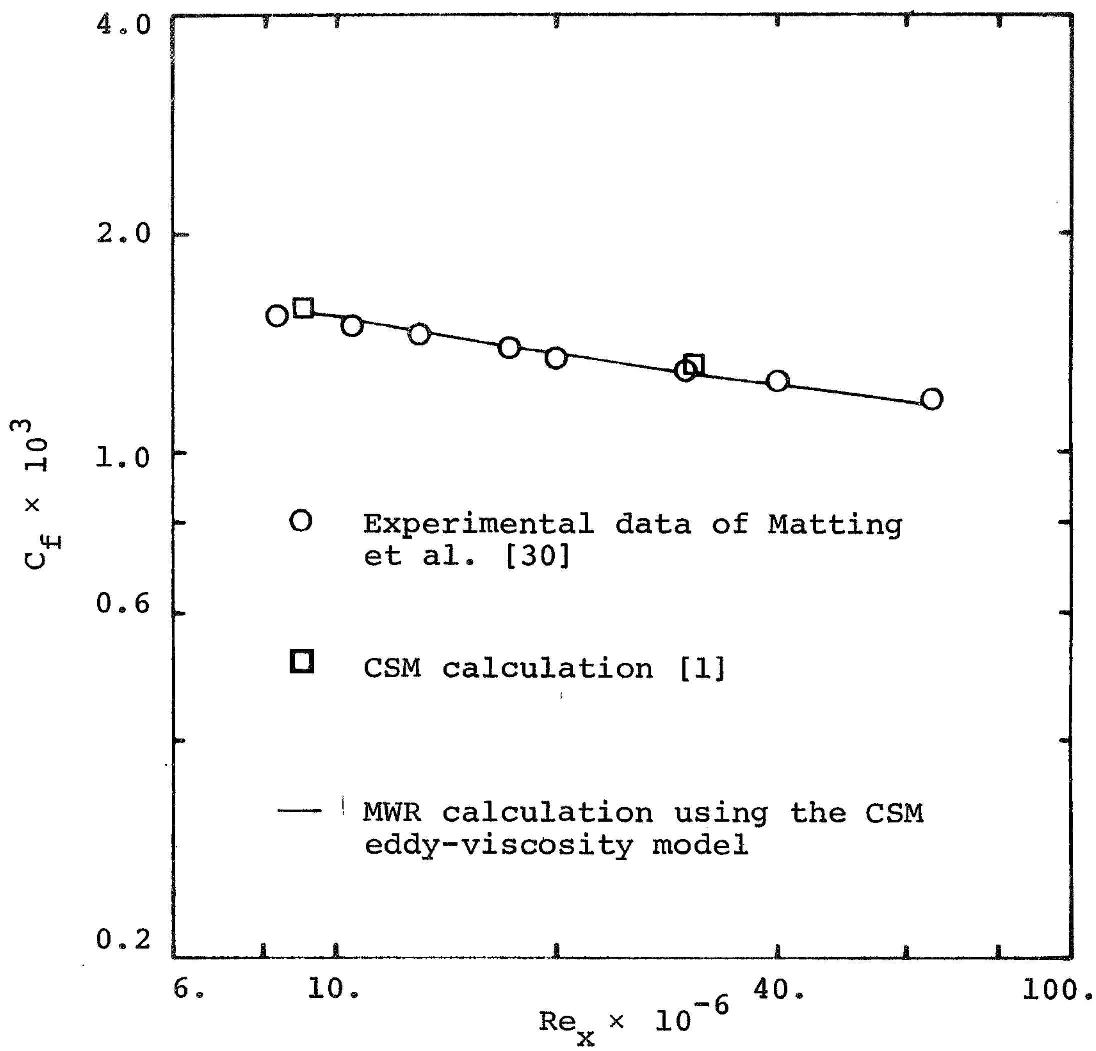

Figure 27: Comparison of Skin-Friction Calculations with Experiment, $M_e = 2.95$

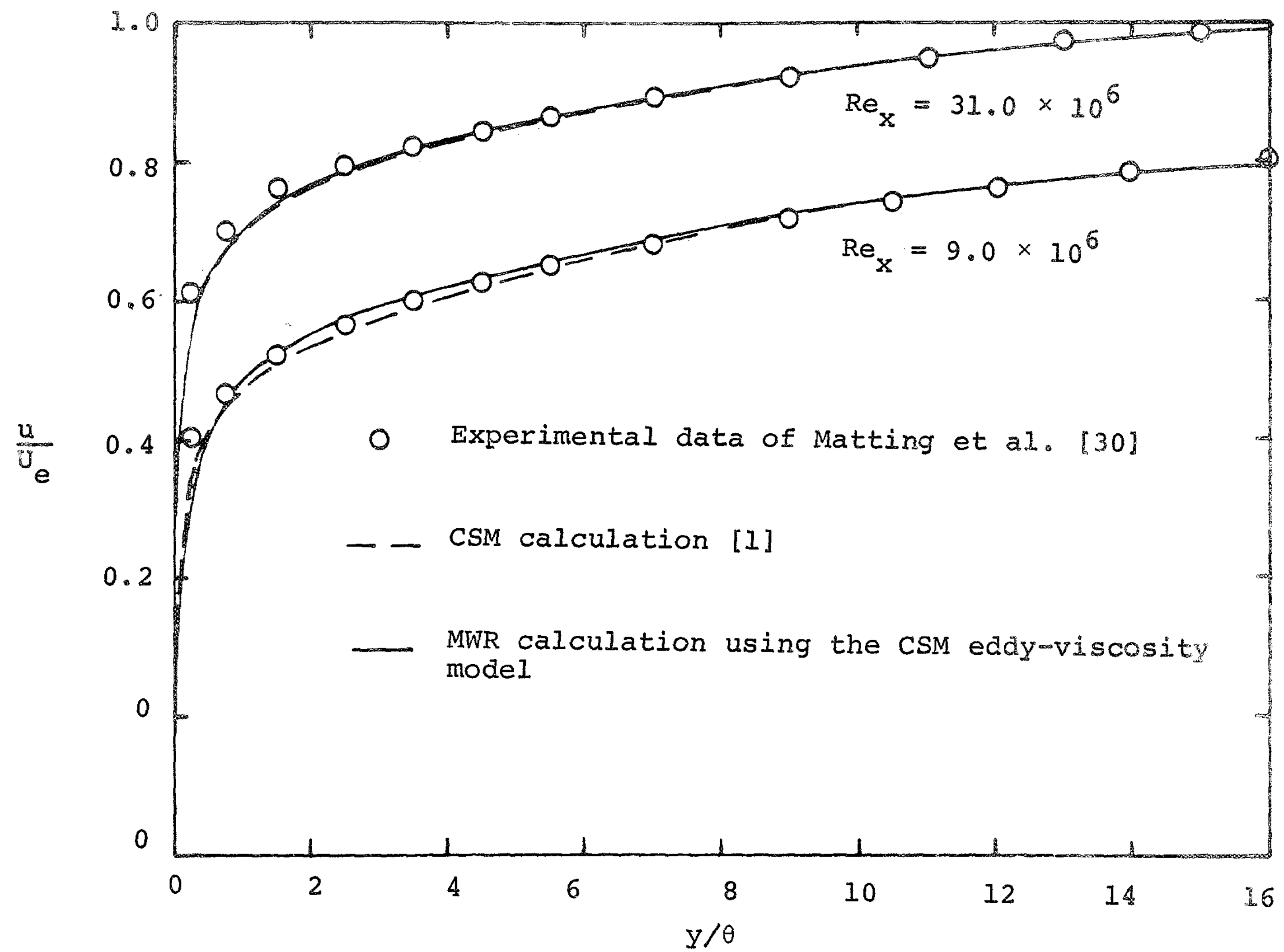

Figure 28: Comparison of Velocity Profile Calculations with Experiment, $M_e = 2.95$

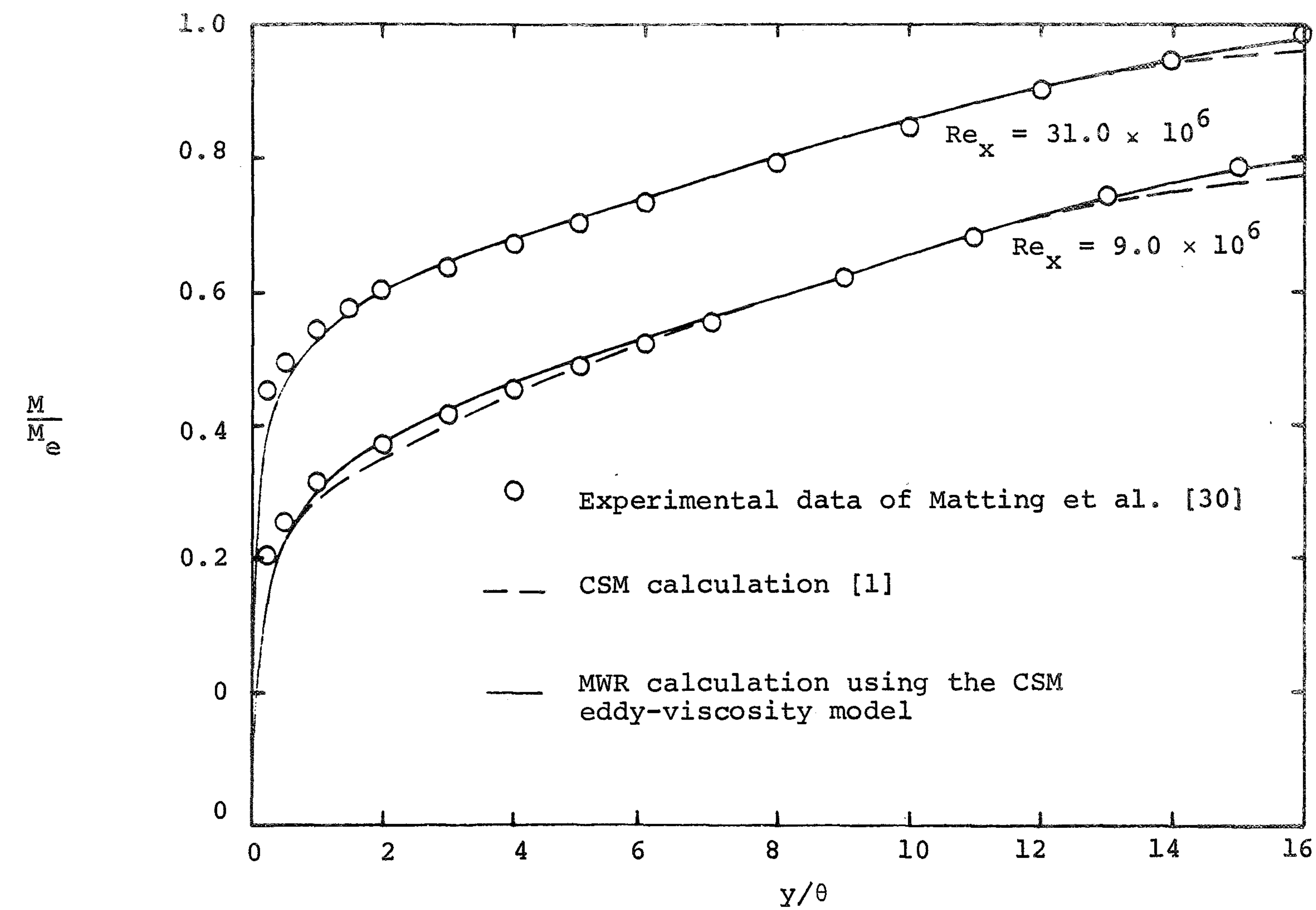

Figure 29: Comparison of Mach-Number Profile Calculations with Experiment, $M_e = 2.95$

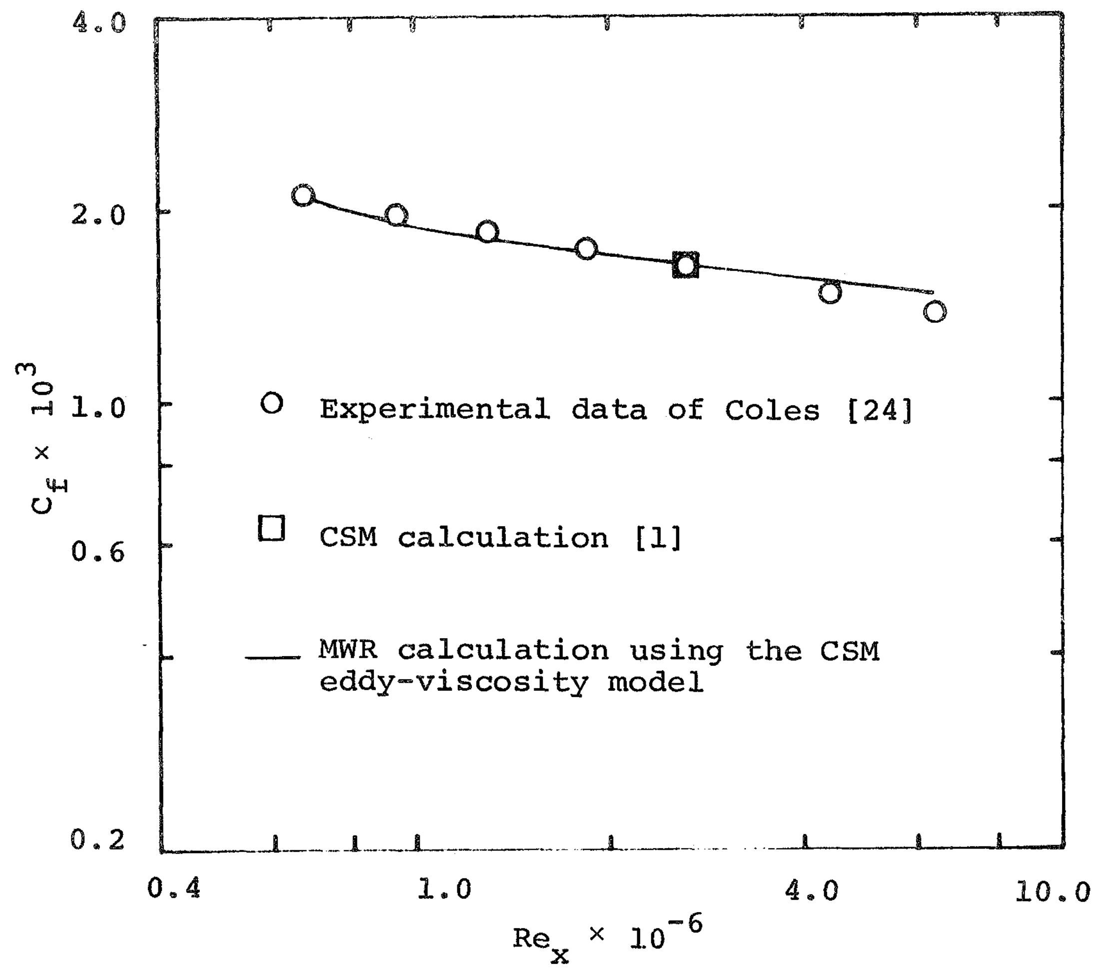

Figure 30: Comparison of Skin-Friction Calculations with Experiment, $M_e = 3.69$

Figures 31 and 32 show the predicted and experimentally measured velocity and Mach-number profiles at the starting location and two downstream locations. The agreement between the MWR predictions and the experimental data is only fair for the Mach-number and velocity profiles at the downstream locations, but the CSM profiles are only fair also. The difference between the predicted and experimental profiles might be attributed to the experimental investigation, since a slight inflection point is noticeable in the experimental Mach-number profiles near a value of $y/\theta = 7$. Such inflections can be caused by external flow disturbances.

The fourth test case was for an adiabatic flat plate with

$$M_e = 4.2$$
$$U_e = 2360 \text{ ft/sec}$$
$$T_w = 539.08°R$$
$$L = 22.39 \text{ ft}$$

Figure 33 compares the skin-friction calculations with the Cebeci-Smith-Mosinskis [1] predictions and with the experimental measurements of Matting, Chapman, Nyholm, and Thomas [30]. The MWR skin-friction calculation is considerably better than the CSM prediction: the maximum error of the CSM prediction is 10.3 percent occurring at $Re_x = 35 \times 10^6$ while the maximum error of the MWR calculation is 3.75 percent at $Re_x = 96 \times 10^6$. Figures 34 and 35 show comparisons for velocity and Mach-number profiles at the initial

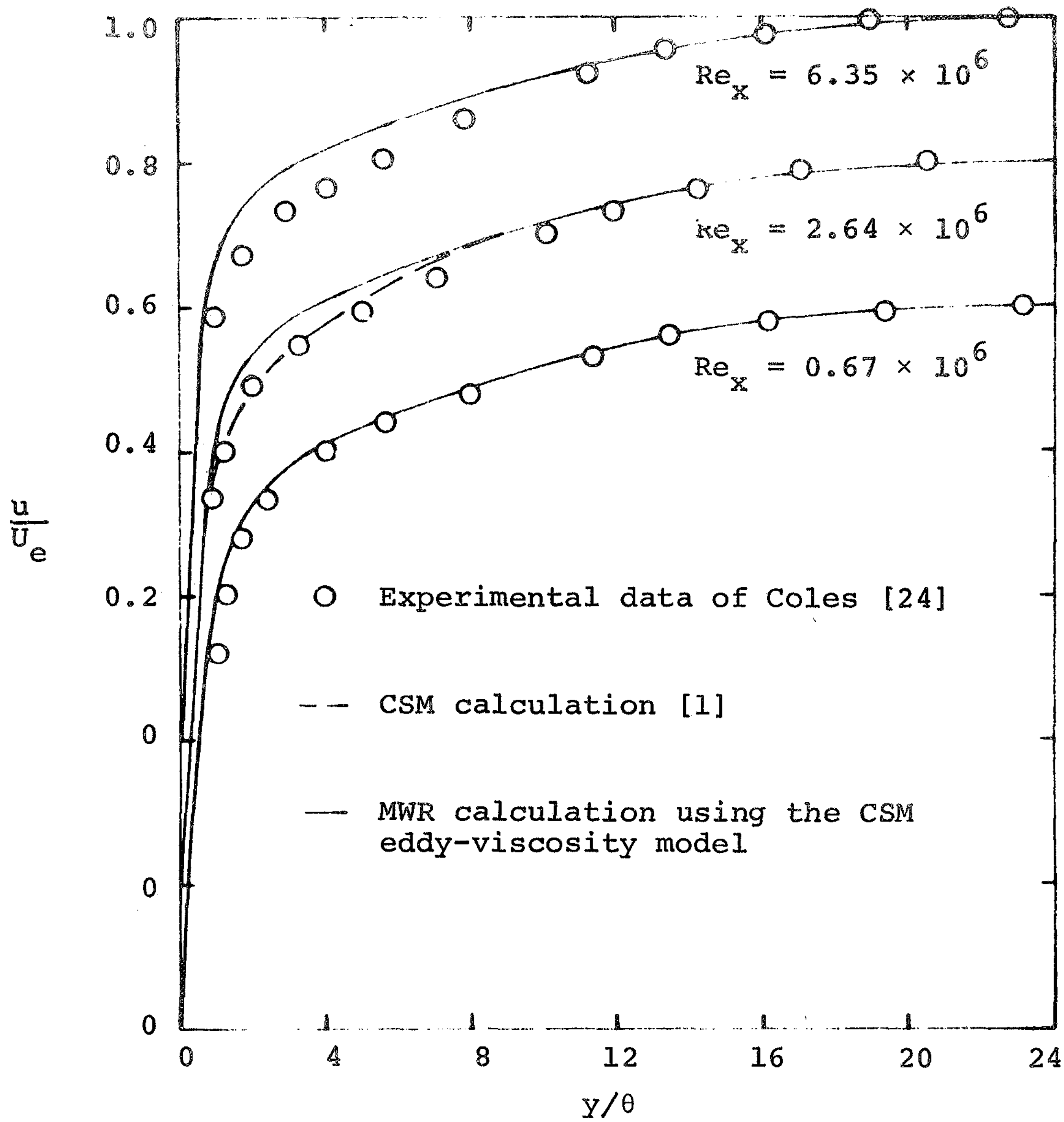

Figure 31: Comparison of Velocity-Profile Calculations with Experiment, $M_e = 3.69$

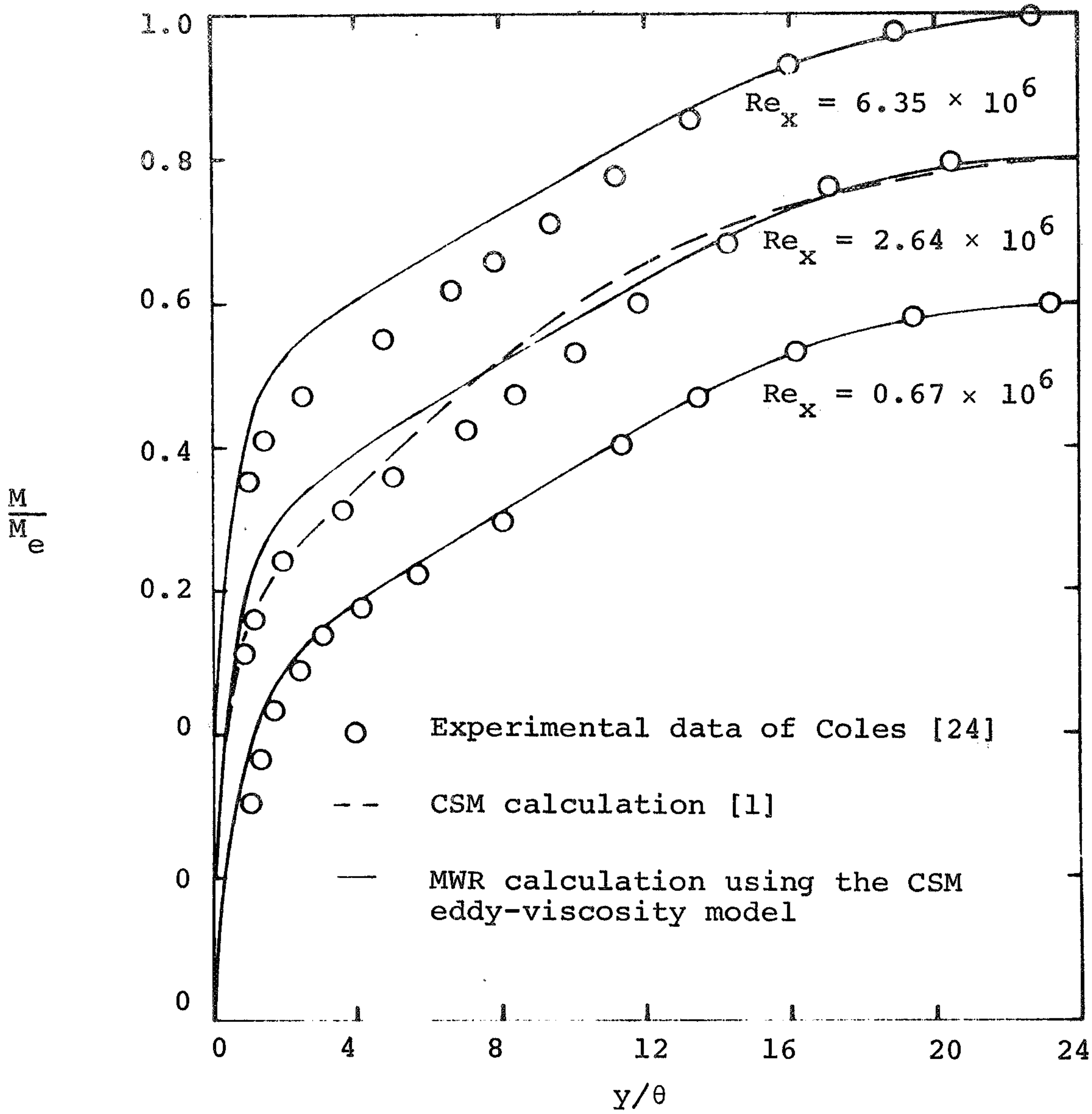

Figure 32: Comparison of Mach-Number Profile Calculations with Experiment, $M_e = 3.69$

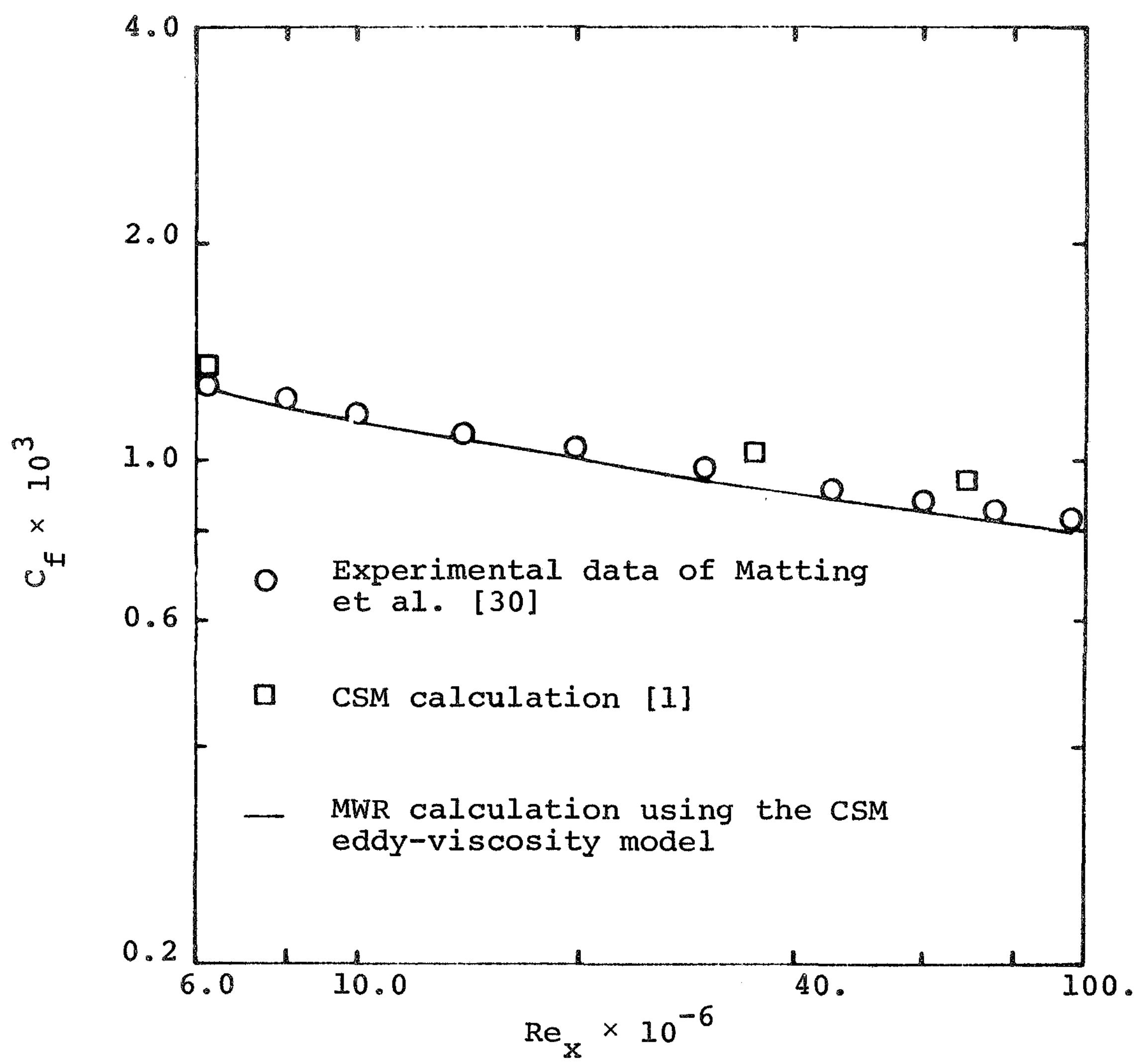

Figure 33: Comparison of Skin-Friction Calculations with Experiment, $M_e = 4.2$

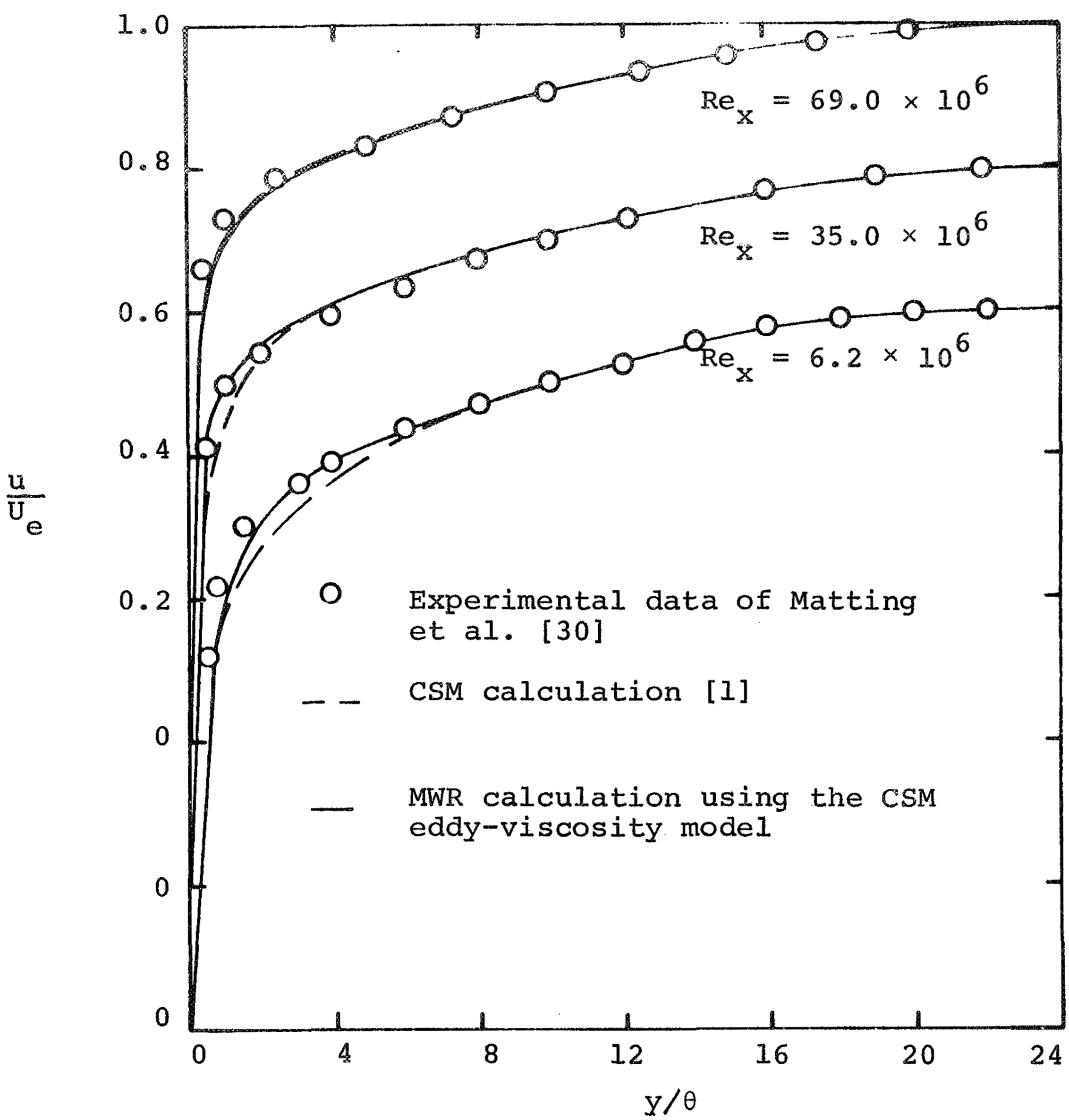

Figure 34: Comparison of Velocity-Profile Calculations with Experiment, $M_e = 4.2$

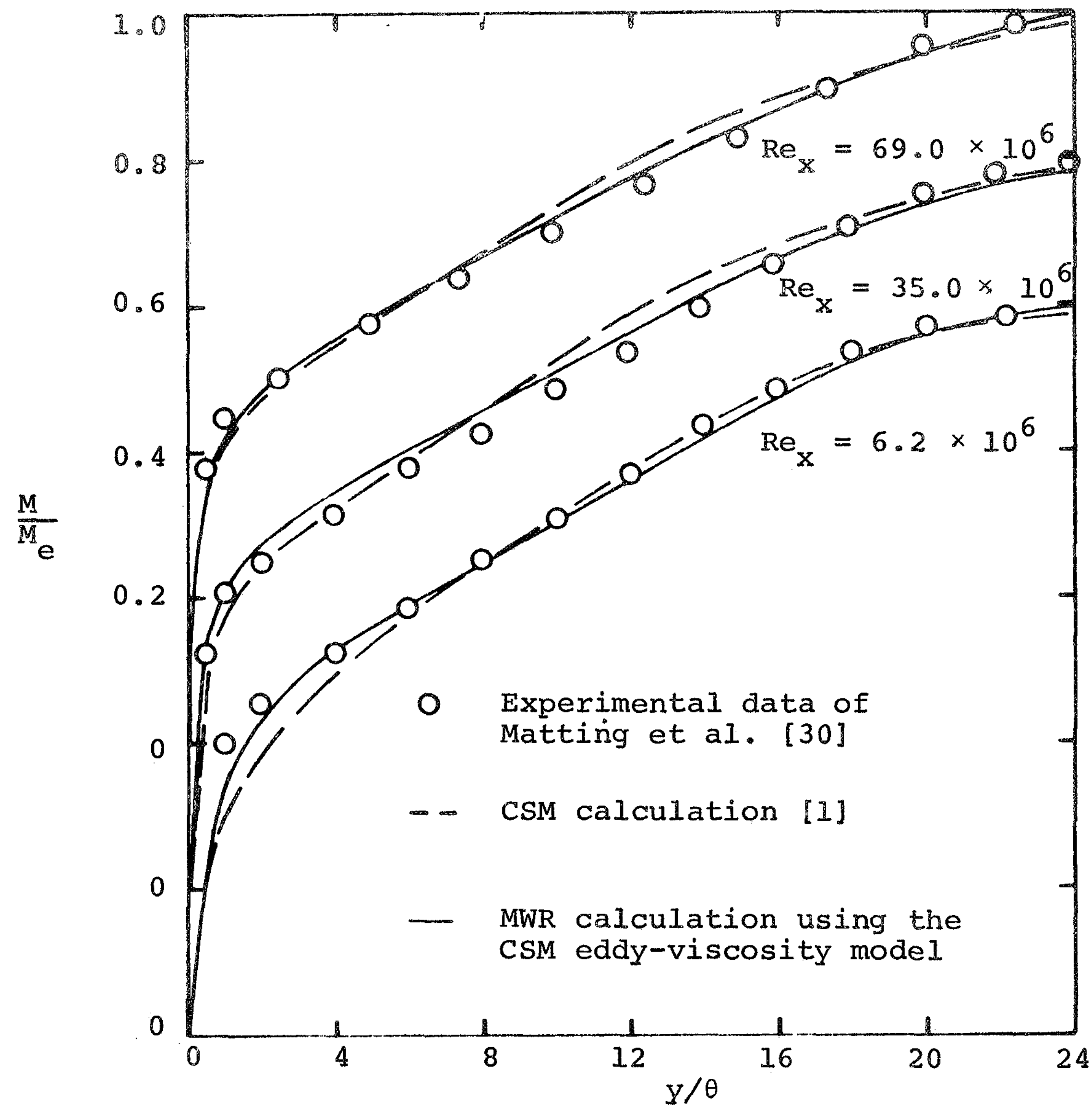

Figure 35: Comparison of Mach-Number Profiles with Experiment, $M_e = 4.2$

x-location and two downstream locations. The profile comparisons are somewhat inconclusive, since the MWR results are better than the CSM results at some x-locations and in some regions of the boundary layer while the opposite is the case at other x-locations and in other regions of the boundary layer. Overall the calculated profiles of the MWR and CSM methods agree well with the experimental measurements.

4.3 Reliability of the Calculations

The MWR results in Figures 24 through 35 agree quite well with the experimental data and in general are as accurate as the Cebeci-Smith-Mosinskis [1] predictions. The convergence properties displayed by the first three MWR approximations are also particularly satisfying (see Appendix C).

In Section 2 special attention was directed to the shear-stress profiles as a possible key to improving the prediction of the boundary-layer parameters for turbulent flow. For this reason, the shear-stress profiles calculated by the MWR technique will be carefully examined. Initially, however, the calculation procedure should be re-emphasized. First, the starting conditions are obtained by the iterative procedure of Section 2.5; this provides a properly behaved shear-stress profile at the initial streamwise location. Second, with these initial conditions the MWR technique calculates the boundary-layer variables at the downstream locations; no iteration or smoothing is used on the CSM eddy-viscosity model at any downstream position. Following this procedure, Figure 36 shows the calculated shear-stress profiles from the MWR solution for the flow with $M_e = 2.54$, and Figure 37 shows the corresponding eddy-viscosity profiles. It is seen that a rather large oscillation in the shear-stress profiles exists at the downstream locations, and the magnitude of this oscillation increases as the calculations proceed downstream. In Figure 37 the match point between the inner and outer eddy-viscosity expressions occurs at $y/\delta = 0.18$; therefore, the oscillatory behavior in Figure 36 exists entirely within the inner region. It is thus very likely that the oscillations in shear stress can be attributed to a sensitivity of the inner-region equation of the CSM eddy-viscosity model (see Section 2.5). Nevertheless, it is important to recall how well the skin friction coefficient, Mach-number profiles, and velocity profiles have been calculated even with the simultaneous development of an oscillatory behavior of the shear-stress profile, at least for the particular flows considered. On the other hand, it is possible that the gross parameters would not be predicted as well for a more difficult flow, say one with a suddenly changing pressure gradient. For such a case, the eddy-viscosity profile might have to be smoothed at every x-station to obtain satisfactory predictions.

Another rather microscopic but very important result

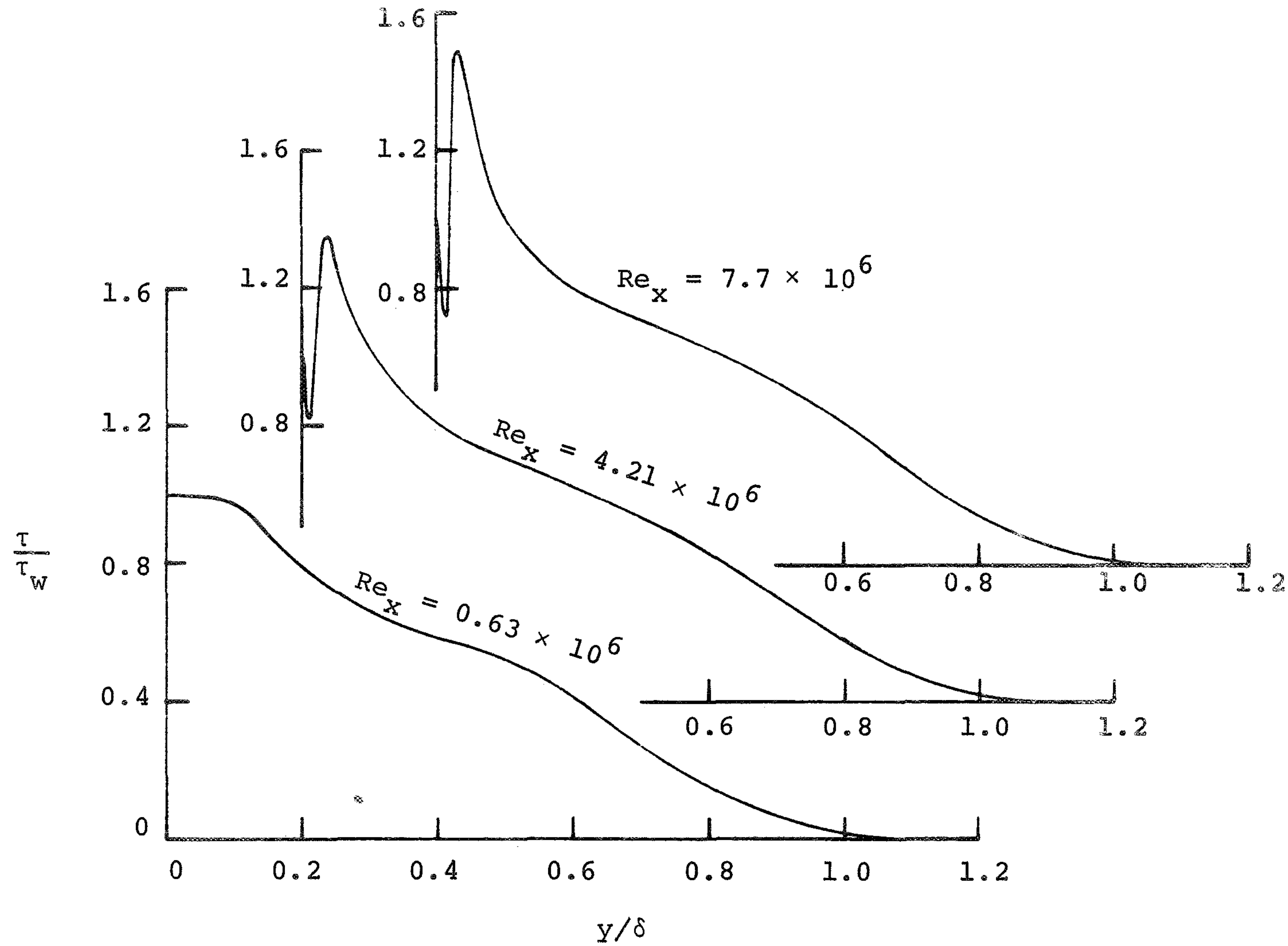

Figure 36: MWR Calculation of Shear-Stress Profiles Using the CSM Eddy-Viscosity Model, $M_e = 2.54$

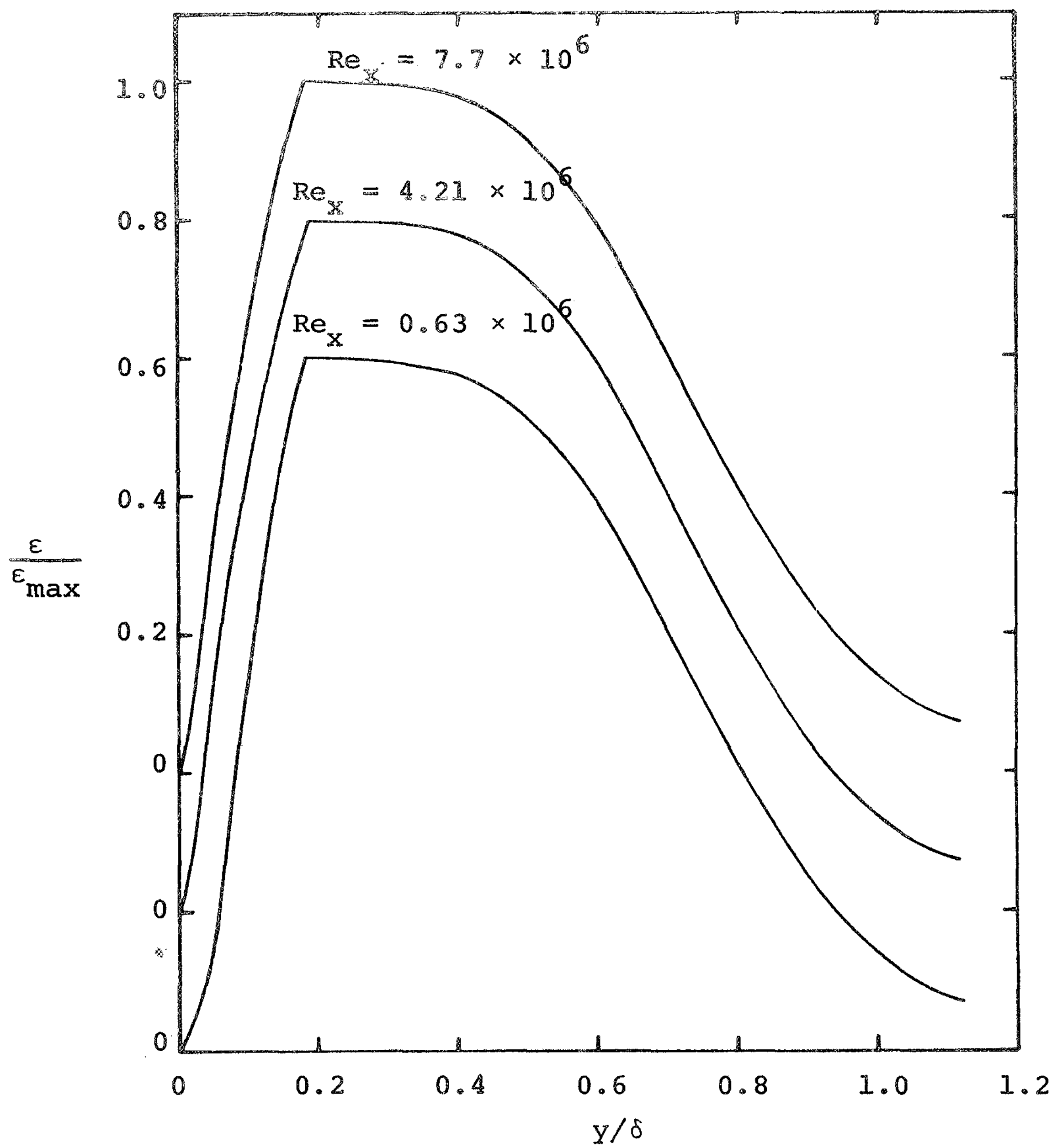

Figure 37: MWR Calculation of Eddy-Viscosity Profiles Using the CSM Eddy-Viscosity Model, $M_e = 2.54$

occurs in the skin-friction prediction near the starting region of the calculations. In fact this result is so close to the starting point that it is not observable on the scales of the previous graphs of skin-friction coefficient. Consequently, the starting region of the skin-friction graph has been magnified greatly, and the results of the MWR solution for the $M_e = 2.54$ flow are shown in Figure 38. The peak in Figure 38 is caused by inaccuracies in evaluating the g_i vector at the initial streamwise location. These inaccuracies cause the calculated value of dC_f/dRe_x to be positive initially, but as the calculation program proceeds downstream, it reverses the skin-friction curve which then follows the trend of the experimental data. Thus, when the initial conditions are rather incompatible with the governing equations, the prediction program corrects these incompatibilities in a very small streamwise distance — a very desirable characteristic of a prediction technique. The mechanism in the prediction program which generates the rapid, corrective response is probably closely related to the sensitivity of the CSM eddy-viscosity model. Perhaps any incorrect behavior in the boundary-layer calculations is quickly sensed by the CSM model, and a corrective response in the form of a shear-stress profile is immediately input to the governing equations at the next calculation step. The same mechanism which was previously blamed for the troublesome sensitivity of the CSM eddy-viscosity model

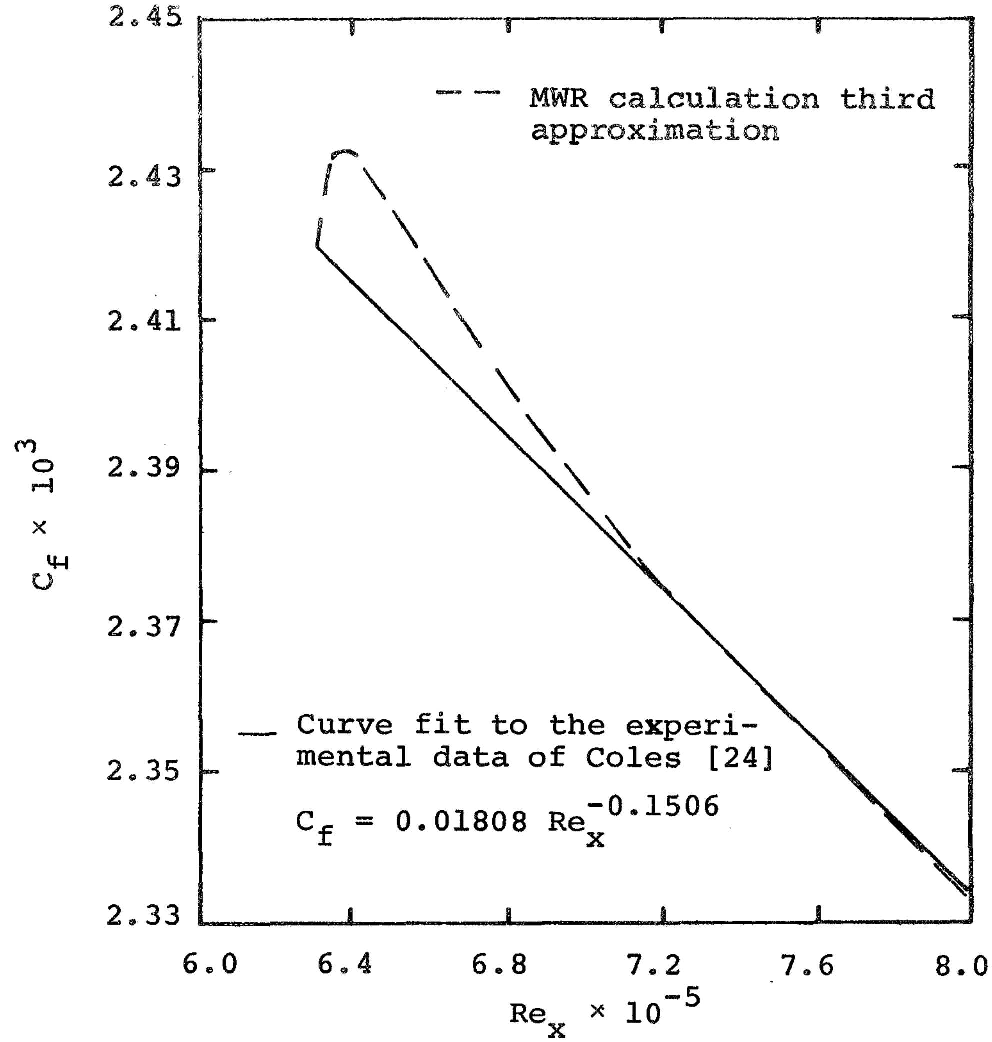

Figure 38: A Greatly Magnified View of the Calculations in the Starting Region, $M_e = 2.54$

is now being suggested as a probable cause for the proper responsiveness of the prediction program. Perhaps the combination of the defining equations for eddy viscosity with the boundary-layer equations generates a sensitivity which must be accommodated in any calculation procedure. This sensitivity may even be necessary for the predictions to display the proper response to numerical disturbances.

Responses analogous to the peak in Figure 38 have been noticed by other investigators. For example, in calculating compressible, turbulent boundary layers by a finite-difference method, Herring and Mellor [8] generate what they call reset initial profiles by making various assumptions on the development of the flow which generated the initial experimental profiles; then in Herring and Mellor's words, "Since there was a slight discontinuity in values like C_f and δ^* between the reset profile and the first profile moving forward, it was found best to allow space to calculate profiles at two or three stations before the initial station." Thus, initial disturbances are not uncommon in prediction programs for turbulent boundary layers.

4.4 The MWR Calculations Using Alternate Shear Models

In the prediction of compressible, turbulent boundary layers using the CSM eddy-viscosity model, there developed anomalous oscillations of the shear-stress profile in the inner region of the boundary layer, even though skin-friction and velocity and Mach-number profile calculations were satisfactory. In Section 4.3 these oscillations were attributed to the sensitivity of the CSM eddy-viscosity model. It would be instructive to see if any shear models could be constructed which would be devoid of oscillations, but would still yield accurate predictions of the boundary-layer parameters. Consequently, the task was undertaken to predict the compressible, turbulent boundary layer with the MWR using alternative shear-stress models which, by construction, would yield well-behaved shear-stress profiles.

As a first attempt, a very simple-minded approach was used even though it could only conceivably be expected to work for the flat-plate flows. In the inner region of the boundary layer, denoted by subscript i, the shear stress was assumed to be a constant,

$$\tau_i = \tau_w \tag{4.1}$$

while in the outer region the CSM eddy-viscosity model was employed, since it yields well-behaved shear-stress profiles there. The junction between the inner and outer regions was defined as the point where the shear stress from the inner-region model equaled the shear stress from the outer-region model. The MWR predicted skin-friction results with this shear model are shown in Figure 39 for a second approximation. These are the results for flow over an adiabatic flat plate at $M_e = 2.54$. The calculations are shown with and without the initialization procedure of

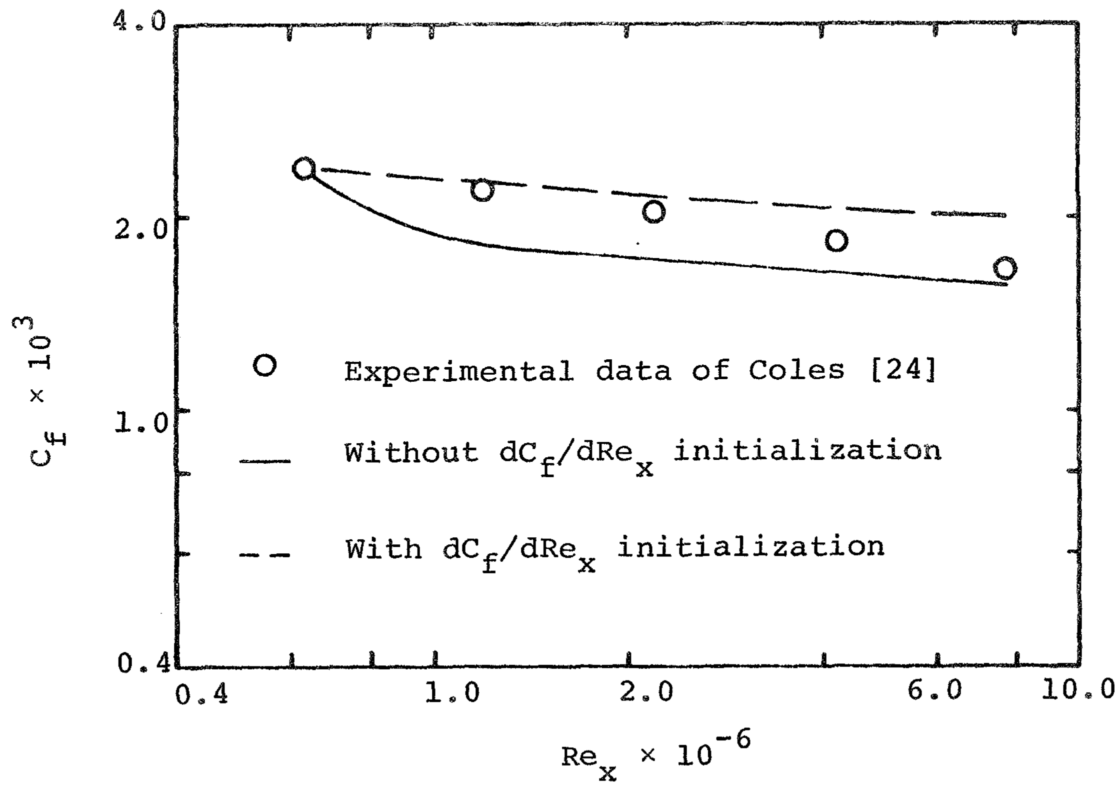

Figure 39: Skin-Friction Calculation from an MWR Second Approximation Using the Inner-Region Shear Model of Equation (4.1), $M_e = 2.54$

Appendix D where a procedure has been developed to artificially match the experimental and calculated values of dC_f/dRe_x at x_o.

In hopes of obtaining better skin-friction predictions, a slightly more sophisticated shear-stress model was next considered for the inner region,

$$\tau_i^* = 1 - 2.3978\ y^{*2} + 2.9266\ y^{*3} \tag{4.2}$$

where $\tau_i^* = \tau_i/\tau_w$ and $y^* = y/\delta$. Equation (4.2) was obtained from an analytical curve fit to the inner-region shear-stress results of Bradshaw [54] on a flat plate in incompressible, turbulent flow. In the outer region the CSM model was again used, and the junction between the two regions was defined as the point where the shear-stress values from the inner and outer equations were equal. The MWR predicted skin-friction results with this shear model are shown in Figure 40 for a second approximation. The calculations were again made for flow over an adiabatic flat plate at $M_e = 2.54$. The predictions are shown both with and without the dC_f/dRe_x initialization of Appendix D. The predictions using equation (4.2) are no better than those using equation (4.1); in fact, the results are nearly identical.

In another attempt to improve the skin-friction calculations, a much more sophisticated shear-stress equation was developed and employed in the prediction program. The

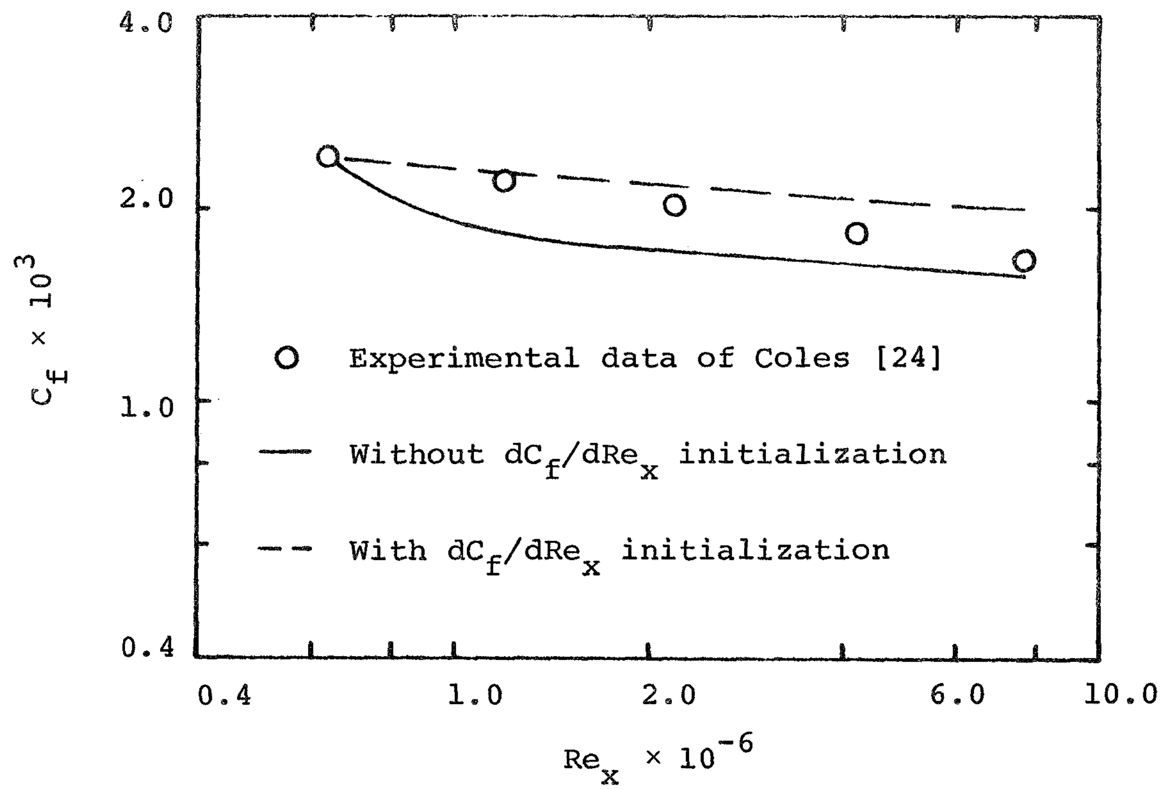

Figure 40: Skin-Friction Calculation from an MWR Second Approximation Using the Inner-Region Shear Model of Equation (4.2), $M_e = 2.54$

idea for this model arose from the work of Clauser [4] where he developed universal velocity profiles for incompressible, turbulent flow over a flat plate. He developed universal correlation functions separately for the inner and outer regions and argued that there must be a parameter tying these two regions together in an overlap region. He chose the shear stress at the wall for the joining parameter. Perhaps the trouble with the two previous alternate shear models was the rough manner in which the separate functions for the two regions were joined; consequently, a model was developed which links the inner and outer regions and has a smooth junction between the two regions.

For this model, it is assumed that a fourth-order polynomial of the form

$$\tau_i^*(y^*) = b_o + b_1 y^* + b_2 {y^*}^2 + b_3 {y^*}^3 + b_4 {y^*}^4 \qquad (4.3)$$

can satisfactorily model the shear-stress behavior in the inner region. The b_i coefficients are constants at a specified x-station and are determined from the following relations:

$$\tau_i^*(1) = 0 \qquad (4.4)$$

$$\frac{\partial \tau_i^*(1)}{\partial y^*} = 0 \qquad (4.5)$$

$$\tau_i^*(0) = 1 \qquad (4.6)$$

$$\frac{\partial \tau_i^*(0)}{\partial y^*} = \frac{\delta}{\tau_w}\frac{dp}{dx} \qquad (4.7)$$

$$\frac{\partial \tau_i^*(y_m^*)}{\partial y^*} = \frac{\partial \tau_o^*(y_m^*)}{\partial y^*} \qquad (4.8)$$

where subscript i denotes the inner region, subscript o the outer region, and y_m^* is the value of y^* at the match point between the two regions. Equations (4.4) through (4.7) satisfy four relevant boundary conditions; equation (4.7) is obtained from the evaluation of the x-momentum equation (3.11) at $y^* = 0$, and equation (4.8) is the matching condition which creates a smooth junction between the inner and outer functions. The CSM eddy-viscosity equation was again used in the outer region, and the combined shear model was incorporated into the MWR prediction program. Again, the skin-friction variation was calculated for an MWR second approximation for flow over an adiabatic flat plate with $M_e = 2.54$ and is shown in Figure 41. Both the calculations with and without the dC_f/dRe_x initialization procedure are shown, and it is seen that these results are slightly worse than those from the simpler shear models of Figures 39 and 40.

Summarizing, the skin-friction coefficient predictions from three alternate shear models show a maximum error in the MWR calculations between 16 percent and 27 percent in Figures 39, 40, and 41. In contrast, the maximum error in a second approximation of the MWR calculations for skin

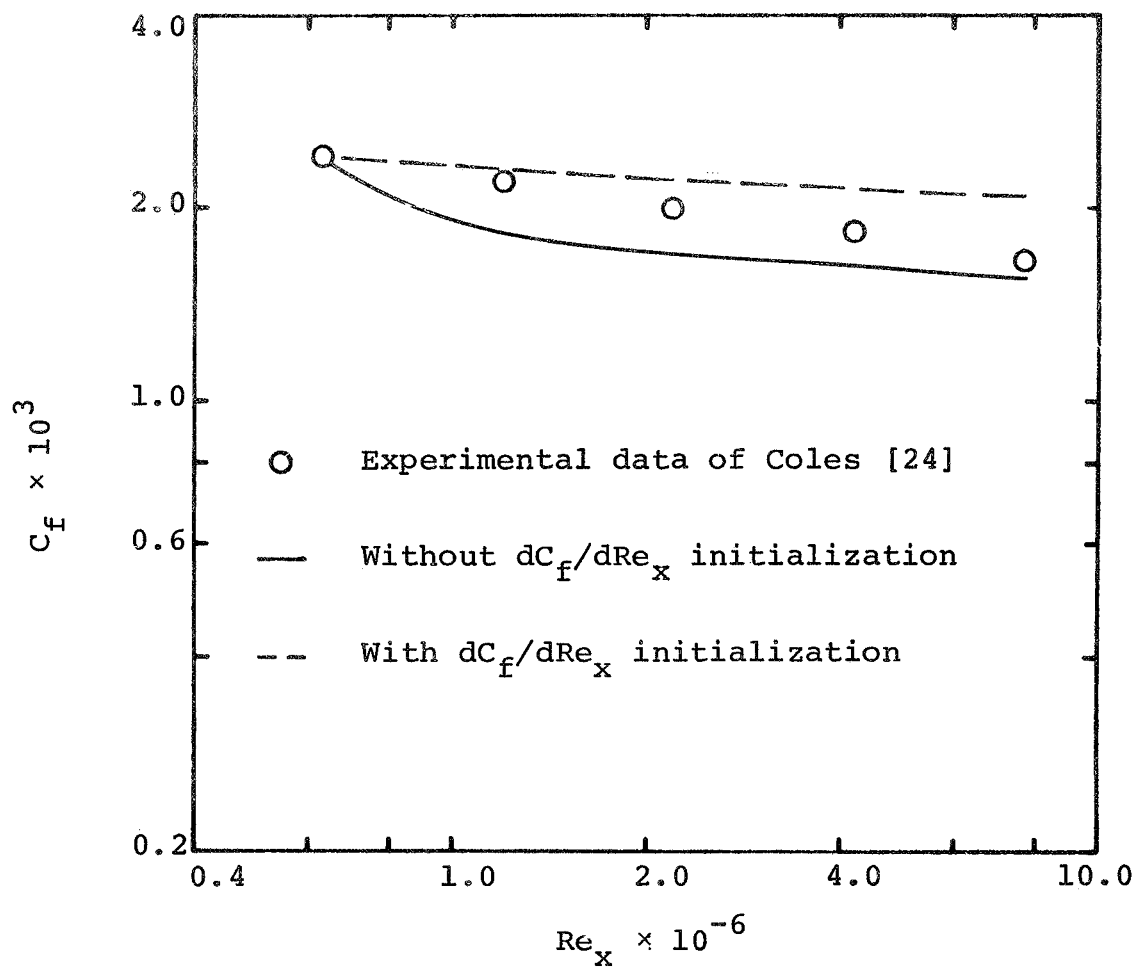

Figure 41: Skin-Friction Calculation from an MWR Second Approximation Using the Inner-Region Shear Model of Equation (4.3), $M_e = 2.54$

friction using the CSM eddy-viscosity model is 10.8 percent as seen in Appendix C. Although the calculations with the alternate shear models are not too bad, nevertheless they are not nearly as good as the predictions with the CSM model. In Figures 39, 40, and 41 the calculations with the alternate shear models, but without the dC_f/dRe_x initialization of Appendix D, start very poorly but then level off and approach the experimental data as Re_x increases. At first this characteristic was thought to be an incompatibility between the starting conditions and the governing differential equations; consequently the analysis of Appendix D was performed to allow the skin-friction variation to start properly. However, the calculated results in Figures 39, 40, and 41 with the dC_f/dRe_x initialization procedure are no better than the results without the initialization procedure: the region of inaccurate calculation is just shifted from low Re_x to high Re_x. It seems that the alternate inner-region models simply do not contain enough physical make-up of the inner layer to be adequately responsive to the developing boundary layer. The hope of using a polynomial in y for the inner shear-stress equation and still calculating the skin friction as accurately as the predictions with the CSM eddy-viscosity model has consequently been abandoned at the present time.

There would be, however, a very practical advantage to obtaining a smoothly varying shear-stress formulation;

namely in providing an order of magnitude reduction in machine calculation time. This contention can be illustrated by considering, as an approximation and with no special claims being made concerning its physical basis, a single polynomial representation for the shear stress across the complete viscous layer. In Section 4.3 it is seen that the calculated shear-stress profiles oscillate in the inner region of the boundary layer when the CSM eddy-viscosity model is used in the MWR prediction program. Complications of these oscillations are believed to propagate into the solution of the ordinary differential equations for the C_j coefficients and to require a very small step size in the ξ-direction (which consequently increases the computer time) in order to obtain accurate solutions for the C_j. To verify that the CSM eddy-viscosity model, with its shear-stress oscillations, necessitates the small $\Delta\xi$ steps, the task is undertaken to predict the compressible, turbulent boundary-layer behavior by using still another shear-stress model which, by construction, will yield smooth shear-stress profiles with no oscillations.

A similarity approach, comparable to that of Chi and Chang [55] and Ross and Robertson [56], is chosen across the entire boundary layer by assuming shear-stress similarity in the nondimensional coordinates τ/τ_w versus y/δ. A third degree polynomial of the form

$$\tau^*(y^*) = a_o + a_1 y^* + a_2 y^{*2} + a_3 y^{*3}$$

is selected where the coefficients of the polynomial are found by the following boundary conditions:

$$\tau^*(1) = 0 \tag{4.9}$$

$$\frac{\partial \tau^*(1)}{\partial y^*} = 0 \tag{4.10}$$

$$\tau^*(0) = 1 \tag{4.11}$$

$$\frac{\partial \tau^*(0)}{\partial y^*} = \frac{\delta}{\tau_w} \frac{dp}{dx} \tag{4.12}$$

The resulting equation for shear stress is

$$\tau^*(y^*) = \frac{\delta}{\tau_w} \frac{dp}{dx} y^*(y^*-1)^2 + y^{*2}(2y^*-3) + 1 \tag{4.13}$$

The behavior of this equation is shown in Figure 42. Equation (4.13) is not proposed as an accurate quantitative description of the physical phenomena by means of which the predicted boundary-layer parameters can be improved; but rather it is proposed as a qualitatively correct, simple, and smooth analytical expression which can be used to study the restriction on the step size $\Delta\xi$ and therefore the machine computation time.

Boundary-layer calculations were performed by the MWR technique for flow over an adiabatic flat plate using equation (4.13) for the shear-stress model. The skin-friction results at $M_e = 2.54$ are shown in Figure 43 for the second approximation with and without the dC_f/dRe_x initialization

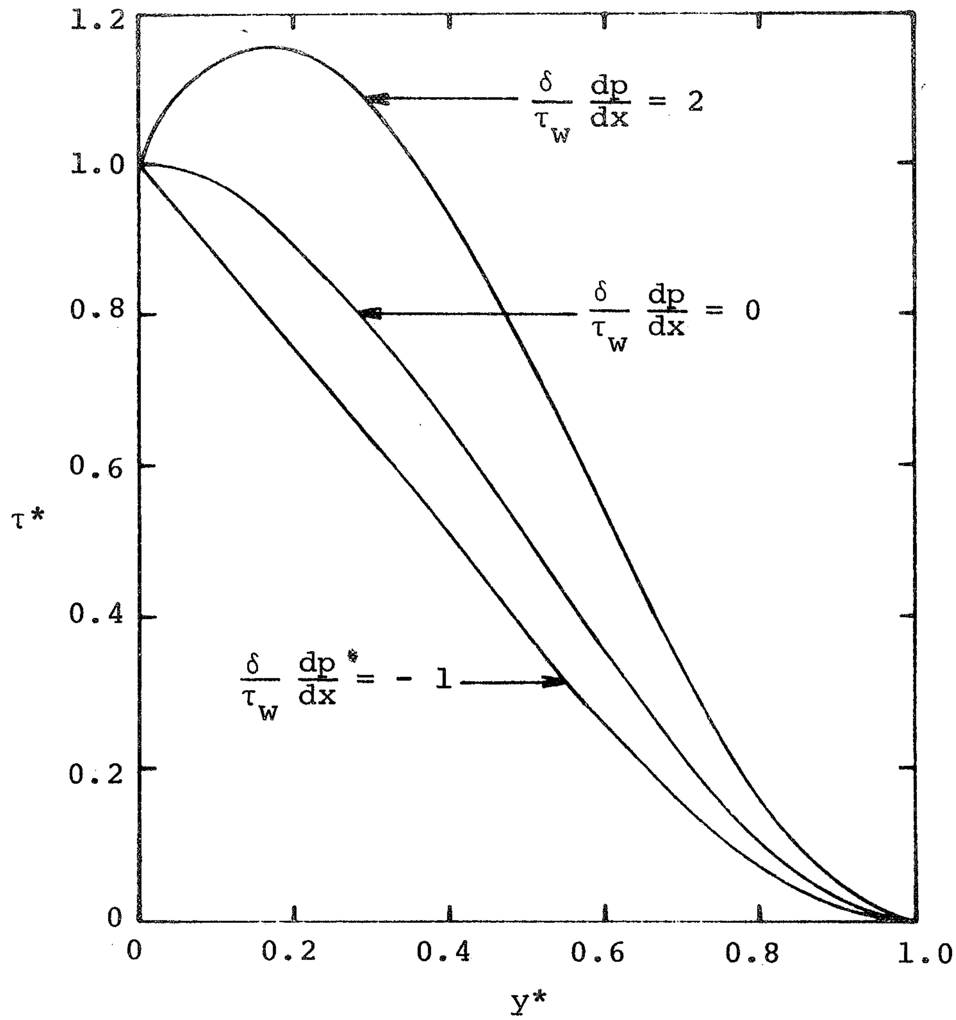

Figure 42: Shear-Stress Profiles Calculated from Equation (4.13)

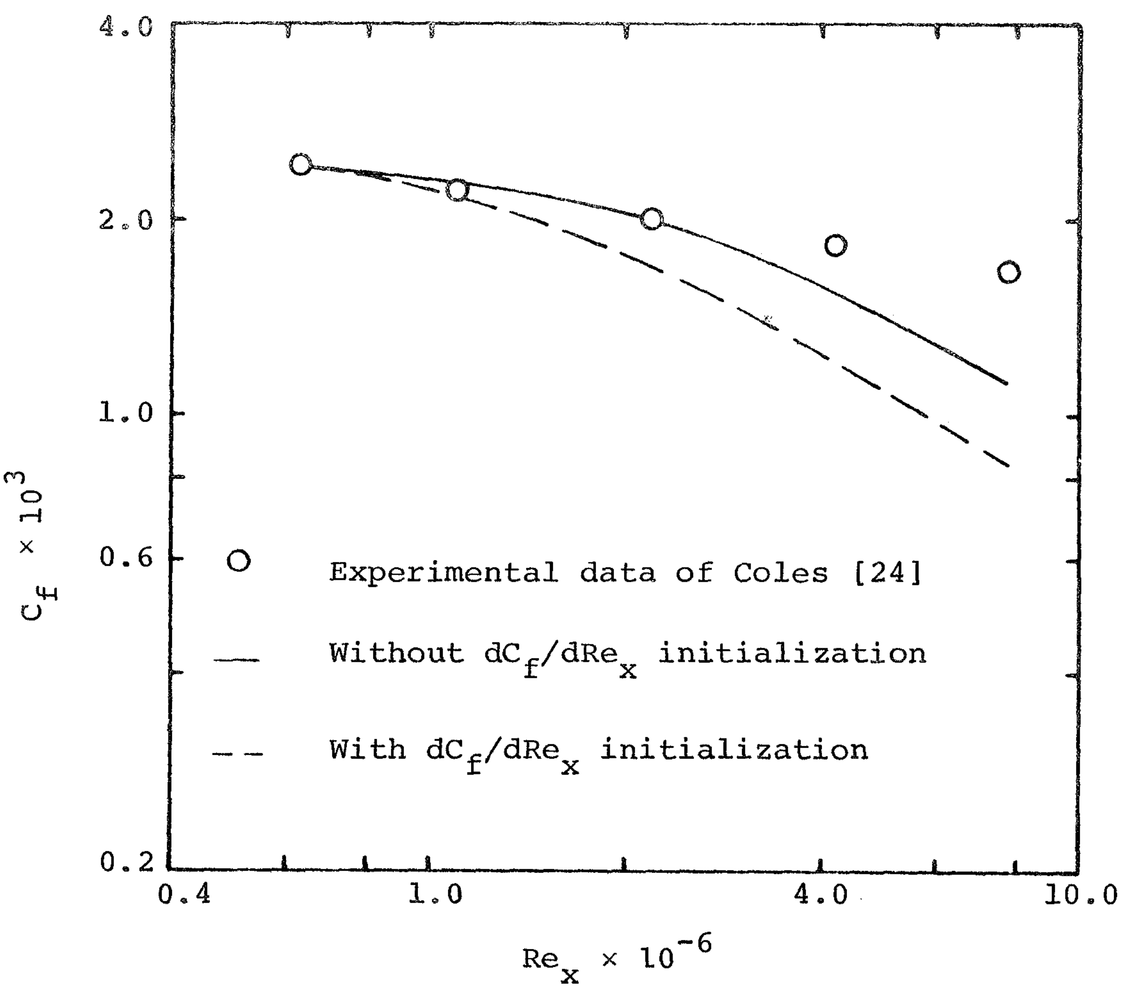

Figure 43: Skin-Friction Calculation from an MWR Second Approximation Using the Shear Model of Equation (4.13), $M_e = 2.54$

procedure. These results are considerably worse than those of the alternate shear models which used separate formulations for the inner and outer regions, since the maximum error of the calculations in Figure 43 is 50 percent. These calculations were made using various values of the step size $\Delta\xi$. Values of $\Delta\xi$ equal to 0.001, 0.01, and 0.03 all gave results for the C_j coefficients which were identical to five significant figures whereas the calculations for the C_j coefficients using the entire CSM model, Section 4.2, required $\Delta\xi$ values of 0.001 and smaller for successive solutions to agree to three significant figures. The results obtained by varying $\Delta\xi$ indicate that the sensitivity and oscillation of the CSM eddy-viscosity model require the use of the very small step size of $\Delta\xi = 0.001$, which consequently inflates the machine calculation time. For example, if a step size of $\Delta\xi = 0.01$ could be used instead of 0.001 with the CSM model in Section 4.2, then the average calculation time for the second approximation of the MWR would be decreased from 150 seconds to less than 19 seconds on a CDC 6500 computer. Thus the requirement of the small step size is attributed to the sensitivity of the CSM eddy-viscosity model, and the potential for accurate predictions of the boundary-layer parameters with an order-of-magnitude reduction in computer time is indicated when a smoothly behaved shear model is found which adequately describes the physical phenomena.

4.5 Summary

The numerical solution procedure for calculating compressible, turbulent boundary layers with the MWR technique was described. Solutions were obtained using the CSM eddy-viscosity model for compressible flow of air over an adiabatic flat plate at four different Mach numbers. The calculated results agreed well with the experimental data, and in general, the results predicted by the MWR were at least as good as the results predicted by the Cebeci-Smith-Mosinskis [1] finite-difference method. The machine calculation time for a second approximation of the MWR was of the same order as the CSM method, but a potential reduction in calculation time by an order of magnitude appears to be possible if a smoothly varying and physically correct shear-stress model can be found. Despite good predictions of skin-friction coefficient and velocity and Mach-number profiles, oscillations in the calculated shear-stress profiles were found to develop at the downstream locations. These oscillations were attributed to the sensitivity of the inner-region equation of the CSM eddy-viscosity model. A nearly microscopic peak in some of the skin-friction calculations was detected near the starting region, and the cause of the peak was found to be slight inaccuracies in the starting values of the shear integrals g_i.

Alternate shear-stress models were developed and employed in place of the CSM eddy-viscosity model in the hope that an improvement of the qualitative behavior of the shear-stress profile would improve the boundary-layer predictions. This was not the case; the predictions using the alternate shear models were considerably worse than those using the CSM eddy-viscosity model. Some important information, however, did result from the use of the alternate shear models. With a similarity model for shear stress, a much larger $\Delta\xi$ step size could be used than that required by the CSM eddy-viscosity model. The resulting machine computation times were consequently reduced by an order of magnitude. Thus the door is opened for the development of a calculation procedure which will predict accurate boundary-layer parameters while requiring a very small machine time. The only missing ingredient is an alternate shear-stress model which will generate results as accurate as those from the CSM model while permitting a much larger step size $\Delta\xi$ than that required by the CSM model.

5. SUMMARY, CONCLUSIONS, AND RECOMMENDATIONS

5.1 Summary

The two main goals of this work are: (1) the examination and selection of turbulent shear information models to be used in a boundary-layer calculation procedure and (2) the development of a calculation procedure for two-dimensional, compressible, turbulent boundary layers.

First, calculations employing various turbulent shear models that have occurred in the literature were noted and compared; and two models were selected for further study in the present investigation. The CSM eddy-viscosity model was ultimately chosen to be incorporated into a prediction program. An iterative procedure was applied at the initial calculation station to correct the erratic behavior of the initial shear-stress profile, and a constant in the CSM model was modified.

Second, a calculation procedure was developed by applying the MWR solution technique to the governing equations for two-dimensional, compressible, turbulent boundary layers. A computer program was written for this solution procedure, and the numerical results were compared with the experiments of Coles [24] and Matting et al. [30] and with the finite-difference solutions of Cebeci et al. [1] for the flow of air over an adiabatic flat plate.

Finally, a shear-stress similarity approach was undertaken to eliminate the effects of the anomalous shear-stress oscillations which arose when the CSM eddy-viscosity model was employed in the prediction program. By means of this similarity approach, the effect of the shear-stress oscillations on the accuracy of the predicted boundary-layer parameters and on the required computation time was studied.

5.2 Conclusions

1. Many eddy-viscosity models yield qualitatively incorrect shear-stress profiles in the inner region of the turbulent boundary layer as is seen by results from previous investigations in the literature as well as by results calculated in the present investigation.
2. An error analysis on the CSM eddy-viscosity model produces a very plausible explanation for the anomalous shear-stress behavior by indicating the strong sensitivity of the model to the velocity profile and to the first y-derivative of the profile.
3. The CSM eddy-viscosity model is one of the best known and highly regarded turbulent shear models in the turbulent boundary-layer literature and therefore is employed in the prediction program of this investigation.
4. A significant improvement of the CSM eddy-viscosity model is achieved in compressible flow by allowing the

constant K_1 to become a function of Mach number; but due to the large degree of scatter in the calculated values of K_1, this function is not as yet well-defined.

5. The present method for comparing turbulent, compressible boundary-layer calculations with experimental data (measured at a fixed x-location and fixed Mach number) is a better indication of the ability of a prediction program than two methods of comparison developed by other investigators.

6. From the boundary-layer predictions with the CSM eddy-viscosity model, it is seen that:

   (i) The convergence properties of the MWR solution are very well-behaved, and a second approximation is sufficient for most engineering purposes.

   (ii) The predicted results for velocity and Mach-number profiles and skin-friction coefficient agree with both experiment and the CSM finite-difference predictions. The resulting calculation times for the MWR second approximation and the CSM method are of the same order.

   (iii) Although the proposed iterative procedure creates a smooth shear-stress distribution initially, it is nevertheless found that shear-stress oscillations develop in the inner region of the boundary layer as the calculations proceed to downstream locations. The cause of these oscillations is probably a result of the sensitivity of the CSM model to the velocity profile.

7. The use of polynomial expressions for shear stress eliminated the oscillations in the shear-stress profiles; the use of these expressions also reduced the computer time by an order of magnitude. A shear model which yields smooth shear-stress profiles, however, has not been found which also yields results of acceptable accuracy.

5.3 Recommendations

Considering the success of the present formulation for compressible, adiabatic, flat-plate flow calculations, this formulation should be extended to pressure-gradient and heat transfer cases. The major obstacle in this extension is in obtaining a smooth and proper shear-stress distribution at the initial calculation station. It is reasonable to expect that the initialization procedure of Hirst and Reynolds [57] or Bradshaw [58] could be extended to compressible flow for this purpose, and the necessary modifications could be made in the program for the initialization procedure and for the handling of the complete energy equation.

In this work several alternate shear models were developed in an attempt to rid the prediction results of the oscillatory shear-stress behavior, but as a result considerable accuracy in the predicted boundary-layer parameters was sacrificed. However, this approach could be very rewarding: if a shear model (devoid of any oscillatory behavior) can be found which adequately models the physical situation, then an accurate prediction program can be developed which will require very small machine calculation times. An alternative to developing a new oscillatory-free model is the modification of an existing model. For example, a simple and practical (though rigorously unpleasing) approach is the numerical smoothing of the oscillations of an existing model at every streamwise station. Such a smoothing procedure could lead to significant improvements in the predicted boundary-layer parameters and to a reduction in computer time. Thus, if one has explicit and physically well-based ideas for the development of a smoothly behaved shear model which will accurately model the physical phenomena, then he should pursue these ideas. However, if one lacks such specific ideas, he would be well-advised to modify some existing shear model in an attempt to reduce its erratically behaved shear-stress profiles.

Previously it was noted that a significant improvement could be made in the CSM eddy-viscosity model if the constant K_1 was allowed to become a function of Mach number. However, due to a large degree of scatter in the calculated values, this functional form was not accurately defined. The accurate specification of this functional form then is obviously an area for further study. It might be possible, for example, to determine the functional form of K_1 from extensive experimental data for the turbulent shear stress and the corresponding mean velocity profiles. This approach should be pursued only after more extensive data is available for turbulent shear stress.

LIST OF REFERENCES

1. Cebeci, T., Smith, A.M.O., and Mosinskis, G., "Calculation of Compressible Adiabatic Turbulent Boundary Layers", AIAA Paper No. 69-687, 1969.

2. Boussinesq, J., "Theory de l'ecoulement Tourbillant", Mém. Prés. par div. Sav. 23, Paris, 1877.

3. Hinze, J. O., Turbulence: An Introduction to its Mechanism and Theory, McGraw-Hill Book Company, New York, 1959.

4. Clauser, F. H., "The Turbulent Boundary Layer", Advances in Applied Mechanics, 4, Academic Press, 1956.

5. Laufer, J., "Thoughts on Compressible Turbulent Boundary Layers", Compilation of Papers Presented at Symposium on Compressible Turbulent Boundary Layers, NASA-Langley Research Center, 1968.

6. Forsnes, V. G. and Abbott, D. E., "A Unified Comparison of Local and Global Turbulent Shear Stress Models Utilized in the Prediction of Two-Dimensional, Incompressible Turbulent Boundary Layers", Technical Report FMTR 69-4, School of Mechanical Engineering, Purdue University, 1969.

7. Alber, I. E. and Coats, D. E., "Analytical Investigations of Equilibrium and Nonequilibrium Compressible Turbulent Boundary Layers", Dynamic Science, Technical Report DYN-1-PU, 1969.

8. Herring, H. J. and Mellor, G. L., "A Method of Calculating Compressible Turbulent Boundary Layers", NASA CR-1144, 1968.

9. Kline, S. J., Morkovin, M. V., Sovran, G., and Cockrell, D. J., (eds.), Proceedings, Computation of Turbulent Boundary Layers - 1968 AFOSR-IFP Stanford Conference, Volume 1: Methods, Predictions, Evaluation and Flow Structure, Thermosciences Division, Department of Mechanical Engineering, Stanford University, 1968.

10. Cebeci, T., "The Behavior of Turbulent Flow Near a Porous Wall with Pressure Gradient", Douglas Aircraft Company, Report No. DAC 70014, 1969.

11. Cebeci, T., and Mosinskis, G. J., "Calculation of Heat and Mass Transfer in Turbulent Flows at Low Mach Numbers", Douglas Aircraft Company, Report No. DAC 70015, 1969.

12. Mellor, G. L., "The Effect of Pressure Gradients on Turbulent Flow Near a Smooth Wall", Journal of Fluid Mechanics, 24, 1966.

13. Van Driest, E. R., "On Turbulent Flow Near a Wall", Journal of the Aeronautical Sciences, 23, 1956.

14. Klebanoff, P. S., "Characteristics of Turbulence in a Boundary Layer with Zero Pressure Gradient", NACA TN 3178, 1954.

15. Laufer, J., "The Structure of Turbulence in Fully Developed Pipe Flow", NACA Report No. 1174, 1954.

16. Van Dyke, M., Perturbation Methods in Fluid Mechanics, Academic Press, New York, 1964.

17. Dvorac, F., Private Communication.

18. Coles, D. E. and Hirst, E. A., Proceedings, Computation of Turbulent Boundary Layers - 1968 AFOSR-IFP Stanford Conference, Volume II: Compiled Data, Thermosciences Division, Department of Mechanical Engineering, Stanford University, 1968.

19. Mellor, G. L. and Herring, H. J., "Two Methods of Calculating Turbulent Boundary-Layer Behavior Based on Numerical Solutions of the Equations of Motion", see Reference 9.

20. Michel, R., Quemard, C., and Durant, R., "Hypothesis on the Mixing Length and Application to the Calculation of the Turbulent Boundary Layers", see Reference 9.

21. Ng, K. H., Patankar, S. V., and Spalding, D. B., "The Hydrodynamic Turbulent Boundary Layer on a Smooth Wall, Calculated by a Finite-Difference Method", see Reference 9.

22. Cebeci, T., and Smith, A.M.O., "A Finite-Difference Solution of the Incompressible Turbulent Boundary-Layer Equations by an Eddy-Viscosity Concept", see Reference 9.

23. Cebeci, T. and Smith, A.M.O., "A Finite-Difference Solution of the Incompressible Turbulent Boundary-Layer Equations by an Eddy-Viscosity Concept", Douglas Aircraft Company, Report No. DAC-67130, 1968.

24. Coles, D. E., "Measurements in the Boundary Layer on a Smooth Flat Plate in Supersonic Flow, III. Measurements in a Flat Plate Boundary Layer at the Jet Propulsion Laboratory", Jet Propulsion Laboratory, California Insitiute of Technology, Report No. 20-71, 1953.

25. Bankston, C. A. and McEligot, D. M., "Turbulent and Laminar Heat Transfer to Gases with Varying Properties in the Entry Region of Circular Ducts", International Journal of Heat and Mass Transfer, 13, 1970.

26. Martellucci, A., Rie, H., and Sontowski, J. J., "Evaluation of Several Eddy Viscosity Models Through Comparison with Measurements in Hypersonic Flows", AIAA Paper No. 69-688, 1969.

27. Crocco, L., "Su di un Valore Massimo del Coefficiente di Transmissione del Calose da una Limina Piana a un Fluido Seconente", Rendiconti R. Accademia dei Lincei, 14, 1931.

28. Van Driest, E. R., "Turbulent Boundary Layer in Compressible Fluids", Journal of the Aeronautical Sciences, 18, 1951.

29. Bushnell, D. M., Johnson, C. B., Harvey, W. D., and Feller, W. F., "Comparison of Prediction Methods and Studies of Relaxation in Hypersonic Turbulent Nozzle-Wall Boundary Layers", NASA TN D-5433, 1969.

30. Matting, F. W., Chapman, D. R., Nyholm, J. R., and Thomas, A. G., "Turbulent Skin Friction at High Mach Numbers and Reynolds Numbers in Air and Helium", NASA TR R-82, 1961.

31. Schubauer, G. B. and Tchen, C. M., Turbulent Flow, No. 9, Princeton Aeronautical Paperbacks, Coleman DuP. Donaldson, General Editor, Princeton University Press, 1961.

32. Cebeci, T. and Smith, A.M.O., "Numerical Solution of the Turbulent Boundary Layer Equations", Douglas Aircraft Company, Report No. DAC 33735, 1967.

33. Schlichting, H., Boundary Layer Theory, Sixth Edition, McGraw-Hill Book Company, New York, 1968.

34. Goldberg, P., "Upstream History and Apparent Stress in Turbulent Boundary Layers", M.I.T. Gas Turbine Laboratory Report No. 85, 1966.

35. Cebeci, T., Lecture Notes.

36. Ludwieg, H., "Bestimung des Verhaltnisses der Austanschkoeffizienten fur Warme and Impuls bei Turbulenten", Grenzschichten, Z. Flugwiss, 4, 1956.

37. Johnson, D. S., "Velocity and Temperature Fluctuation Measurements in a Turbulent Boundary Layer Downstream of a Stepwise Discontinuity in Wall Temperature", Journal of Applied Mechanics Transactions ASME, Series E, 26, 1959.

38. Rotta, J. C., "Recent Developments in Calculation Methods for Turbulent Boundary Layers with Pressure Gradients and Heat Transfer", Journal of Applied Mechanics, Paper No. 66-APM-F, 1966.

39. Reynolds, W. C., "A Morphology of the Prediction Methods", see Reference 9.

40. Bethel, H. E. and Abbott, D. E., "On the Convergence and Exactness of Solutions of the Laminar Boundary Layer Equations Using the N-Parameter Integral Formulation of Galerkin-Kantorovich-Dorodnitsyn", Technical Report FMTR-66-2, School of Mechanical Engineering, Purdue University, 1966.

41. Koob, S. J. and Abbott, D. E., "An Integral Differential Difference Method Analysis of Viscous Flow Over an Impulsively Accelerated Semi-Infinite Plate", Technical Report FMTR-68-2, School of Mechanical Engineering, Purdue University, 1968.

42. Spalding, D. B., "Theories of the Turbulent Boundary Layer", Applied Mechanics Reviews, 20, 8, 1967.

43. Abbott, D. E., Deiwert, G. S., Forsnes, V. G., and Deboy, G. R., "Application of the Method of Weighted Residuals to the Turbulent Boundary Layer Equations; Part I: The Method of Weighted Residuals as a Solution Technique. Part II: A Two-Parameter Prediction Technique", see Reference 9.

44. Ero, M.I.O., "Shock Induced Unsteady Flow of a Compressible Real Gas Over a Flat Plate", Ph.D. Thesis, Purdue University, 1968.

45. Nielson, J. N., Goodwin, F. K., and Kuhn, G. D., "Review of the Method of Integral Relations Applied to Viscous Interaction Problems Including Separation", Nielson Engineering and Research, Inc., Paper No. 7, 1969.

46. Bossel, H. H., "Boundary Layer Computation by an N-Parameter Integral Method Using Exponentials", University of California, Santa Barbara, Report UCSB-ME-69-8. 1969.

47. Deiwert, G. S. and Abbott, D. E., "Analytical Prediction of the Incompressible Turbulent Boundary Layer with Arbitrary Pressure Distribution", Journal of Hydronautics, 4, 1, 1970.

48. Johnson, C. B. and Bushnell, D. M., "Power Law Velocity-Profile-Exponent Variations with Reynolds Number, Wall Cooling, and Mach Number in a Turbulent Boundary Layer", NASA TN D-5753, 1970.

49. Pasiuk, L., Hastings, S. M., and Chatham, R., "Experimental Reynolds Analogy Factor for a Compressible Turbulent Boundary Layer with a Pressure Gradient", NOLTR 64-200, 1965.

50. Winter, K. G., Smith, K. G., and Rotta, J. C., "Turbulent Boundary Layer Studies on a Waisted Body of Revolution in Subsonic and Supersonic Flow", AGARDograph 97, Part I, 1965.

51. Schultz-Grunow, F., "New Frictional Resistance Law for Smooth Plates", NACA TM 986, 1941.

52. Smith, D. W. and Walker, J. H., "Skin-Friction Measurements in Incompressible Flow", NACA TN 4231, 1958.

53. Ralston, A. and Wilf, H. S., Mathematical Methods for Digital Computers, Wiley, New York/London, 1960.

54. Bradshaw, P. and Ferris, D. H., "The Effect of Initial Conditions on the Development of Turbulent Boundary Layers", National Physical Laboratory, Aero Report 1223, 1967.

55. Chi, S. W. and Chang, C. C., "Effective Viscosity in a Turbulent Boundary Layer", AIAA Journal, 7, 1, 1969.

56. Ross, D. and Robertson, J. M., "Shear Stress in a Turbulent Boundary Layer", Journal of Applied Physics, 21, 6, 1950.

57. Hirst, E. A. and Reynolds, W. C., "An Integral Prediction Method for Turbulent Boundary Layers Using the Turbulent Kinetic Energy Equation", see Reference 9.

58. Bradshaw, P. and Ferriss, D. H., "Derivation of a Shear-Stress Transport Equation from the Turbulent Energy Equation", see Reference 9.

APPENDIX A

DIFFERENTIATION FORMULA FOR A FUNCTION TABULATED AT VARIABLY-SPACED VALUES OF THE ARGUMENT

A.1 Analysis

Assume a function is given at several points as shown in Figure A1. Let

$$\Delta r_+ = r_{i+1} - r_i \tag{A.1}$$

and

$$\Delta r_- = r_i - r_{i-1} \tag{A.2}$$

Now expanding W in a Taylor series about the point r_i and evaluating the series at r_{i-1} and r_{i+1} yields

$$W_{i-1} = W_i - \Delta r_- \frac{\partial W_i}{\partial r} + \frac{\Delta r_-^2}{2!} \frac{\partial^2 W_i}{\partial r^2} - \frac{\Delta r_-^3}{3!} \frac{\partial^3 W_i}{\partial r^3} + \ldots \tag{A.3}$$

and

$$W_{i+1} = W_i + \Delta r_+ \frac{\partial W_i}{\partial r} + \frac{\Delta r_+^2}{2!} \frac{\partial^2 W_i}{\partial r^2} + \frac{\Delta r_+^3}{3!} \frac{\partial^3 W_i}{\partial r^3} + \ldots \tag{A.4}$$

Combining equations (A.3) and (A.4) so as to eliminate the second order terms gives

$$\frac{\partial W_i}{\partial r} = \left[\frac{\Delta r_-}{\Delta r_+} W_{i+1} - \frac{\Delta r_+}{\Delta r_-} W_{i-1} + \left(\frac{\Delta r_+}{\Delta r_-} - \frac{\Delta r_-}{\Delta r_+} \right) W_i \right] \Big/ (\Delta r_- + \Delta r_+)$$
$$- \frac{\Delta r_- \, \Delta r_+}{3!} \frac{\partial^3 W_i}{\partial r^3} + \ldots . \tag{A.5}$$

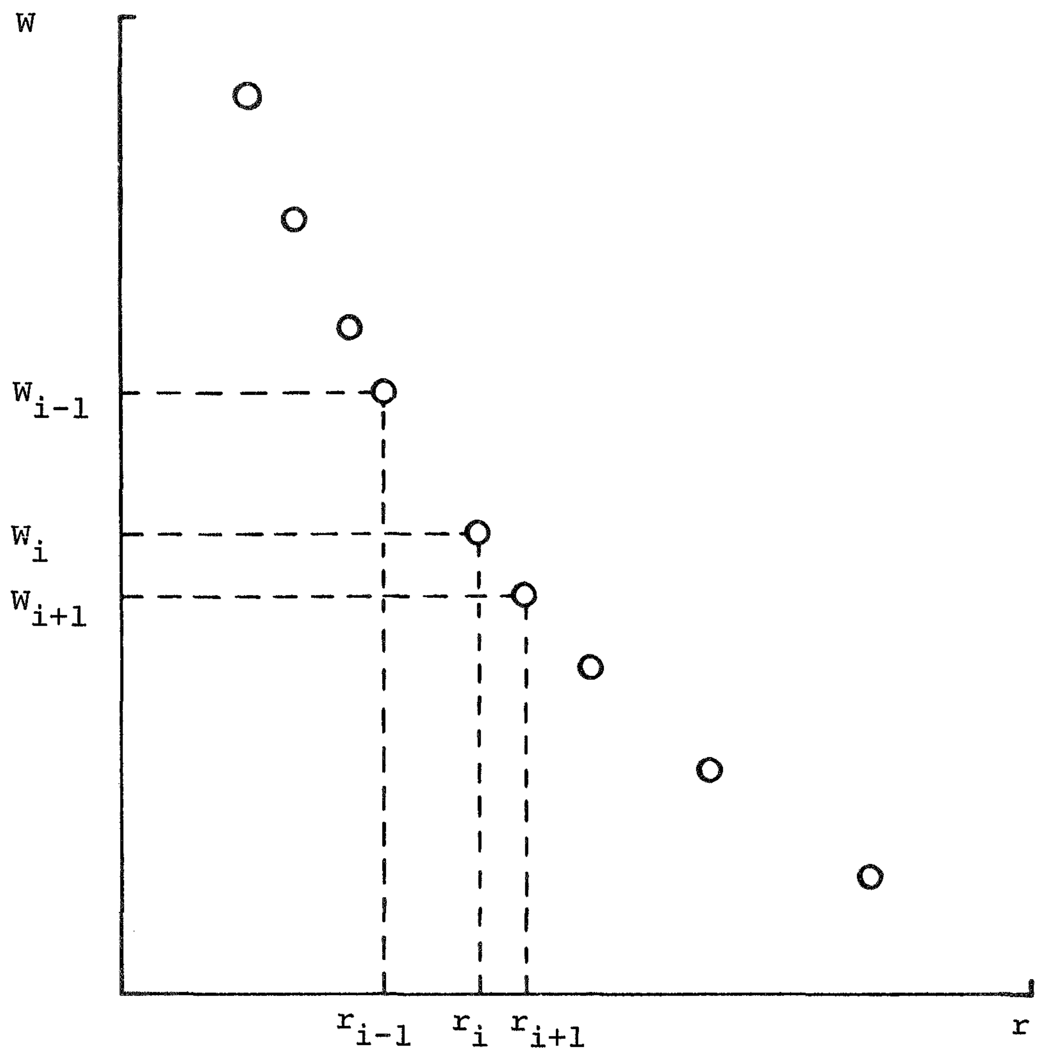

Figure A1: A Function Specified at a Discrete Number of Variably Spaced Points where the remainder or error term is

$$\frac{\Delta r_- \, \Delta r_+}{3!} \, \frac{\partial^3 W(S)}{\partial r^3} \tag{A.6}$$

and

$$r_{i-1} < S < r_{i+1} \tag{A.7}$$

Thus, equation (A.5) without the third derivative term is a second-order differentiation scheme, since the error is proportional to the product of two spacings of the argument variable.

Equation (A.5) was used to calculate the first derivative of tabular, experimental, velocity profiles at all the interior data points while the derivative on the wall was calculated from the measured skin-friction value, and the derivative at the last data point was taken to be zero.

APPENDIX B

COMPUTER PROGRAM

```
36536,DEBOY,T200,CM 60000,P20,L11000.
MAP(ON)
RUN(S).
LGO.
'
      PROGRAM MAIN(INPUT,OUTPUT,TAPE5=INPUT,TAPE6=OUTPUT)
C
C     THE MAIN PROGRAM IS USED TO READ IN DATA,EVALUATE DEFINITE
C     INTEGRALS, PERFORM MATRIX MANIPULATIONS, AND SET UP THE
C     INTEGRATION LOGIC
C
      DIMENSION AINV(49),AINVSH(7),F(50),U(50),FCT(50),QINT(50),
     1    A(7,7),ASINGL(49),LWORK(7),MWORK(7),SHINT(7),C(7),
     2    PRMT(5),DERC(7),AUX(16,7),PHIO(50),POLLEG(8)
      EXTERNAL DERIV,OUTP
      COMMON B1INIT,AINV,SHINT,CFINIT,REOX,QL,ICOUNT,NU,U,F,TE,UE,N,TO,
     1    QMUE,ROE,REINF,TW,QME,GAMMA,QMUW,ROW,RESUBX,CF,A,XSUBO,PHIO
      COMMON QK1,RE1,RE2
      READ(5,503) N,NU,QL,XSUBO
      READ(5,504) QME,CFO,QMOMTO,TW
      READ(5,504) TE,PE,TO,GAMMA
      READ(5,504) RGAS,CSUBP,QK1
      READ(5,504) RE1,RE2
      READ(5,502) (F(I),I=1,NU)
      READ(5,502) (U(I),I=1,NU)
C
C     N= ORDER OF THE MWR APPROXIMATION
C     NU= NUMBER OF POINTS AT WHICH F(I) IS ENTERED
C     QL= FINAL VALUE OF LONGITUDINAL COORDINATE, FT
C     XSUBO= INITIAL VALUE OF LONGITUDINAL COORDINATE, FT
C     QME= FREE STREAM MACH NUMBER
C     CFO= INITIAL VALUE OF CF
C     QMOMTO= INITIAL VALUE OF MOMENTUM THICKNESS, FT
C     TW= WALL TEMPERATURE,DEGREES R
C     TE=FREE STREAM TEMPERATURE, DEGREES R
C     PE= FREE STREAM PRESSURE LB/FT**2
C     TO= TOTAL TEMPERATURE IN THE FREE STREAM, DEGREES R
C     GAMMA= RATIO OF SPECIFIC HEATS
C     RGAS= GAS CONSTANT, FT-LBF/LBM-R
C      CSUBP= SPECIFIC HEAT AT CONSTANT PRESSURE, BTU/LBM-R
C     QK1= OPTIMUM VALUE OF THE CONSTANT K1 IN EQUATION (2.12)
C     RE1 AND RE2= DOWNSTREAM VALUES OF REYNOLDS NUMBER (BASED ON X)
C     WHERE VELOCITY PROFILE AND MACH NUMBER PROFILE OUTPUTS ARE
C     DESIRED
C     F= INITIAL VELOCITY PROFILE FUNCTION IN EQUATION (3.39)
C     U= NONDIMENSIONALIZED VELOCITY VALUES
C
    2 NM1=N-1
      ICOUNT=-1
C
C     CALCULATE FLUID AND FLOW PROPERTIES
C
      QMUE=3.59E-7*(TE/492.)**1.5*684./(TE+192.)
      QMUW=3.59E-7*(TW/492.)**1.5*684./(TW+192.)
      UE=QME*49.02*SQRT(TE)
      ROE=PE/RGAS/TE/32.2
      ROW=TE/TW*ROE
      REINF=ROE*UE*QL/QMUE
      QQQ=2.*QMUW*SQRT(REINF)*ROW/ROE/ROE/UE/QL
C
C     WRITE FLUID AND FLOW PROPERTIES
C
      WRITE(6,600) NU
```

```
      ~~WRITE(6,613)~~
      WRITE(6,610) TE,UE,PE,ROE,ROW,REINF
      WRITE(6,601)
      WRITE(6,602) (F(I),U(I),I=1,NU)
C
C     SET INITIAL CONDITIONS ON THE C(J) COEFFICIENTS
C
      C(1)=1.0
      IF(N.EQ.1) GO TO 40
      DO 33 I=2,N
   33 C(I)=0.0
   40 CONTINUE
C
C     EVALUATE DEFINITE INTEGRALS AND MATRICES AND PERFORM NECESSARY
C     MATRIX MULTIPLICATION AND INVERSION
C
      DO 32 I=1,N
      DO 31 J=1,N
      DO 30 K=1,NU
      TWOUM1=2.*U(K)-1.0
      IF(I.GE.J) MAX=I-1
      IF(J.GE.I) MAX=J-1
      CALL LEP(POLLEG,TWOUM1,MAX)
   30 FCT(K)=POLLEG(I)*POLLEG(J)*U(K)*F(K)
      CALL QTFG(U,FCT,QINT,NU)
   31  A(I,J)=QINT(NU)
   32 CONTINUE
      DO 20 I=1,NU
   20  PHIO(I)=F(I)
      WRITE(6,603)
      WRITE(6,604) ((A(I,J),I=1,N),J=1,N)
      CALL ARRAY(2,N,N,7,7,ASINGL,A)
      WRITE(6,605)
      NSQ=N**2
      WRITE(6,604) (ASINGL(I),I=1,NSQ)
      CALL MINV(ASINGL,N,DET,LWORK,MWORK)
C    NOW ASINGL IS THE INVERSE OF A
     DO 14 I=1,NSQ
   14 AINV(I)=ASINGL(I)
      WRITE(6,606)
      WRITE(6,604) (AINV(I),I=1,NSQ)
      SHINT(1)=0.0
      B1INIT=ROW/ROE*QMUW/QMUE
      CFINIT = QQQ
      REOX=ROE*UE/QMUE
      WRITE(6,609) B1INIT,CFINIT,REOX
C
C     SPECIFY PARAMETERS REQUIRED TO CALL HPCG, AND CALL HPCG
C
      PRMT(1)=XSUBO/QL
      PRMT(2)=1.0
      PRMT(3)=.001
      PRMT(4)=.01*C(1)
      QN=N
      DO 34 I=1,N
   34 DERC(I)=1./QN
      CALL HPCG(PRMT,C,DERC,N,IHLF,DERIV,OUTP,AUX)
C
C     LIST ALL INPUT AND OUTPUT FORMATS
C
  600 FORMAT(//,10X,3HNU=,1I3,//)
  601 FORMAT(/,15X,1HF,19X,1HU,/)
  602 FORMAT(2F20.6)
  603 FORMAT(///,9X,6HA(I,J),/)
  604 FORMAT(1E20.6)
  605 FORMAT(///,9X,6HASINGL,/)
```

```
606   FORMAT(///,9X,4HAINV,/)
607   FORMAT(///,15X,5HSHINT,14X,6HAINVSH,/)
608   FORMAT(2E20.6)
609   FORMAT(///,3X,7HB1INIT=,1E14.6,10X,7HCFINIT=,1E14.6,
    1      10X,5HREOX=,1E14.6,//)
610   FORMAT(1X,6E19.6)
613   FORMAT(//,18X,2HTE,17X,2HUE,17X,2HPE,16X,3HROE,16X,3HROW,
    1      14X,5HREINF)
501   FORMAT(1I20)
502   FORMAT(4F20.6)
503   FORMAT(2I20,2F20.2)
504   FORMAT(4F20.2)
      N=N+1
      END
C
C     SUBROUTINE DERIV CONTAINS THE ORDINARY DIFFERENTIAL EQUATIONS
C     FOR THE C(J) COEFFICIENTS AND EVALUATES ALL TERMS IN THESE
C     ORDINARY DIFFERENTIAL EQUATIONS
C
      SUBROUTINE DERIV(ZET,C,DERC)
      DIMENSION AINV(49),AINVSH(7),B(7),C(7),AINVB(7),DERC(7),
    1      SHINT(7),U(50),F(50),A(7,7),PHIO(50)
      COMMON B1INIT,AINV,SHINT,CFINIT,REOX,QL,ICOUNT,NU,U,F,TE,UE,N,TO,
    1      QMUE,ROE,REINF,TW,QME,GAMMA,QMUW,ROW,RESUBX,CF,A,XSUBO,PHIO
      COMMON QK1,RE1,RE2
      CJPHIO=0.0
      DO 12 J=1,N
   12 CJPHIO=CJPHIO+C(J)*(-1.0)**(J-1)*PHIO(1)
      DO 11 I=1,N
   11  B(I)=-HIPO(I)*B1INIT/CJPHIO
      CALL GMPRD(AINV,B,AINVB,N,N,1)
      RESUBX=REOX*(ZET*QL)
      CF=CFINIT/CJPHIO
      CALL SHINTE(C)
      CALL GMPRD(AINV,SHINT,AINVSH,N,N,1)
      DO 10 J=1,N
   10 DERC(J)=AINVB(J)-AINVSH(J)
C
C     WRITE DESIRED OUTPUT VARIABLES
C
      IF(ICOUNT.EQ.0) Z=ICOUNT
      IF(ZET.LT.Z) GO TO 33
      WRITE(6,602) ZET
      WRITE(6,603) (SHINT(I),I=1,N)
      WRITE(6,600)
      WRITE(6,601) (B(I),AINVB(I),AINVSH(I),DERC(I),C(I),I=1,N)
      Z=ZET+.01
   33 CONTINUE
  600 FORMAT(12X,1HB,21X,5HAINVB,15X,6HAINVSH,15X,4HDERC,15X,1HC,/)
  601 FORMAT(5E20.6)
  602 FORMAT(//,1X,4HZET=,1F12.6)
  603 FORMAT(1X,6HSHINT=,1F6.2)
      RETURN
      END
C
C     SUBROUTINE OUTP EVALUATES AND WRITES DESIRED OUTPUT VARIABLES
C
      SUBROUTINE OUTP(ZET,C,DERC,IHLF,NDIM,PRMT)
      DIMENSION C(7),DERC(7),PRMT(5),AINV(49),ROSTTH(50),U(50),F(50),
    1      T(50),TOTE(50),QMUOMU(50),FCT(50),ROSTAR(50),QNEW(50),
    2      THETA(50),QINT(50),Y(50),QNEWE(50),QNUEON(50),  SHFCT(50),
    3      CHI(50),X(50),SHINT(7),A(7,7),PHIO(50)
      COMMON B1INIT,AINV,SHINT,CFINIT,REOX,QL,ICOUNT,NU,U,F,TE,UE,N,TO,
    1      QMUE,ROE,REINF,TW,QME,GAMMA,QMUW,ROW,RESUBX,CF,A,XSUBO,PHIO
      COMMON QK1,RE1,RE2
      PRMT(4)=.01*C(1)
```

```
      CJPHI0=0.0
      DO 12 J=1,N
   12 CJPHI0=CJPHI0+C(J)*(-1.0)**(J-1)*PHI0(1)
      CF=CFINIT/CJPHI0
      CJA1J=0.0
      DO 13 J=1,N
   13 CJA1J=CJA1J+C(J)*A(1,J)
      QMOMTH=QL/SQRT(REINF)*CJA1J
      RESUBX=REOX*(ZET*QL)
      IF(ICOUNT.EQ.0) Z=ICOUNT
      IF(ZET.LT.Z) GO TO 32
      Z=ZET+.01
      WRITE(6,660) RESUBX,CF,ZET,QMOMTH
  660 FORMAT(/,35X,7HRESUBX=,1E14.6,10X,3HCF=,1E14.6,10X,4HZET=,
     1    1F12.6,4X,7HQMOMTH=,1E14.6)
      WRITE(6,661) IHLF
  661 FORMAT(10X,5HIHLF=,1I2)
   32 CONTINUE
      RETURN
      END
C
C     SUBROUTINE SHINTE EVALUATES THE SHINT(J) VECTOR REQUIRED IN
C     SUBROUTINE DERIV
C
      SUBROUTINE SHINTE(C)
      DIMENSION ROSTTH(50),C(7),U(50),F(50),T(50),TOTE(50),
     1    ROSTAR(50),THETA(50),QINT(50),Y(50),ETA(50),UOUE(50),
     2    QMUOMU(50),FCT(50),ROOROE(50),QNU(50),
     3 SHFCT(50),SHINT(7),AINV(49),A(7,7),DUDY(50),EPI(50),
     4    EPO(50),EP(50),BETA(50),PHI0(50),TAU(50),QMOME(50)
      DIMENSION TAUO(50),TAUI(50),TAUIYM(50)
      COMMON B1INIT,AINV,SHINT,CFINIT,REOX,QL,ICOUNT,NU,U,F,TE,UE,N,TO,
     1    QMUE,ROE,REINF,TW,QME,GAMMA,QMUW,ROW,RESUBX,CF,A,XSUBO,PHI0
      COMMON QK1,RE1,RE2
C
C     EVALUATE FLOW VARIABLES REQUIRED BY THE EDDY-VISCOSITY MODEL
C
      NM1=N-1
      DO 13 I=1,NU
      ZZZ=2.*U(I)-1.
      CALL LEP(QINT,ZZZ,NM1)
      CJPJM1=0.0
      DO 10 J=1,N
   10 CJPJM1=CJPJM1+C(J)*QINT(J)
      ROSTTH(I)=CJPJM1*PHI0(I)/(1.-U(I))
      T(I)=TW*(1.+(TO/TW-1.)*U(I)+(TE/TO-1.)*TO/TW*U(I)**2)
      TOTE(I)=T(I)/TE
      ROSTAR(I)=1./TOTE(I)
   13 THETA(I)=ROSTTH(I)/ROSTAR(I)
      CALL QTFG(U,THETA,QINT,NU)
      DO 12 I=1,NU
   12 Y(I)=QL/SQRT(REINF)*QINT(I)
      NDATA=NU
      QNUW=QMUW/ROW
      X=RESUBX/REOX
      QNUE=QMUE/ROE
      NTOTAL=NDATA
      DO 14 I=1,NTOTAL
      ETA(I)=SQRT(REINF)/QL*Y(I)
      UOUE(I)=U(I)
      QMUOMU(I)=3.59E-7/QMUE*(T(I)/492.)**1.5*684./(T(I)+192.)
      FCT(I)=1.-UOUE(I)
      TOTE(I)=T(I)/TE
      ROOROE(I)=1./TOTE(I)
   14 QNU(I)=QMUOMU(I)*QMUE/(ROOROE(I)*ROE)
      CALL QTFG(Y,FCT,QINT,NTOTAL)
```

```
      DELKST=QINT(NTOTAL)
      DO 15 I=1,NDATA
   15  FCT(I)=1.-ROOROE(I)*UOUE(I)
      CALL QTFG(Y,FCT,QINT,NTOTAL)
      DELST=QINT(NTOTAL)
      DO 16 I=1,NDATA
   16  DUDY(I)=UE*SQRT(REINF)/QL/THETA(I)
      TAUW=DUDY(1)*QMUOMU(1)*QMUE
C
C     EVALUATE THE EDDY-VISCOSITY PROFILE FROM THE CSM EDDY-VISCOSITY
C     MODEL
C
      DO 17 I=1,NDATA
      EPI(I)=QK1**2*Y(I)**2*(1.0-EXP(-Y(I)/26./QNU(I)*
     1     (TAUW/ROOROE(I)/ROE)**.5))**2*DUDY(I)
      EPO(I)=.0168*UE*DELKST/(1.0+5.5*(Y(I)/Y(NDATA-1))**6)
      IF(EPI(I).LT.EPO(I)) EP(I)=EPI(I)
      IF (EPI(I).GE.EPO(I))  EP(I)=EPO(I)
   17 BETA(I)=1.0+EP(I)/QNU(I)
C
C     EVALUATE THE SHINT(J) VECTOR
C
      DO 30 J=1,N
      DO 31 I=1,NU
      ZZZ=2.*U(I)-1.
   31 SHFCT(I)=QMUOMU(I)*BETA(I)/THETA(I)*HI2P(J,ZZZ)
      CALL QTFG(UOUE,SHFCT,QINT,NTOTAL)
   30 SHINT(J)=QINT(NTOTAL)
      ICOUNT=ICOUNT+1
      IF(ICOUNT.NE.0) GO TO 19
   20  WRITE(6,623)
      DO 18 I=1,NDATA
      QINT(I)=QMUOMU(I)*QMUE*BETA(I)*DUDY(I)
   18  QMOME(I)=UOUE(I)*SQRT(1./TOTE(I))
C
C     WRITE DESIRED PROFILES AND VARIABLES
C
      WRITE(6,624) (DUDY(I),EPI(I),EPO(I),Y(I),UOUE(I),
     1     QINT(I),QMOME(I),I=1,NDATA)
  623  FORMAT(//,16X,4HDUDY,16X,3HEPI,16X,3HEPO,17X,1HY,16X,
     1     4HUOUE,14X,3HTAU,7X,5HQMOME,/)
  624  FORMAT(1X,6E19.6,1F10.4)
      WRITE(6,622) SHINT(2),DELST
      GO TO 21
  622 FORMAT(10X,6HSHINT=,1E20.4,40X,6HDELST=,1E20.4)
   19  CONTINUE
      IF(RESUBX.GE.RE1.AND.RESUBX.LE.(RE1+.2E6)) GO TO 20
      IF(RESUBX.GE.RE2.AND.RESUBX.LE.(RE2+.2E6)) GO TO 20
   21  CONTINUE
      RETURN
      END
C
C     FUNCTION HI2P CALCULATES THE SECOND DERIVATIVE OF THE WEIGHTING
C     FUNCTION HSUBI WHERE X= 2*UOUE-1.  THIS FUNCTION IS APPLICABLE
C     UP TO AND INCLUDING THE SIXTH APPROXIMATION.
C
      FUNCTION HI2P(I,X)
      GO TO(10,20,30,40,50,60,70),I
   10 HI2P=0.0
      RETURN
   20 HI2P=-4.0
      RETURN
   30 HI2P=6.-18.*X
      RETURN
   40 HI2P=30.*X-60.*X**2+6.
      RETURN
```

```
   50 HI2P=0.25*(420.*X**2-60.-700.*X**3+180.*X)
      RETURN
   60 HI2P=.25*(1260.*X**3-420.*X-1890.*X**4+840.*X**2-30.)
      RETURN
   70 CONTINUE
      RETURN
      END
C
C     FUNCTION HIPO EVALUATES THE FIRST DERIVATIVE OF THE WEIGHTING
C     FUNCTION HSUBI AT UOUE= 0.  THIS FUNCTION IS APPLICABLE UP TO
C     AND INCLUDING THE SIXTH APPROXIMATION.
C
      FUNCTION HIPO(I)
      GO TO(10,20,30,40,50,60,70),I
   10 HIPO=-1.
      RETURN
   20 HIPO=3.
      RETURN
   30 HIPO=-7.
      RETURN
   40 HIPO=13.
      RETURN
   50  HIPO=-21.
      RETURN
   60 HIPO=31.
      RETURN
   70 CONTINUE
      RETURN
      END
C
C     THE FOLLOWING SUBROUTINES WERE OBTAINED FROM THE SUBROUTINE
C     LIBRARY OF THE PURDUE UNIVERSITY COMPUTER CENTER
C
C                                                                       MINV 001
C     ..................................................................MINV 002
C                                                                       MINV 003
C        SUBROUTINE MINV                                                MINV 004
C                                                                       MINV 005
C        PURPOSE                                                        MINV 006
C           INVERT A MATRIX                                             MINV 007
C                                                                       MINV 008
C        USAGE                                                          MINV 009
C           CALL MINV(A,N,D,L,M)                                        MINV 010
C                                                                       MINV 011
C        DESCRIPTION OF PARAMETERS                                      MINV 012
C           A - INPUT MATRIX, DESTROYED IN COMPUTATION AND REPLACED BY  MINV 013
C               RESULTANT INVERSE.                                      MINV 014
C           N - ORDER OF MATRIX A                                       MINV 015
C           D - RESULTANT DETERMINANT                                   MINV 016
C           L - WORK VECTOR OF LENGTH N                                 MINV 017
C           M - WORK VECTOR OF LENGTH N                                 MINV 018
C                                                                       MINV 019
C        REMARKS                                                        MINV 020
C           MATRIX A MUST BE A GENERAL MATRIX                           MINV 021
C                                                                       MINV 022
C        SUBROUTINES AND FUNCTION SUBPROGRAMS REQUIRED                  MINV 023
C           NONE                                                        MINV 024
C                                                                       MINV 025
C        METHOD                                                         MINV 026
C           THE STANDARD GAUSS-JORDAN METHOD IS USED. THE DETERMINANT   MINV 027
C           IS ALSO CALCULATED. A DETERMINANT OF ZERO INDICATES THAT    MINV 028
C           THE MATRIX IS SINGULAR.                                     MINV 029
C                                                                       MINV 030
C                                                                       MINV 032
      SUBROUTINE MINV(A,N,D,L,M)                                        MINV 033
      DIMENSION A(1),L(1),M(1)                                          MINV 034
```

```
C
C        ...............................................................
C
C        IF A DOUBLE PRECISION VERSION OF THIS ROUTINE IS DESIRED, THE
C        C IN COLUMN 1 SHOULD BE REMOVED FROM THE DOUBLE PRECISION
C        STATEMENT WHICH FOLLOWS.
C
C     DOUBLE PRECISION A,D,BIGA,HOLD
C
C        THE C MUST ALSO BE REMOVED FROM DOUBLE PRECISION STATEMENTS
C        APPEARING IN OTHER ROUTINES USED IN CONJUNCTION WITH THIS
C        ROUTINE.
C
C        THE DOUBLE PRECISION VERSION OF THIS SUBROUTINE MUST ALSO
C        CONTAIN DOUBLE PRECISION FORTRAN FUNCTIONS.  ABS IN STATEMENT
C        10 MUST BE CHANGED TO DABS.
C
C        ...............................................................
C
C        SEARCH FOR LARGEST ELEMENT
C
      D=1.0
      NK=-N
      DO 80 K=1,N
      NK=NK+N
      L(K)=K
      M(K)=K
      KK=NK+K
      BIGA=A(KK)
      DO 20 J=K,N
      IZ=N*(J-1)
      DO 20 I=K,N
      IJ=IZ+I
   10 IF( ABS(BIGA)- ABS(A(IJ))) 15,20,20
   15 BIGA=A(IJ)
      L(K)=I
      M(K)=J
   20 CONTINUE
C
C        INTERCHANGE ROWS
C
      J=L(K)
      IF(J-K) 35,35,25
   25 KI=K-N
      DO 30 I=1,N
      KI=KI+N
      HOLD=-A(KI)
      JI=KI-K+J
      A(KI)=A(JI)
   30 A(JI) =HOLD
C
C        INTERCHANGE COLUMNS
C
   35 I=M(K)
      IF(I-K) 45,45,38
   38 JP=N*(I-1)
      DO 40 J=1,N
      JK=NK+J
      JI=JP+J
      HOLD=-A(JK)
      A(JK)=A(JI)
   40 A(JI) =HOLD
C
C        DIVIDE COLUMN BY MINUS PIVOT (VALUE OF PIVOT ELEMENT IS
C        CONTAINED IN BIGA)
C
```

```
   45 IF(BIGA) 48,46,48
   46 D=0.0
      RETURN
   48 DO 55 I=1,N
      IF(I-K) 50,55,50
   50 IK=NK+I
      A(IK)=A(IK)/(-BIGA)
   55 CONTINUE
C
C        REDUCE MATRIX
C
      DO 65 I=1,N
      IK=NK+I
      HOLD=A(IK)
      IJ=I-N
      DO 65 J=1,N
      IJ=IJ+N
      IF(I-K) 60,65,60
   60 IF(J-K) 62,65,62
   62 KJ=IJ-I+K
      A(IJ)=HOLD*A(KJ)+A(IJ)
   65 CONTINUE
C
C        DIVIDE ROW BY PIVOT
C
      KJ=K-N
      DO 75 J=1,N
      KJ=KJ+N
      IF(J-K) 70,75,70
   70 A(KJ)=A(KJ)/BIGA
   75 CONTINUE
C
C        PRODUCT OF PIVOTS
C
      D=D*BIGA
C
C        REPLACE PIVOT BY RECIPROCAL
C
      A(KK)=1.0/BIGA
   80 CONTINUE
C
C        FINAL ROW AND COLUMN INTERCHANGE
C
      K=N
  100 K=(K-1)
      IF(K) 150,150,105
  105 I=L(K)
      IF(I-K) 120,120,108
  108 JQ=N*(K-1)
      JR=N*(I-1)
      DO 110 J=1,N
      JK=JQ+J
      HOLD=A(JK)
      JI=JR+J
      A(JK)=-A(JI)
  110 A(JI) =HOLD
  120 J=M(K)
      IF(J-K) 100,100,125
  125 KI=K-N
      DO 130 I=1,N
      KI=KI+N
      HOLD=A(KI)
      JI=KI-K+J
      A(KI)=-A(JI)
  130 A(JI) =HOLD
      GO TO 100
```

```
 150 RETURN                                                              MINV 166
     END                                                                 MINV 167
C                                                                        GMPRD003
C       SUBROUTINE GMPRD                                                 GMPRD004
C                                                                        GMPRD005
C       PURPOSE                                                          GMPRD006
C          MULTIPLY TWO GENERAL MATRICES TO FORM A RESULTANT GENERAL     GMPRD007
C          MATRIX                                                        GMPRD008
C                                                                        GMPRD009
C       USAGE                                                            GMPRD010
C          CALL GMPRD(A,B,R,N,M,L)                                       GMPRD011
C                                                                        GMPRD012
C       DESCRIPTION OF PARAMETERS                                        GMPRD013
C          A - NAME OF FIRST INPUT MATRIX                                GMPRD014
C          B - NAME OF SECOND INPUT MATRIX                               GMPRD015
C          R - NAME OF OUTPUT MATRIX                                     GMPRD016
C          N - NUMBER OF ROWS IN A                                       GMPRD017
C          M - NUMBER OF COLUMNS IN A AND ROWS IN B                      GMPRD018
C          L - NUMBER OF COLUMNS IN B                                    GMPRD019
C                                                                        GMPRD020
C       REMARKS                                                          GMPRD021
C          ALL MATRICES MUST BE STORED AS GENERAL MATRICES               GMPRD022
C          MATRIX R CANNOT BE IN THE SAME LOCATION AS MATRIX A           GMPRD023
C          MATRIX R CANNOT BE IN THE SAME LOCATION AS MATRIX B           GMPRD024
C          NUMBER OF COLUMNS OF MATRIX A MUST BE EQUAL TO NUMBER OF ROWGMPRD025
C          OF MATRIX B                                                   GMPRD026
C                                                                        GMPRD027
C       SUBROUTINES AND FUNCTION SUBPROGRAMS REQUIRED                    GMPRD028
C          NONE                                                          GMPRD029
C                                                                        GMPRD030
C       METHOD                                                           GMPRD031
C          THE M BY L MATRIX B IS PREMULTIPLIED BY THE N BY M MATRIX A   GMPRD032
C          AND THE RESULT IS STORED IN THE N BY L MATRIX R.              GMPRD033
C                                                                        GMPRD034
C     ..................................................................GMPRD035
C                                                                        GMPRD036
      SUBROUTINE GMPRD(A,B,R,N,M,L)                                      GMPRD037
      DIMENSION A(1),B(1),R(1)                                           GMPRD038
C                                                                        GMPRD039
      IR=0                                                               GMPRD040
      IK=-M                                                              GMPRD041
      DO 10 K=1,L                                                        GMPRD042
      IK=IK+M                                                            GMPRD043
      DO 10 J=1,N                                                        GMPRD044
      IR=IR+1                                                            GMPRD045
      JI=J-N                                                             GMPRD046
      IB=IK                                                              GMPRD047
      R(IR)=0                                                            GMPRD048
      DO 10 I=1,M                                                        GMPRD049
      JI=JI+N                                                            GMPRD050
      IB=IB+1                                                            GMPRD051
   10 R(IR)=R(IR)+A(JI)*B(IB)                                            GMPRD052
      RETURN                                                             GMPRD053
      END                                                                GMPRD054
C                                                                        ARRAY001
C     ..................................................................ARRAY002
C                                                                        ARRAY003
C        SUBROUTINE ARRAY                                                ARRAY004
C                                                                        ARRAY005
C        PURPOSE                                                         ARRAY006
C           CONVERT DATA ARRAY FROM SINGLE TO DOUBLE DIMENSION OR VICE   ARRAY007
C           VERSA.  THIS SUBROUTINE IS USED TO LINK THE USER PROGRAM     ARRAY008
C           WHICH HAS DOUBLE DIMENSION ARRAYS AND THE SSP SUBROUTINES    ARRAY009
C           WHICH OPERATE ON ARRAYS OF DATA IN A VECTOR FASHION.         ARRAY010
C                                                                        ARRAY011
C        USAGE                                                           ARRAY012
```

```
C           CALL ARRAY (MODE,I,J,N,M,S,D)
C
C        DESCRIPTION OF PARAMETERS
C           MODE - CODE INDICATING TYPE OF CONVERSION
C                     1 - FROM SINGLE TO DOUBLE DIMENSION
C                     2 - FROM DOUBLE TO SINGLE DIMENSION
C           I    - NUMBER OF ROWS IN ACTUAL DATA MATRIX
C           J    - NUMBER OF COLUMNS IN ACTUAL DATA MATRIX
C           N    - NUMBER OF ROWS SPECIFIED FOR THE MATRIX D IN
C                  DIMENSION STATEMENT
C           M    - NUMBER OF COLUMNS SPECIFIED FOR THE MATRIX D IN
C                  DIMENSION STATEMENT
C           S    - IF MODE=1, THIS VECTOR CONTAINS, AS INPUT, A DATA
C                  MATRIX OF SIZE I BY J IN CONSECUTIVE LOCATIONS
C                  COLUMN-WISE.  IF MODE=2, IT CONTAINS A DATA MATRIX
C                  OF THE SAME SIZE AS OUTPUT.  THE LENGTH OF VECTOR S
C                  IS IJ, WHERE IJ=I*J.
C           D    - IF MODE=1, THIS MATRIX (N BY M) CONTAINS, AS OUTPUT,
C                  A DATA MATRIX OF SIZE I BY J IN FIRST I ROWS AND
C                  J COLUMNS.  IF MODE=2, IT CONTAINS A DATA MATRIX OF
C                  THE SAME SIZE AS INPUT.
C
C        REMARKS
C           VECTOR S CAN BE IN THE SAME LOCATION AS MATRIX D.  VECTOR S
C           IS REFERRED AS A MATRIX IN OTHER SSP ROUTINES, SINCE IT
C           CONTAINS A DATA MATRIX.
C           THIS SUBROUTINE CONVERTS ONLY GENERAL DATA MATRICES (STORAGE
C           MODE OF 0).
C
C        SUBROUTINES AND FUNCTION SUBROUTINES REQUIRED
C           NONE
C
C        METHOD
C           REFER TO THE DISCUSSION ON VARIABLE DATA SIZE IN THE SECTION
C           DESCRIBING OVERALL RULES FOR USAGE IN THIS MANUAL.
C
C     ..................................................................
C
      SUBROUTINE ARRAY (MODE,I,J,N,M,S,D)
      DIMENSION S(1),D(1)
C
      NI=N-I
C
C        TEST TYPE OF CONVERSION
C
      IF(MODE-1) 100, 100, 120
C
C        CONVERT FROM SINGLE TO DOUBLE DIMENSION
C
  100 IJ=I*J+1
      NM=N*J+1
      DO 110 K=1,J
      NM=NM-NI
      DO 110 L=1,I
      IJ=IJ-1
      NM=NM-1
  110 D(NM)=S(IJ)
      GO TO 140
C
C        CONVERT FROM DOUBLE TO SINGLE DIMENSION
C
  120 IJ=0
      NM=0
      DO 130 K=1,J
      DO 125 L=1,I
      IJ=IJ+1
```

```
      NM=NM+1                                                           ARRAY079
  125 S(IJ)=D(NM)                                                       ARRAY080
  130 NM=NM+NI                                                          ARRAY081
C                                                                       ARRAY082
  140 RETURN                                                            ARRAY083
      END                                                               ARRAY084
C                                                                       TFG 001
C     ..................................................................TFG 002
C                                                                       TFG 003
C        SUBROUTINE QTFG                                                TFG 004
C                                                                       TFG 005
C        PURPOSE                                                        TFG 006
C           TO COMPUTE THE VECTOR OF INTEGRAL VALUES FOR A GIVEN        TFG 007
C           GENERAL TABLE OF ARGUMENT AND FUNCTION VALUES.              TFG 008
C                                                                       TFG 009
C        USAGE                                                          TFG 010
C           CALL QTFG (X,Y,Z,NDIM)                                      TFG 011
C                                                                       TFG 012
C        DESCRIPTION OF PARAMETERS                                      TFG 013
C           X      - THE INPUT VECTOR OF ARGUMENT VALUES.               TFG 014
C           Y      - THE INPUT VECTOR OF FUNCTION VALUES.               TFG 015
C           Z      - THE RESULTING VECTOR OF INTEGRAL VALUES. Z MAY BE  TFG 016
C                    IDENTICAL WITH X OR Y.                             TFG 017
C           NDIM   - THE DIMENSION OF VECTORS X,Y,Z.                    TFG 018
C                                                                       TFG 019
C        REMARKS                                                        TFG 020
C           NO ACTION IN CASE NDIM LESS THAN 1.                         TFG 021
C                                                                       TFG 022
C        SUBROUTINES AND FUNCTION SUBPROGRAMS REQUIRED                  TFG 023
C           NONE                                                        TFG 024
C                                                                       TFG 025
C        METHOD                                                         TFG 026
C           BEGINNING WITH Z(1)=0, EVALUATION OF VECTOR Z IS DONE BY    TFG 027
C           MEANS OF TRAPEZOIDAL RULE (SECOND ORDER FORMULA).           TFG 028
C           FOR REFERENCE, SEE                                          TFG 029
C           F.B.HILDEBRAND, INTRODUCTION TO NUMERICAL ANALYSIS,         TFG 030
C           MCGRAW-HILL, NEW YORK/TORONTO/LONDON, 1956, PP.75.          TFG 031
C                                                                       TFG 032
C     ..................................................................TFG 033
C                                                                       TFG 034
      SUBROUTINE QTFG(X,Y,Z,NDIM)                                       TFG 035
C                                                                       TFG 036
C                                                                       TFG 037
      DIMENSION X(1),Y(1),Z(1)                                          TFG 038
C                                                                       TFG 039
      SUM2=0.                                                           TFG 040
      IF(NDIM-1)4,3,1                                                   TFG 041
C                                                                       TFG 042
C     INTEGRATION LOOP                                                  TFG 043
    1 DO 2 I=2,NDIM                                                     TFG 044
      SUM1=SUM2                                                         TFG 045
      SUM2=SUM2+.5*(X(I)-X(I-1))*(Y(I)+Y(I-1))                          TFG 046
    2 Z(I-1)=SUM1                                                       TFG 047
    3 Z(NDIM)=SUM2                                                      TFG 048
    4 RETURN                                                            TFG 049
      END                                                               TFG 050
C
C     ..................................................................
C
C        SUBROUTINE LEP
C
C        PURPOSE
C           COMPUTE THE VALUES OF THE LEGENDRE POLYNOMIALS P(N,X)
C           FOR ARGUMENT VALUE X AND ORDERS 0 UP TO N.
C
C        USAGE
```

```
C             CALL LEP(Y,X,N)
C
C          DESCRIPTION OF PARAMETERS
C             Y   - RESULT VECTOR OF DIMENSION N+1 CONTAINING THE VALUES
C                   OF LEGENDRE POLYNOMIALS OF ORDER 0 UP TO N
C                   FOR GIVEN ARGUMENT X.
C                   VALUES ARE ORDERED FROM LOW TO HIGH ORDER
C             X   - ARGUMENT OF LEGENDRE POLYNOMIAL
C             N   - ORDER OF LEGENDRE POLYNOMIAL
C
C          REMARKS
C             N LESS THAN 0 IS TREATED AS IF N WERE 0
C
C          SUBROUTINES AND FUNCTION SUBPROGRAMS REQUIRED
C             NONE
C
C          METHOD
C             EVALUATION IS BASED ON THE RECURRENCE EQUATION FOR
C             LEGENDRE POLYNOMIALS P(N,X)
C             P(N+1,X)=2*X*P(N,X)-P(N-1,X)-(X*P(N,X)-P(N-1,X))/(N+1),
C             WHERE THE FIRST TERM IN BRACKETS IS THE ORDER,
C             THE SECOND IS THE ARGUMENT.
C             STARTING VALUES ARE P(0,X)=1, P(1,X)=X
C
C     ..................................................................
C
      SUBROUTINE LEP(Y,X,N)
C
      DIMENSION Y(1)
C
C        TEST OF ORDER
      Y(1)=1.
      IF(N)1,1,2
    1 RETURN
C
    2 Y(2)=X
      IF(N-1)1,1,3
C
    3 DO 4 I=2,N
      G=X*Y(I)
    4 Y(I+1)=G-Y(I-1)+G-(G-Y(I-1))/FLOAT(I)
      RETURN
      END
C
C
C     ..................................................................
C
C        SUBROUTINE HPCG
C
C        PURPOSE
C           TO SOLVE A SYSTEM OF FIRST ORDER ORDINARY GENERAL
C           DIFFERENTIAL EQUATIONS WITH GIVEN INITIAL VALUES.
C
C        USAGE
C           CALL HPCG (PRMT,Y,DERY,NDIM,IHLF,FCT,OUTP,AUX)
C           PARAMETERS FCT AND OUTP REQUIRE AN EXTERNAL STATEMENT.
C
C        DESCRIPTION OF PARAMETERS
C           PRMT   - AN INPUT AND OUTPUT VECTOR WITH DIMENSION GREATER
C                    OR EQUAL TO 5, WHICH SPECIFIES THE PARAMETERS OF
C                    THE INTERVAL AND OF ACCURACY AND WHICH SERVES FOR
C                    COMMUNICATION BETWEEN OUTPUT SUBROUTINE (FURNISHED
C                    BY THE USER) AND SUBROUTINE HPCG. EXCEPT PRMT(5)
C                    THE COMPONENTS ARE NOT DESTROYED BY SUBROUTINE
C                    HPCG AND THEY ARE
C           PRMT(1)- LOWER BOUND OF THE INTERVAL (INPUT),
```

```
C        PRMT(2)  - UPPER BOUND OF THE INTERVAL (INPUT).
C        PRMT(3)  - INITIAL INCREMENT OF THE INDEPENDENT VARIABLE
C                   (INPUT).
C        PRMT(4)  - UPPER ERROR BOUND (INPUT). IF ABSOLUTE ERROR IS
C                   GREATER THAN PRMT(4), INCREMENT GETS HALVED.
C                   IF INCREMENT IS LESS THAN PRMT(3) AND ABSOLUTE
C                   ERROR LESS THAN PRMT(4)/50, INCREMENT GETS DOUBLED.
C                   THE USER MAY CHANGE PRMT(4) BY MEANS OF HIS
C                   OUTPUT SUBROUTINE.
C        PRMT(5)  - NO INPUT PARAMETER. SUBROUTINE HPCG INITIALIZES
C                   PRMT(5)=0. IF THE USER WANTS TO TERMINATE
C                   SUBROUTINE HPCG AT ANY OUTPUT POINT, HE HAS TO
C                   CHANGE PRMT(5) TO NON-ZERO BY MEANS OF SUBROUTINE
C                   OUTP. FURTHER COMPONENTS OF VECTOR PRMT ARE
C                   FEASIBLE IF ITS DIMENSION IS DEFINED GREATER
C                   THAN 5. HOWEVER SUBROUTINE HPCG DOES NOT REQUIRE
C                   AND CHANGE THEM. NEVERTHELESS THEY MAY BE USEFUL
C                   FOR HANDING RESULT VALUES TO THE MAIN PROGRAM
C                   (CALLING HPCG) WHICH ARE OBTAINED BY SPECIAL
C                   MANIPULATIONS WITH OUTPUT DATA IN SUBROUTINE OUTP.
C        Y        - INPUT VECTOR OF INITIAL VALUES.  (DESTROYED)
C                   LATERON Y IS THE RESULTING VECTOR OF DEPENDENT
C                   VARIABLES COMPUTED AT INTERMEDIATE POINTS X.
C        DERY     - INPUT VECTOR OF ERROR WEIGHTS.  (DESTROYED)
C                   THE SUM OF ITS COMPONENTS MUST BE EQUAL TO 1.
C                   LATERON DERY IS THE VECTOR OF DERIVATIVES, WHICH
C                   BELONG TO FUNCTION VALUES Y AT A POINT X.
C        NDIM     - AN INPUT VALUE, WHICH SPECIFIES THE NUMBER OF
C                   EQUATIONS IN THE SYSTEM.
C        IHLF     - AN OUTPUT VALUE, WHICH SPECIFIES THE NUMBER OF
C                   BISECTIONS OF THE INITIAL INCREMENT. IF IHLF GETS
C                   GREATER THAN 10, SUBROUTINE HPCG RETURNS WITH
C                   ERROR MESSAGE IHLF=11 INTO MAIN PROGRAM.
C                   ERROR MESSAGE IHLF=12 OR IHLF=13 APPEARS IN CASE
C                   PRMT(3)=0 OR IN CASE SIGN(PRMT(3)).NE.SIGN(PRMT(2)-
C                   PRMT(1)) RESPECTIVELY.
C        FCT      - THE NAME OF AN EXTERNAL SUBROUTINE USED. IT
C                   COMPUTES THE RIGHT HAND SIDES DERY OF THE SYSTEM
C                   TO GIVEN VALUES OF X AND Y. ITS PARAMETER LIST
C                   MUST BE X,Y,DERY. THE SUBROUTINE SHOULD NOT
C                   DESTROY X AND Y.
C        OUTP     - THE NAME OF AN EXTERNAL OUTPUT SUBROUTINE USED.
C                   ITS PARAMETER LIST MUST BE X,Y,DERY,IHLF,NDIM,PRMT.
C                   NONE OF THESE PARAMETERS (EXCEPT, IF NECESSARY,
C                   PRMT(4),PRMT(5),...) SHOULD BE CHANGED BY
C                   SUBROUTINE OUTP. IF PRMT(5) IS CHANGED TO NON-ZERO,
C                   SUBROUTINE HPCG IS TERMINATED.
C        AUX      - AN AUXILIARY STORAGE ARRAY WITH 16 ROWS AND NDIM
C                   COLUMNS.
C
C     REMARKS
C        THE PROCEDURE TERMINATES AND RETURNS TO CALLING PROGRAM, IF
C        (1) MORE THAN 10 BISECTIONS OF THE INITIAL INCREMENT ARE
C            NECESSARY TO GET SATISFACTORY ACCURACY (ERROR MESSAGE
C            IHLF=11),
C        (2) INITIAL INCREMENT IS EQUAL TO 0 OR HAS WRONG SIGN
C            (ERROR MESSAGES IHLF=12 OR IHLF=13),
C        (3) THE WHOLE INTEGRATION INTERVAL IS WORKED THROUGH,
C        (4) SUBROUTINE OUTP HAS CHANGED PRMT(5) TO NON-ZERO.
C
C     SUBROUTINES AND FUNCTION SUBPROGRAMS REQUIRED
C        THE EXTERNAL SUBROUTINES FCT(X,Y,DERY) AND
C        OUTP(X,Y,DERY,IHLF,NDIM,PRMT) MUST BE FURNISHED BY THE USER.
C
C     METHOD
C        EVALUATION IS DONE BY MEANS OF HAMMINGS MODIFIED PREDICTOR-
```

```
C           CORRECTOR METHOD. IT IS A FOURTH ORDER METHOD, USING 4
C           PRECEEDING POINTS FOR COMPUTATION OF A NEW VECTOR Y OF THE
C           DEPENDENT VARIABLES.
C           FOURTH ORDER RUNGE-KUTTA METHOD SUGGESTED BY RALSTON IS
C           USED FOR ADJUSTMENT OF THE INITIAL INCREMENT AND FOR
C           COMPUTATION OF STARTING VALUES.
C           SUBROUTINE HPCG AUTOMATICALLY ADJUSTS THE INCREMENT DURING
C           THE WHOLE COMPUTATION BY HALVING OR DOUBLING.
C           TO GET FULL FLEXIBILITY IN OUTPUT, AN OUTPUT SUBROUTINE
C           MUST BE CODED BY THE USER.
C           FOR REFERENCE, SEE
C             (1)  RALSTON/WILF, MATHEMATICAL METHODS FOR DIGITAL
C                  COMPUTERS, WILEY, NEW YORK/LONDON, 1960, PP.95-109.
C             (2)  RALSTON, RUNGE-KUTTA METHODS WITH MINIMUM ERROR BOUNDS,
C                  MTAC, VOL.16, ISS.80 (1962), PP.431-437.
C
C     ..................................................................
C
      SUBROUTINE HPCG(PRMT,Y,DERY,NDIM,IHLF,FCT,OUTP,AUX)
C
C
      DIMENSION PRMT(1),Y(1),DERY(1),AUX(16,1)
      N=1
      IHLF=0
      X=PRMT(1)
      H=PRMT(3)
      PRMT(5)=0.
      DO 1 I=1,NDIM
      AUX(16,I)=0.
      AUX(15,I)=DERY(I)
    1 AUX(1,I)=Y(I)
      IF(H*(PRMT(2)-X))3,2,4
C
C     ERROR RETURNS
    2 IHLF=12
      GOTO 4
    3 IHLF=13
C
C     COMPUTATION OF DERY FOR STARTING VALUES
    4 CALL FCT(X,Y,DERY)
C
C     RECORDING OF STARTING VALUES
      CALL OUTP(X,Y,DERY,IHLF,NDIM,PRMT)
      IF(PRMT(5))6,5,6
    5 IF(IHLF)7,7,6
    6 RETURN
    7 DO 8 I=1,NDIM
    8 AUX(8,I)=DERY(I)
C
C     COMPUTATION OF AUX(2,I)
      ISW=1
      GOTO 100
C
    9 X=X+H
      DO 10 I=1,NDIM
   10 AUX(2,I)=Y(I)
C
C     INCREMENT H IS TESTED BY MEANS OF BISECTION
   11 IHLF=IHLF+1
      X=X-H
      DO 12 I=1,NDIM
   12 AUX(4,I)=AUX(2,I)
      H=.5*H
      N=1
      ISW=2
      GOTO 100
```

```
C                                                                       PCG 156
   13 X=X+H                                                             PCG 157
      CALL FCT(X,Y,DERY)                                                PCG 158
      N=2                                                               PCG 159
      DO 14 I=1,NDIM                                                    PCG 160
      AUX(2,I)=Y(I)                                                     PCG 161
   14 AUX(9,I)=DERY(I)                                                  PCG 162
      ISW=3                                                             PCG 163
      GOTO 100                                                          PCG 164
C                                                                       PCG 165
C     COMPUTATION OF TEST VALUE DELT                                    PCG 166
   15 DELT=0.                                                           PCG 167
      DO 16 I=1,NDIM                                                    PCG 168
   16 DELT=DELT+AUX(15,I)*ABS(Y(I)-AUX(4,I))                            PCG 169
      DELT=.06666667*DELT                                               PCG 170
      IF(DELT-PRMT(4))19,19,17                                          PCG 171
   17 IF(IHLF-10)11,18,18                                               PCG 172
C                                                                       PCG 173
C     NO SATISFACTORY ACCURACY AFTER 10 BISECTIONS. ERROR MESSAGE.      PCG 174
   18 IHLF=11                                                           PCG 175
      X=X+H                                                             PCG 176
      GOTO 4                                                            PCG 177
C                                                                       PCG 178
C     THERE IS SATISFACTORY ACCURACY AFTER LESS THAN 11 BISECTIONS.     PCG 179
   19 X=X+H                                                             PCG 180
      CALL FCT(X,Y,DERY)                                                PCG 181
      DO 20 I=1,NDIM                                                    PCG 182
      AUX(3,I)=Y(I)                                                     PCG 183
   20 AUX(10,I)=DERY(I)                                                 PCG 184
      N=3                                                               PCG 185
      ISW=4                                                             PCG 186
      GOTO 100                                                          PCG 187
C                                                                       PCG 188
   21 N=1                                                               PCG 189
      X=X+H                                                             PCG 190
      CALL FCT(X,Y,DERY)                                                PCG 191
      X=PRMT(1)                                                         PCG 192
      DO 22 I=1,NDIM                                                    PCG 193
      AUX(11,I)=DERY(I)                                                 PCG 194
   220Y(I)=AUX(1,I)+H*(.375*AUX(8,I)+.7916667*AUX(9,I)                  PCG 195
     1-.2083333*AUX(10,I)+.04166667*DERY(I))                            PCG 196
   23 X=X+H                                                             PCG 197
      N=N+1                                                             PCG 198
      CALL FCT(X,Y,DERY)                                                PCG 199
      CALL OUTP(X,Y,DERY,IHLF,NDIM,PRMT)                                PCG 200
      IF(PRMT(5))6,24,6                                                 PCG 201
   24 IF(N-4)25,200,200                                                 PCG 202
   25 DO 26 I=1,NDIM                                                    PCG 203
      AUX(N,I)=Y(I)                                                     PCG 204
   26 AUX(N+7,I)=DERY(I)                                                PCG 205
      IF(N-3)27,29,200                                                  PCG 206
C                                                                       PCG 207
   27 DO 28 I=1,NDIM                                                    PCG 208
      DELT=AUX(9,I)+AUX(9,I)                                            PCG 209
      DELT=DELT+DELT                                                    PCG 210
   28 Y(I)=AUX(1,I)+.3333333*H*(AUX(8,I)+DELT+AUX(10,I))                PCG 211
      GOTO 23                                                           PCG 212
C                                                                       PCG 213
   29 DO 30 I=1,NDIM                                                    PCG 214
      DELT=AUX(9,I)+AUX(10,I)                                           PCG 215
      DELT=DELT+DELT+DELT                                               PCG 216
   30 Y(I)=AUX(1,I)+.375*H*(AUX(8,I)+DELT+AUX(11,I))                    PCG 217
      GOTO 23                                                           PCG 218
C                                                                       PCG 219
C                                                                       PCG 220
C     ***************************************************************** PCG 221
```

```
C     THE FOLLOWING PART OF SUBROUTINE HPCG COMPUTES BY MEANS OF
C     RUNGE-KUTTA METHOD STARTING VALUES FOR THE NOT SELF-STARTING
C     PREDICTOR-CORRECTOR METHOD.
  100 DO 101 I=1,NDIM
      Z=H*AUX(N+7,I)
      AUX(5,I)=Z
  101 Y(I)=AUX(N,I)+.4*Z
C     Z IS AN AUXILIARY STORAGE LOCATION
C
      Z=X+.4*H
      CALL FCT(Z,Y,DERY)
      DO 102 I=1,NDIM
      Z=H*DERY(I)
      AUX(6,I)=Z
  102 Y(I)=AUX(N,I)+.2969776*AUX(5,I)+.1587596*Z
C
      Z=X+.4557372*H
      CALL FCT(Z,Y,DERY)
      DO 103 I=1,NDIM
      Z=H*DERY(I)
      AUX(7,I)=Z
  103 Y(I)=AUX(N,I)+.2181004*AUX(5,I)-3.050965*AUX(6,I)+3.832865*Z
C
      Z=X+H
      CALL FCT(Z,Y,DERY)
      DO 104 I=1,NDIM
  104 Y(I)=AUX(N,I)+.1747603*AUX(5,I)-.5514807*AUX(6,I)
     1+1.205536*AUX(7,I)+.1711848*H*DERY(I)
      GOTO(9,13,15,21),ISW
C     *****************************************************************
C
C
C     POSSIBLE BREAK-POINT FOR LINKAGE
C
C
C     STARTING VALUES ARE COMPUTED.
C     NOW START HAMMINGS MODIFIED PREDICTOR-CORRECTOR METHOD.
  200 ISTEP=3
  201 IF(N-8)204,202,204
C
C     N=8 CAUSES THE ROWS OF AUX TO CHANGE THEIR STORAGE LOCATIONS
  202 DO 203 N=2,7
      DO 203 I=1,NDIM
      AUX(N-1,I)=AUX(N,I)
  203 AUX(N+6,I)=AUX(N+7,I)
      N=7
C
C     N LESS THAN 8 CAUSES N+1 TO GET N
  204 N=N+1
C
C     COMPUTATION OF NEXT VECTOR Y
      DO 205 I=1,NDIM
      AUX(N-1,I)=Y(I)
  205 AUX(N+6,I)=DERY(I)
      X=X+H
  206 ISTEP=ISTEP+1
      DO 207 I=1,NDIM
     0DELT=AUX(N-4,I)+1.333333*H*(AUX(N+6,I)+AUX(N+6,I)-AUX(N+5,I)+
     1AUX(N+4,I)+AUX(N+4,I))
      Y(I)=DELT-.9256198*AUX(16,I)
  207 AUX(16,I)=DELT
C     PREDICTOR IS NOW GENERATED IN ROW 16 OF AUX, MODIFIED PREDICTOR
C     IS GENERATED IN Y. DELT MEANS AN AUXILIARY STORAGE.
C
      CALL FCT(X,Y,DERY)
C     DERIVATIVE OF MODIFIED PREDICTOR IS GENERATED IN DERY
```

```
C
      DO 208 I=1,NDIM
     0DELT=.125*(9.*AUX(N-1,I)-AUX(N-3,I)+3.*H*(DERY(I)+AUX(N+6,I)+
     1AUX(N+6,I)-AUX(N+5,I)))
      AUX(16,I)=AUX(16,I)-DELT
  208 Y(I)=DELT+.07438017*AUX(16,I)
C
C     TEST WHETHER H MUST BE HALVED OR DOUBLED
      DELT=0.
      DO 209 I=1,NDIM
  209 DELT=DELT+AUX(15,I)*ABS(AUX(16,I))
      IF(DELT-PRMT(4))210,222,222
C
C     H MUST NOT BE HALVED. THAT MEANS Y(I) ARE GOOD.
  210 CALL FCT(X,Y,DERY)
      CALL OUTP(X,Y,DERY,IHLF,NDIM,PRMT)
      IF(PRMT(5))212,211,212
  211 IF(IHLF-11)213,212,212
  212 RETURN
  213 IF(H*(X-PRMT(2)))214,212,212
  214 IF(ABS(X-PRMT(2))-.1*ABS(H))212,215,215
  215 IF(DELT-.02*PRMT(4))216,216,201
C
C
C     H COULD BE DOUBLED IF ALL NECESSARY PRECEEDING VALUES ARE
C     AVAILABLE
  216 IF(IHLF)201,201,217
  217 IF(N-7)201,218,218
  218 IF(ISTEP-4)201,219,219
  219 IMOD=ISTEP/2
      IF(ISTEP-IMOD-IMOD)201,220,201
  220 H=H+H
      IHLF=IHLF-1
      ISTEP=0
      DO 221 I=1,NDIM
      AUX(N-1,I)=AUX(N-2,I)
      AUX(N-2,I)=AUX(N-4,I)
      AUX(N-3,I)=AUX(N-6,I)
      AUX(N+6,I)=AUX(N+5,I)
      AUX(N+5,I)=AUX(N+3,I)
      AUX(N+4,I)=AUX(N+1,I)
      DELT=AUX(N+6,I)+AUX(N+5,I)
      DELT=DELT+DELT+DELT
  2210AUX(16,I)=8.962963*(Y(I)-AUX(N-3,I))-3.361111*H*(DERY(I)+DELT
     1+AUX(N+4,I))
      GOTO 201
C
C
C     H MUST BE HALVED
  222 IHLF=IHLF+1
      IF(IHLF-10)223,223,210
  223 H=.5*H
      ISTEP=0
      DO 224 I=1,NDIM
     0Y(I)=.00390625*(80.*AUX(N-1,I)+135.*AUX(N-2,I)+40.*AUX(N-3,I)+
     1AUX(N-4,I))-.1171875*(AUX(N+6,I)-6.*AUX(N+5,I)-AUX(N+4,I))*H
     0AUX(N-4,I)=.00390625*(12.*AUX(N-1,I)+135.*AUX(N-2,I)+
     1108.*AUX(N-3,I)+AUX(N-4,I))-.0234375*(AUX(N+6,I)+18.*AUX(N+5,I)-
     29.*AUX(N+4,I))*H
      AUX(N-3,I)=AUX(N-2,I)
  224 AUX(N+4,I)=AUX(N+5,I)
      X=X-H
      DELT=X-(H+H)
      CALL FCT(DELT,Y,DERY)
      DO 225 I=1,NDIM
      AUX(N-2,I)=Y(I)
```

```
      AUX(N+5,I)=DERY(I)
  225 Y(I)=AUX(N-4,I)
      DELT=DELT-(H+H)
      CALL FCT(DELT,Y,DERY)
      DO 226 I=1,NDIM
      DELT=AUX(N+5,I)+AUX(N+4,I)
      DELT=DELT+DELT+DELT
     0AUX(16,I)=8.962963*(AUX(N-1,I)-Y(I))-3.361111*H*(AUX(N+6,I)+DELT
     1+DERY(I))
  226 AUX(N+3,I)=DERY(I)
      GOTO 206
      END
```

APPENDIX C

CONVERGENCE OF THE MWR SOLUTIONS

C.1 Discussion

Calculations were made for the first, second, and third approximations of the MWR by employing the CSM eddy-viscosity model in the turbulent shear information terms. The calculated velocity profiles, Mach-number profiles, and skin-friction distribution are shown in Figures C1 to C15 for four different free-stream Mach numbers and all three approximations. The convergence properties of these solutions are particularly satisfying, since very little success has previously been obtained for approximations above the second order for turbulent flow. The skin-friction calculations converge toward the experimental data for successive approximations. The calculations of velocity and Mach-number profiles also display convergence in the sense that the third approximation is always much nearer to the second than the second approximation is to the first; however, the profile calculations are not always convergent to the experimental data. This may be because the comparison between calculation and experiment is not totally valid for velocity and Mach-number profiles as discussed in Section 3.8.

The small difference between the third approximation

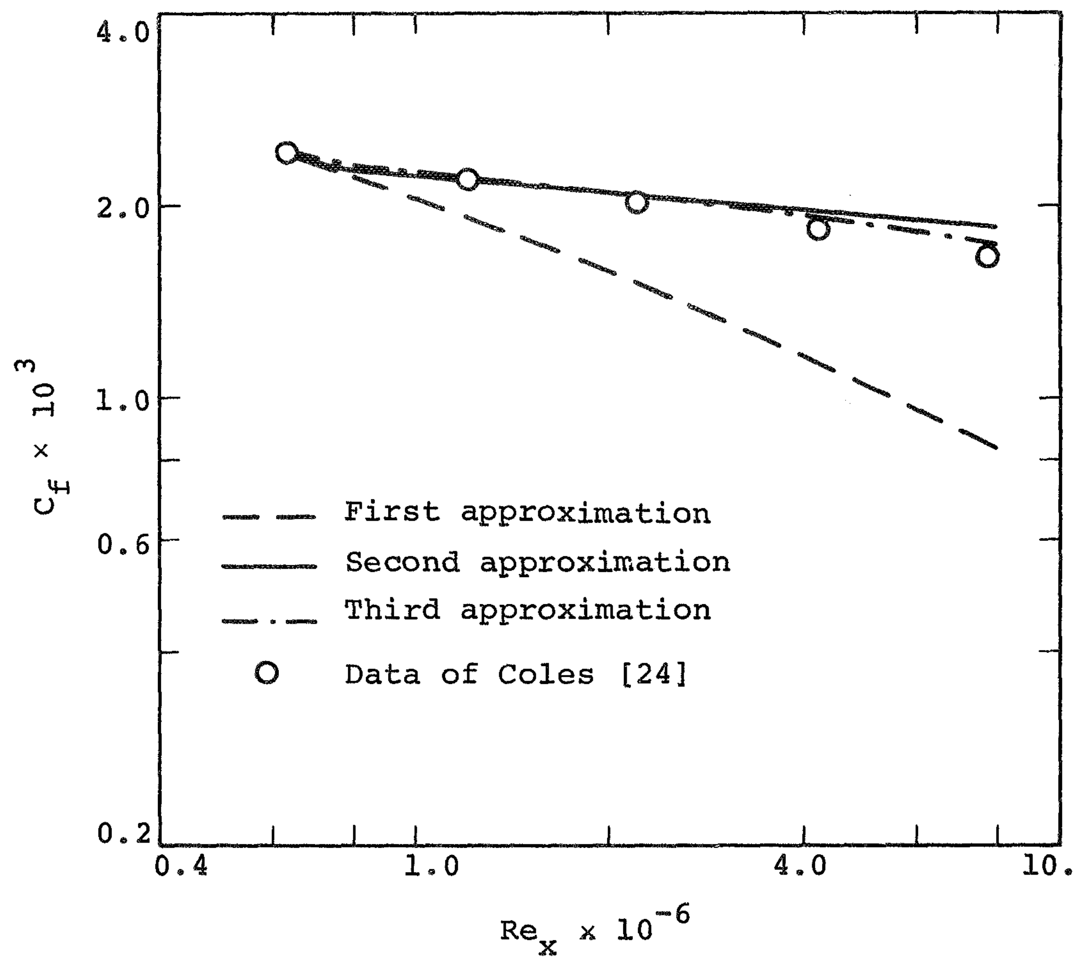

Figure C1: Comparison of the MWR Skin-Friction Calculations with Experiment, $M_e = 2.54$

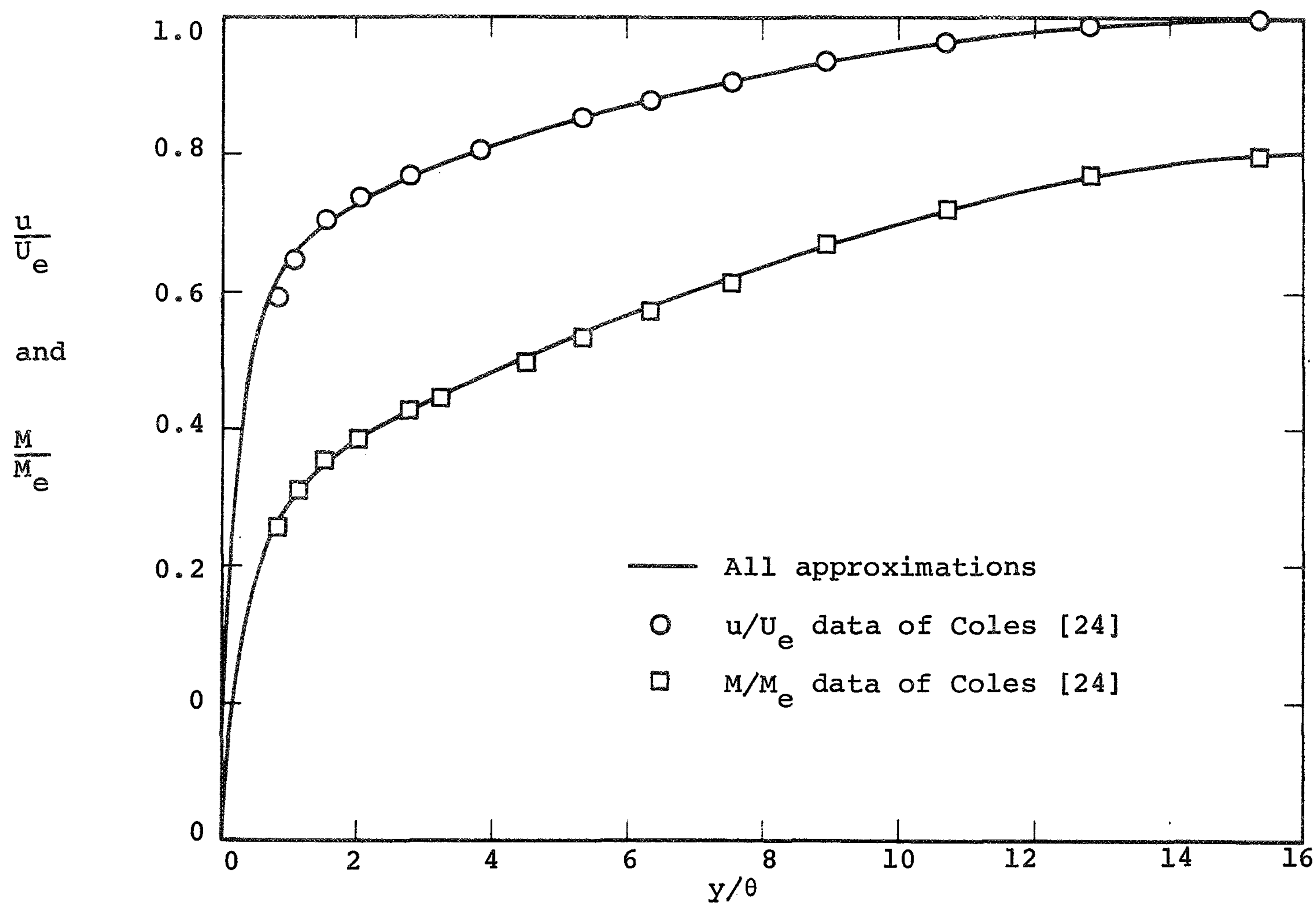

Figure C2: Comparison of the MWR Profile Calculations with Experiment, $M_e = 2.54$, $Re_x = 0.63 \times 10^6$

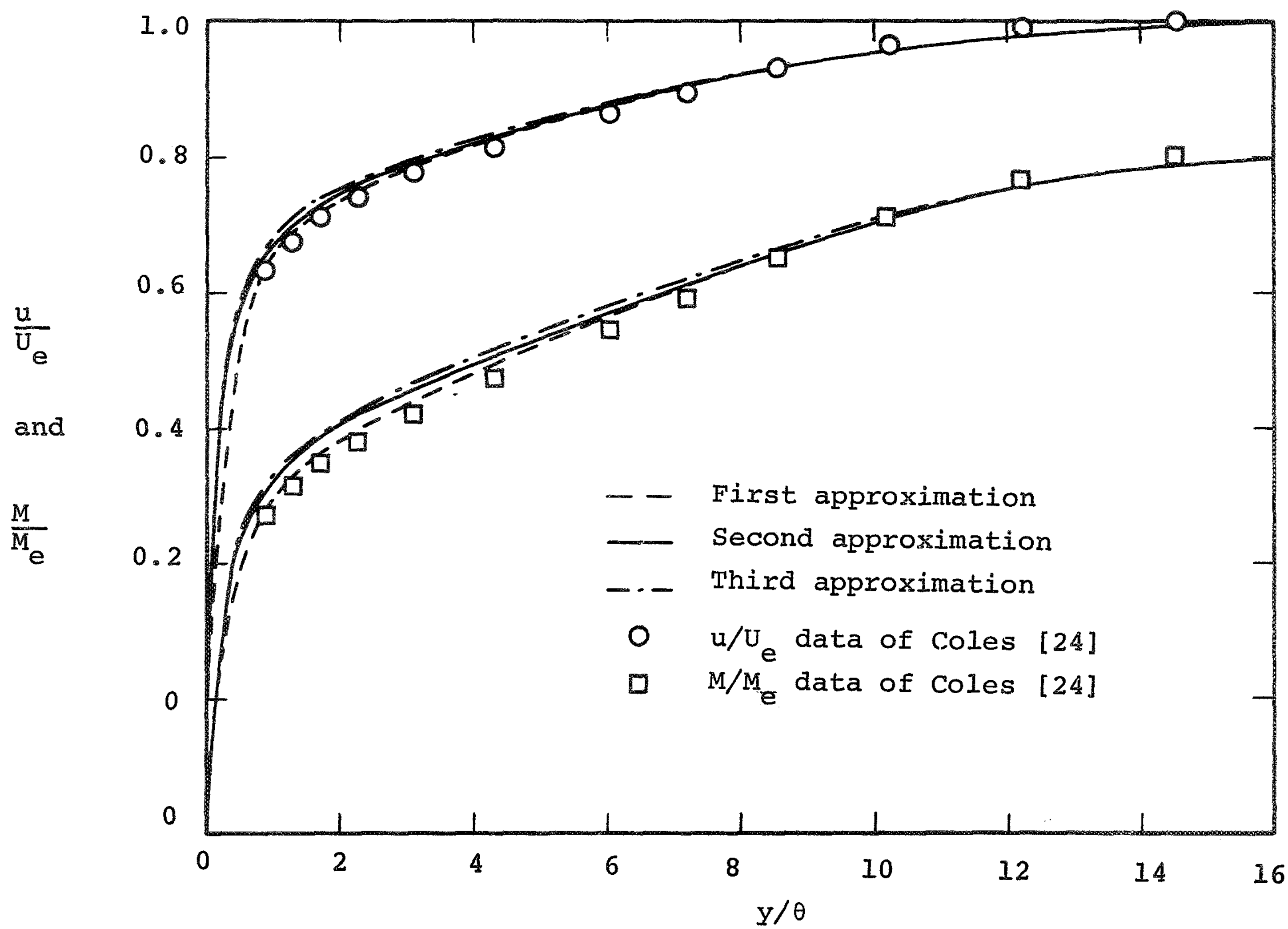

Figure C3: Comparison of the MWR Profile Calculations with Experiment, $M_e = 2.54$, $Re_x = 4.21 \times 10^6$

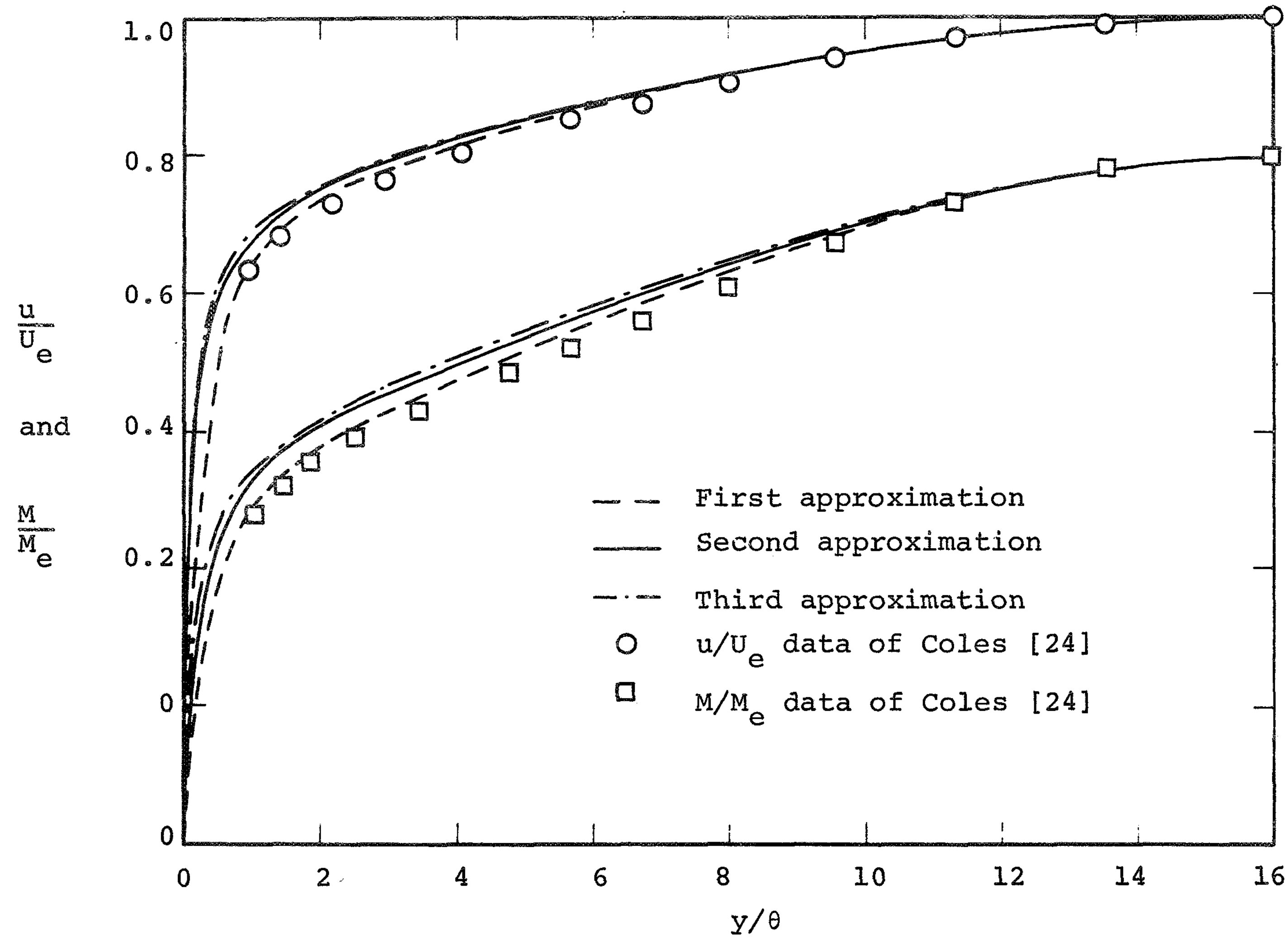

Figure C4: Comparison of the MWR Profile Calculations with Experiment, $M_e = 2.54$, $Re_x = 7.7 \times 10^6$

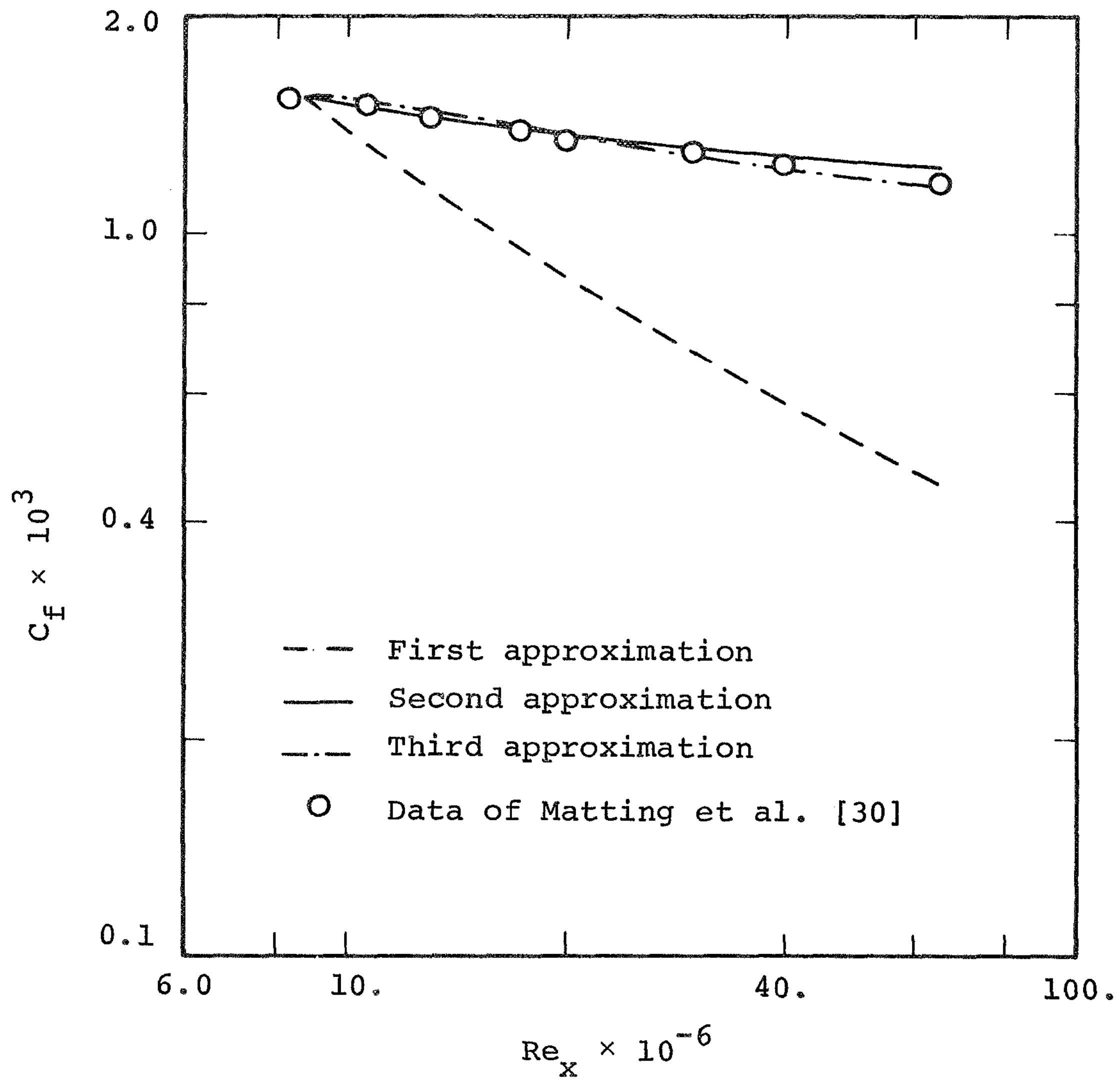

Figure C5: Comparison of the MWR Skin-Friction Calculations with Experiment, $M_e = 2.95$

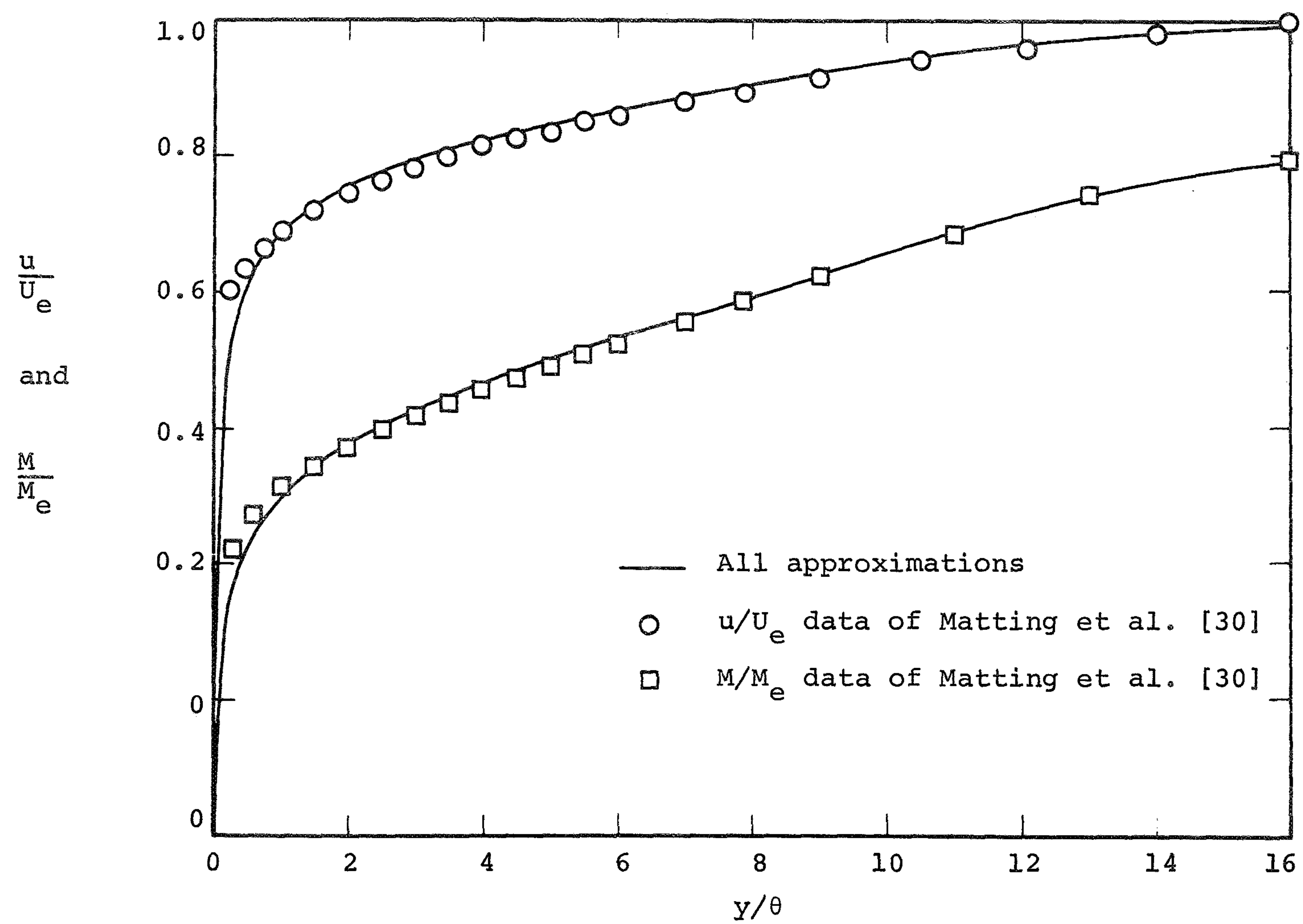

Figure C6: Comparison of the MWR Profile Calculations with Experiment, $M_e = 2.95$, $Re_x = 9.0 \times 10^6$

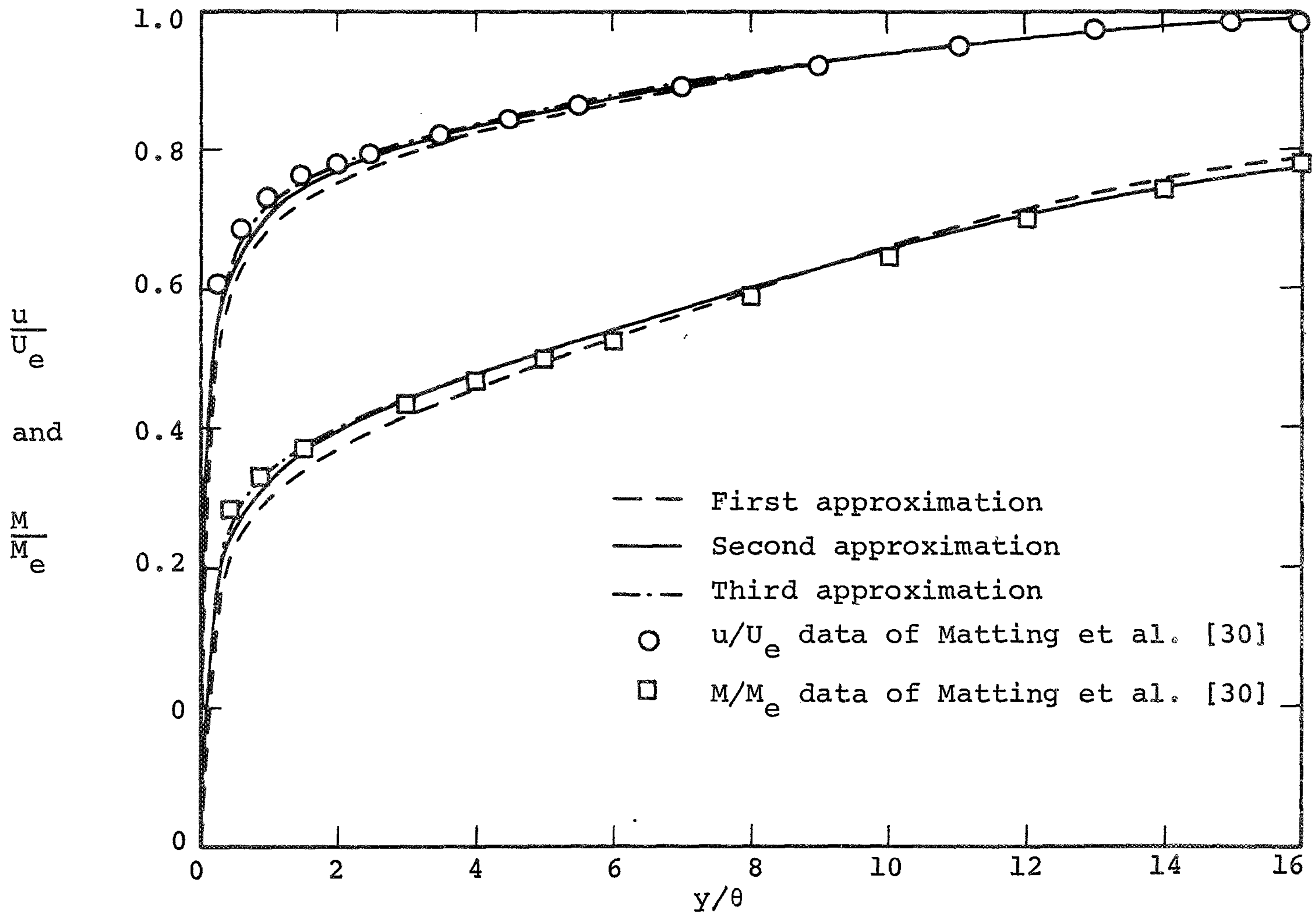

Figure C7: Comparison of the MWR Profile Calculations with Experiment, $M_e = 2.95$, $Re_x = 31. \times 10^6$

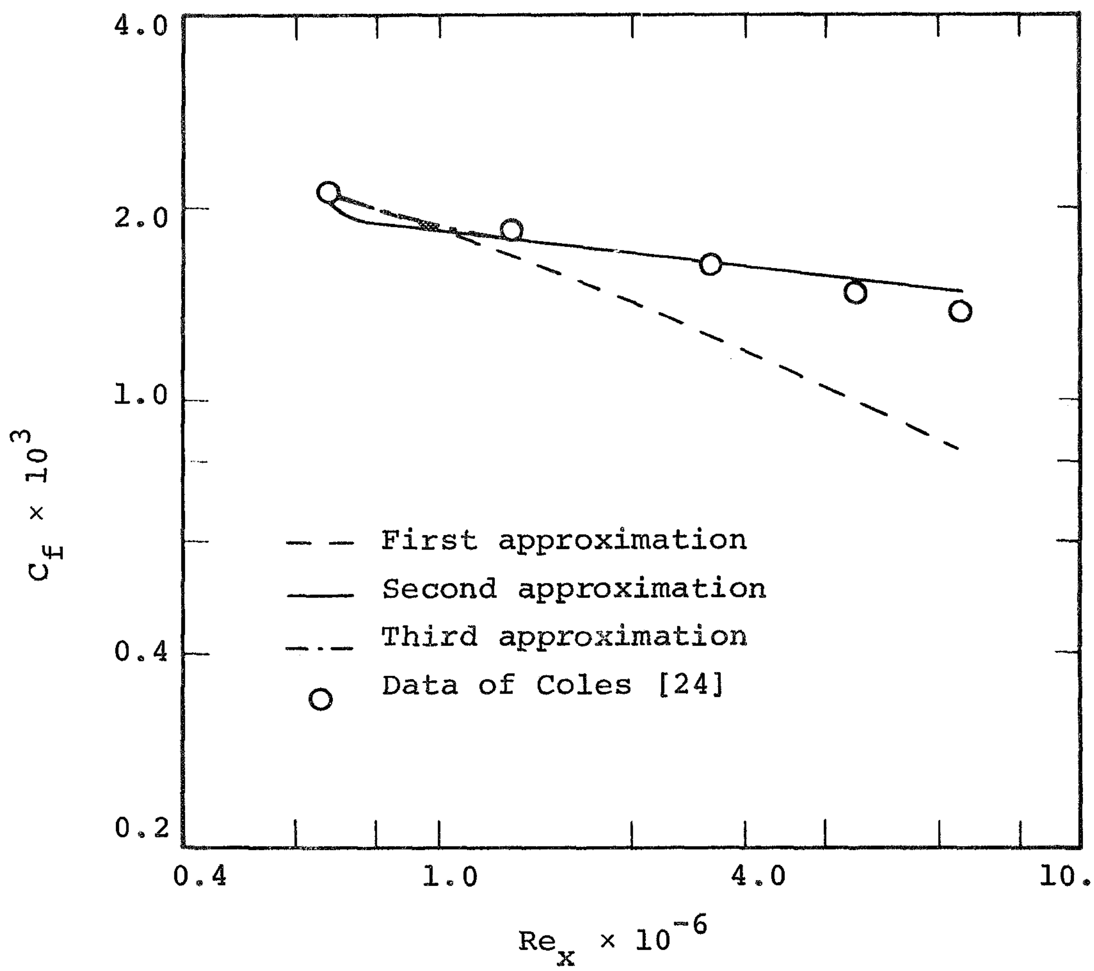

Figure C8: Comparison of the MWR Skin-Friction Calculations with Experiment, $M_e = 3.69$

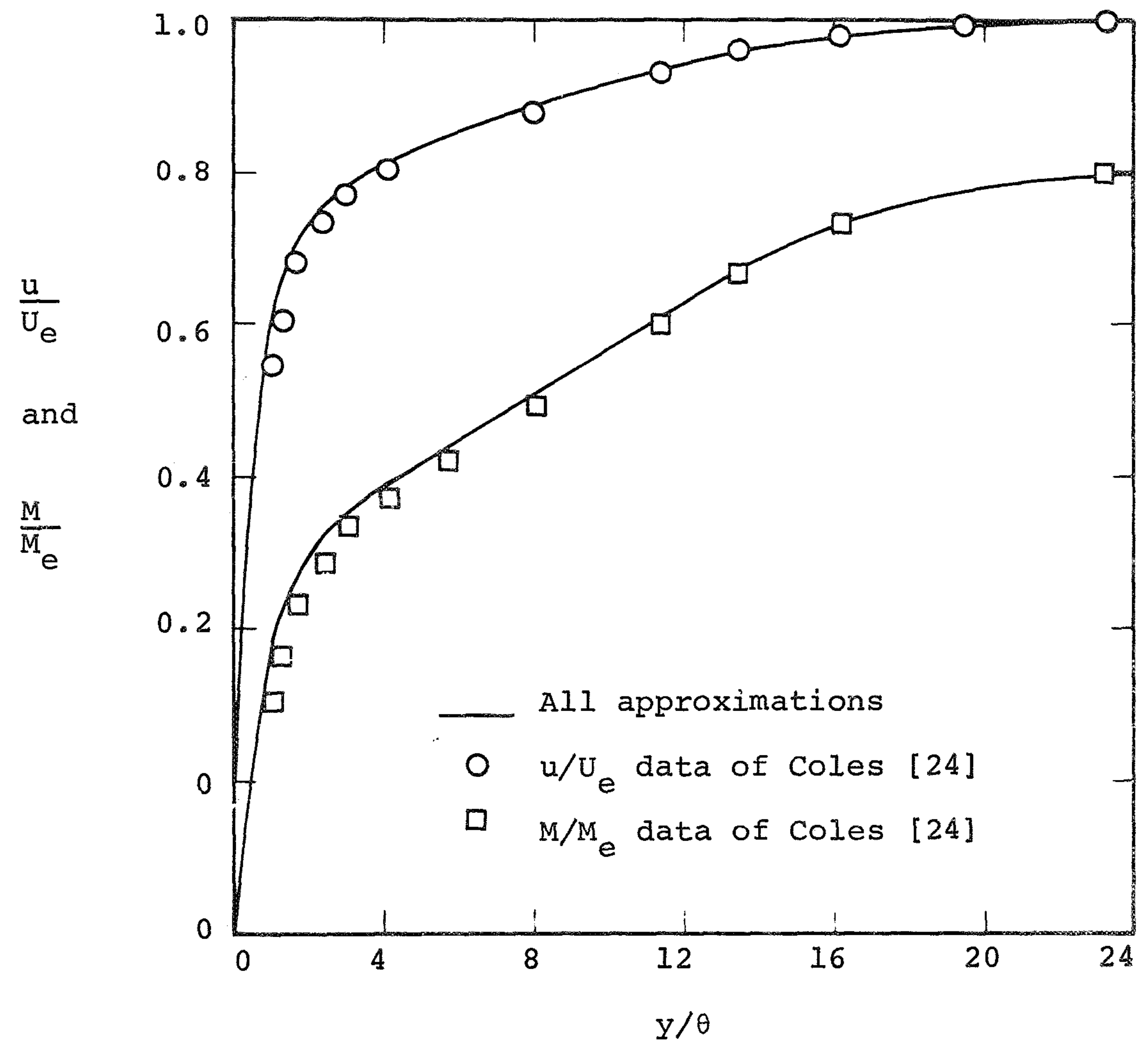

Figure C9: Comparison of the MWR Profile Calculations with Experiment, $M_e = 3.69$, $Re_x = 0.67 \times 10^6$

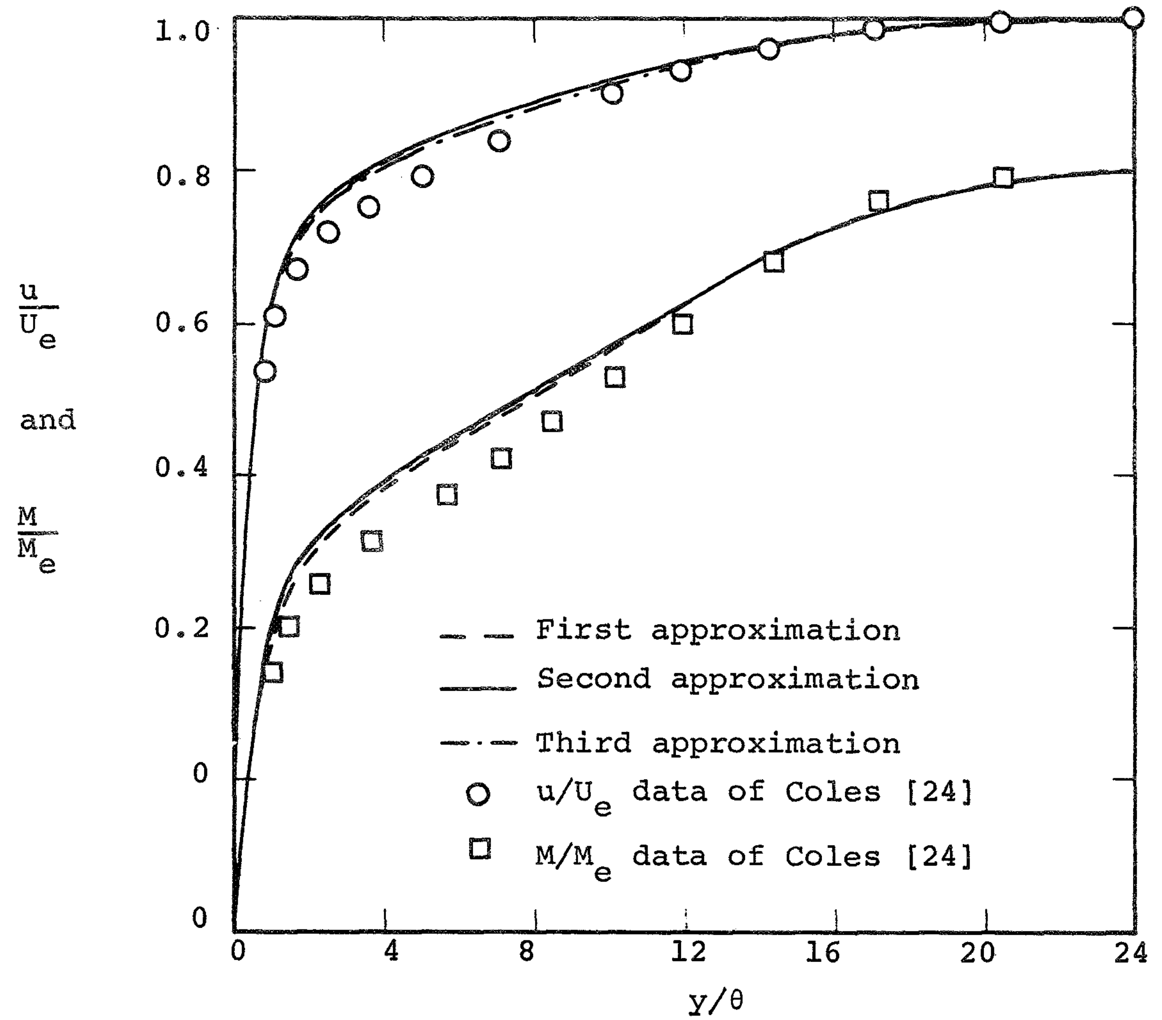

Figure C10: Comparison of the MWR Profile Calculations with Experiment, $M_e = 3.69$, $Re_x = 2.64 \times 10^6$

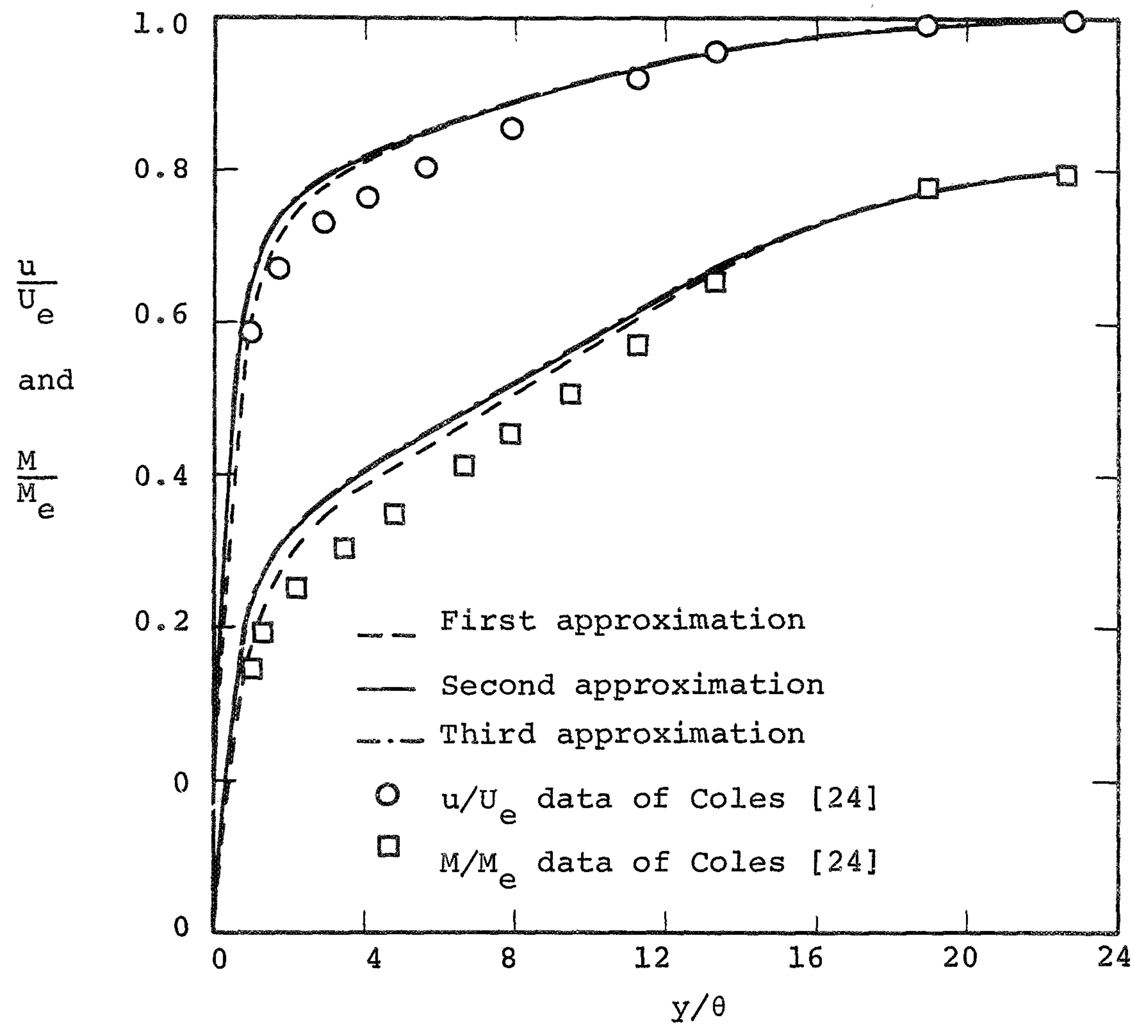

Figure C11: Comparison of the MWR Profile Calculations with Experiment, $M_e = 3.69$, $Re_x = 6.35 \times 10^6$

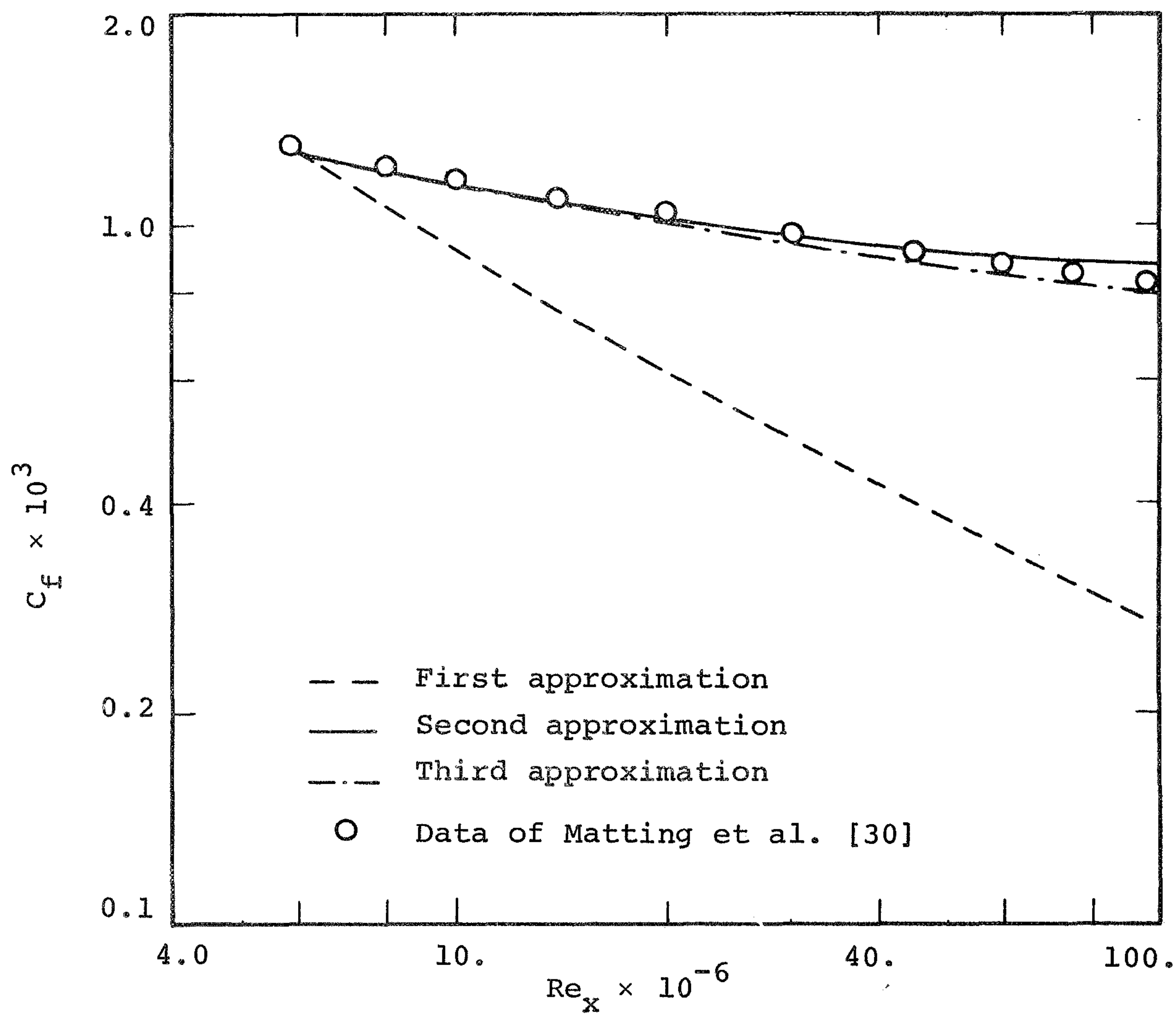

Figure C12: Comparison of the MWR Skin-Friction Calculations with Experiment, $M_e = 4.2$

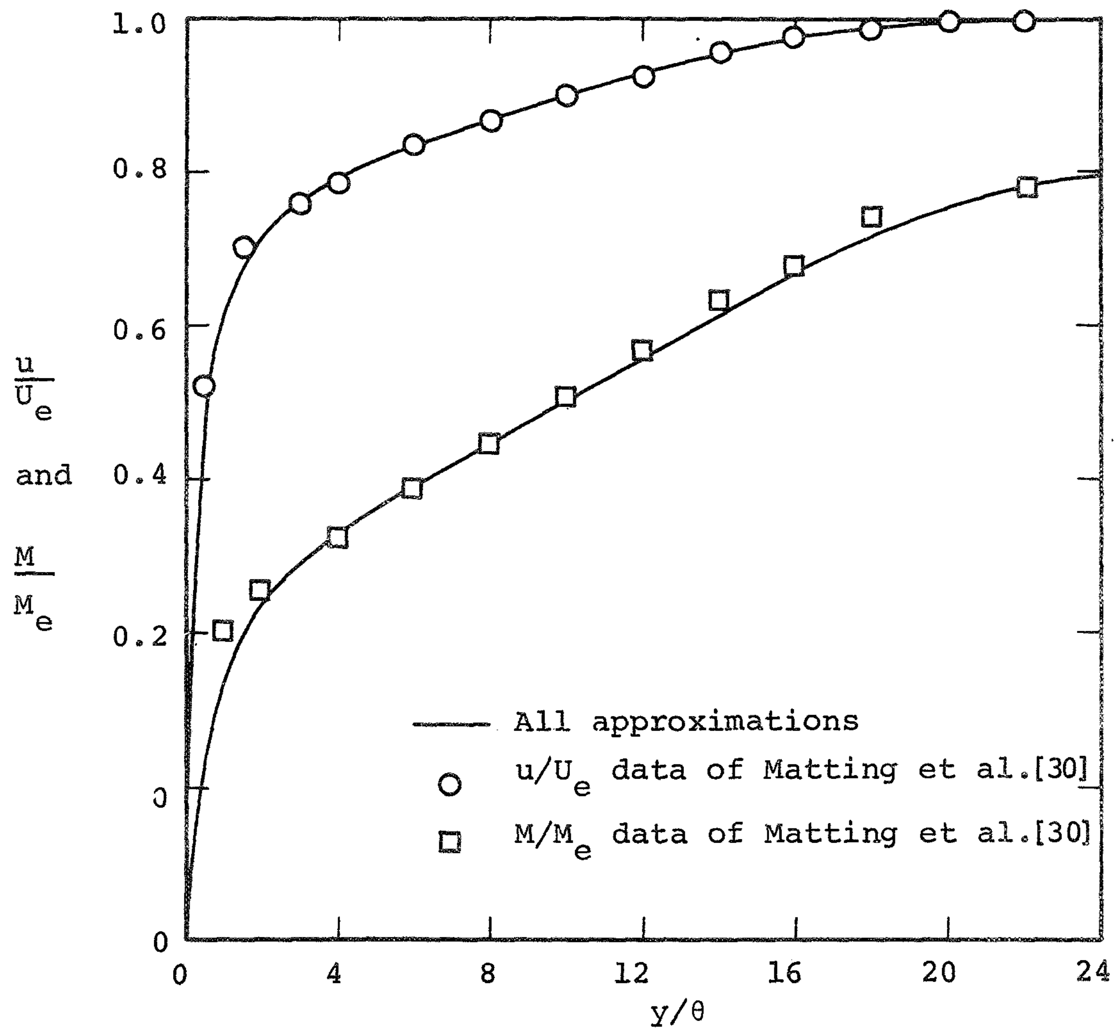

Figure C13: Comparison of the MWR Profile Calculations with Experiment, $M_e = 4.2$, $Re_x = 6.2 \times 10^6$

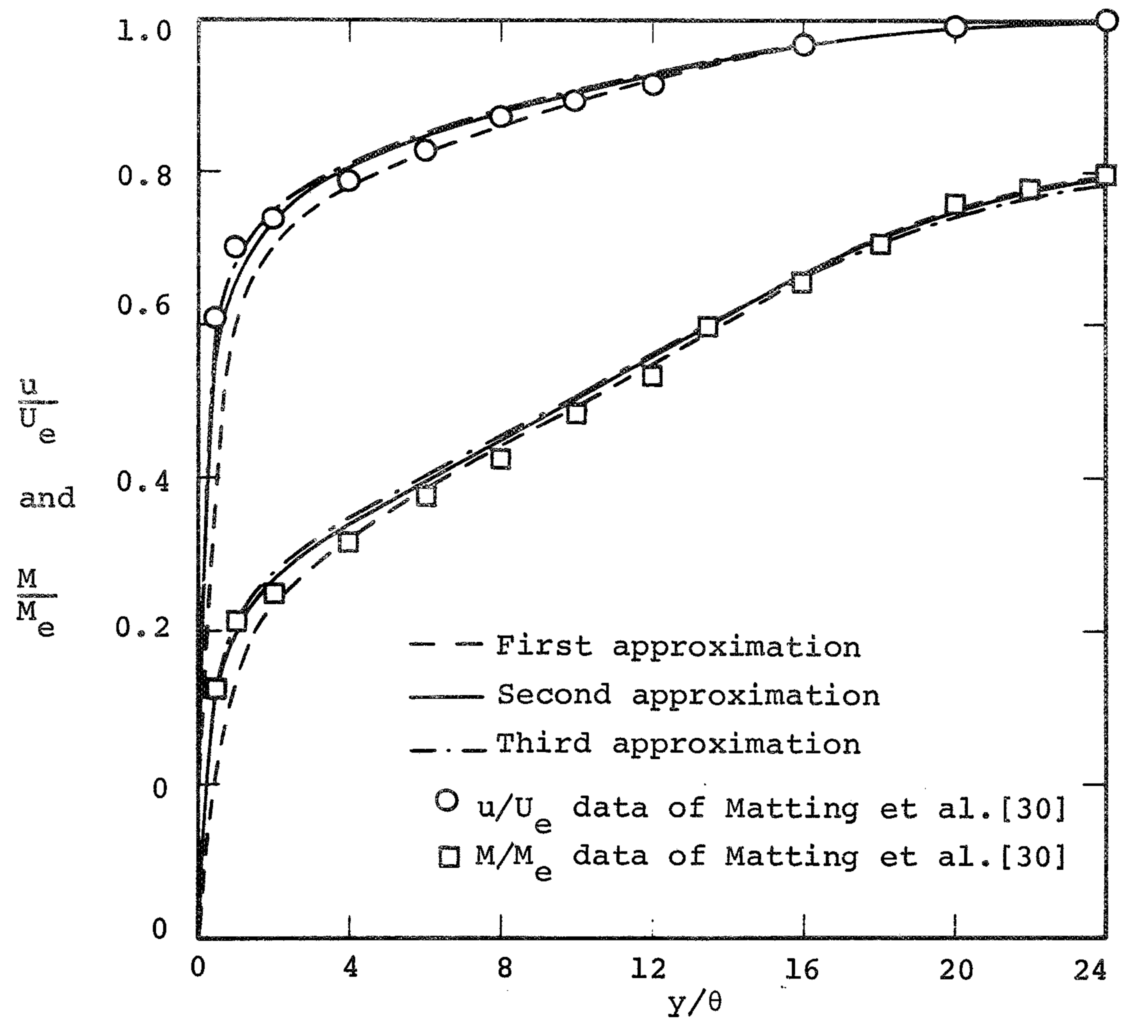

Figure C14: Comparison of the MWR Profile Calculations with Experiment, $M_e = 4.2$, $Re_x = 35. \times 10^6$

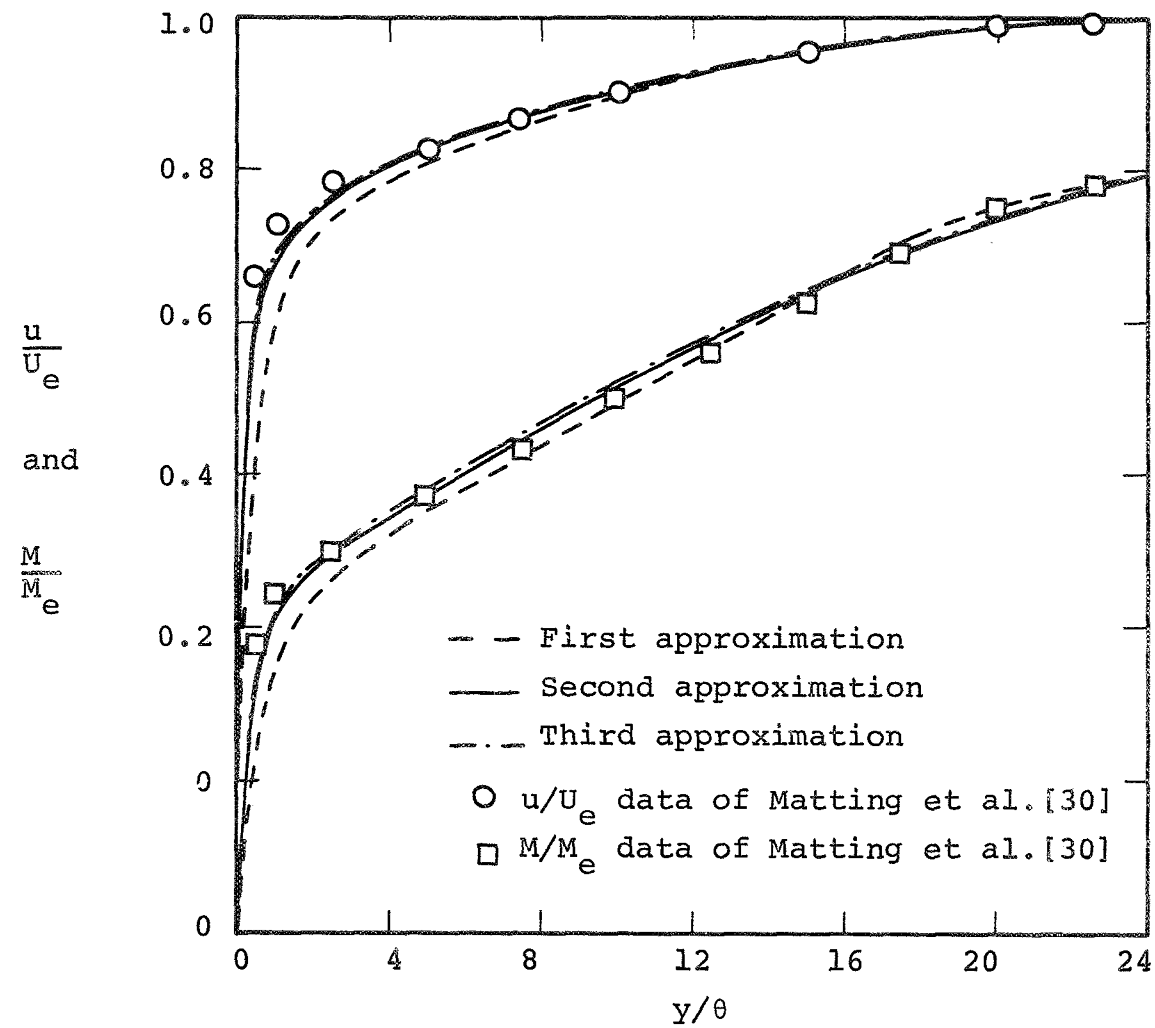

Figure C15: Comparison of the MWR Profile Calculations with Experiment, $M_e = 4.2$, $Re_x = 69. \times 10^6$

and the second in this work supports the contention of Forsnes and Abbott [C1] and Deiwert and Abbott [C2] that the second approximation is sufficient for most engineering purposes.

LIST OF REFERENCES

C1. Forsnes, V. G. and Abbott, D. E., "A Unified Comparison of Local and Global Turbulent Shear-Stress Models Utilized in the Prediction of Two-Dimensional, Incompressible Turbulent Boundary Layers", Technical Report FMTR 69-4, School of Mechanical Engineering, Purdue University, 1969.

C2. Deiwert, G. S. and Abbott, D. E., "Analytical Prediction of the Incompressible Turbulent Boundary Layer with Arbitrary Pressure Distribution", Journal of Hydronautics, 4, 1, 1970.

APPENDIX D

AN INITIALIZATION PROCEDURE FOR dC_f/dRe_x

D.1 Introduction

A method is devised by which the calculated value of dC_f/dRe_x at the initial calculation station of the MWR prediction procedure can be forced to match the experimental value of dC_f/dRe_x at x_o. For the purposes of this report, the experimental value of dC_f/dRe_x at x_o is defined as the value obtained by: (1) fitting a straight line to the experimental results on a plot of log C_f versus log Re_x in the region near x_o, (2) determining the equation which represents this straight line, $C_f = aRe_x^b$, and (3) analytically differentiating this equation at x_o.

D.2 Analysis

The basic assumption underlying this dC_f/dRe_x initialization procedure is that the fractional error in the calculated value of the shear integral g_2 at x_o is assumed to be the same as the fractional error in the calculated values of g_2 at all streamwise stations. For the present the initialization procedure is restricted to a second approximation of the MWR.

From equation (3.74), reproduced below,

$$C_f = \frac{2\mu_w \rho_w^*}{\rho_\infty U_r L} \; \frac{\sqrt{Re_r}}{(-1)^{j-1} C_j F(0)} \tag{3.74}$$

it is seen that

$$C_f = \frac{2\mu_w \rho_w^*}{\rho_r U_r L} \frac{\sqrt{Re_r}}{F(0)(C_1 - C_2)} \tag{D.1}$$

for a second approximation. Differentiation of equation (D.1) yields

$$\frac{dC_f}{d\xi} = - \frac{C_f}{C_1 - C_2} \left(\frac{dC_1}{d\xi} - \frac{dC_2}{d\xi} \right) \tag{D.2}$$

Equation (3.55), reproduced below,

$$\frac{dC_k}{d\xi} = \frac{U_{e_\xi}}{U_e} A_{ki}^{-1} I_{ij} C_j - A_{ki}^{-1} B_i - \frac{\mu_e}{\mu_r} A_{ki}^{-1} g_i \tag{3.55}$$

simplifies to

$$\frac{dC_k}{d\xi} = UAIC_k - AINB_k - \frac{\mu_e}{\mu_r} A_{ki}^{-1} g_i \tag{D.3}$$

where

$$UAIC_k = \frac{U_{e_\xi}}{U_e} A_{ki}^{-1} I_{ij} C_j \tag{D.4}$$

and

$$AINB_k = A_{ki}^{-1} B_i \tag{D.5}$$

Substitution of equation (D.3) into equation (D.2) and conversion to the physical variable x yield

$$\frac{dC_f}{dx} = - \frac{1}{L} \frac{\rho_e U_e}{\rho_r U_r} \frac{C_f}{C_1 - C_2} \left[UAIC_1 - UAIC_2 - AINB_1 + AINB_2 - \frac{\mu_e}{\mu_r} \left(A_{12}^{-1} - A_{22}^{-1} \right) g_2 \right] \tag{D.6}$$

The experimental value of dC_f/dRe_x at the initial station x_o is substituted into equation (D.6), the remaining terms are also evaluated at x_o, and the equation is solved for the value of g_2 - denote this value by the symbol $g_{2_{desired}}$. This is the value of g_2 at x_o which, if used in the MWR calculation program, will yield the experimental value of dC_f/dRe_x at x_o. Now the value of g_2 at x_o is calculated by using a specified shear model - denote this value by the symbol $g_{2_{model}}$. This value of g_2, substituted into equation (D.6), would most likely yield a value of dC_f/dRe_x different than the experimental value of dC_f/dRe_x at x_o. Then in the prediction program whenever a value of g_2 is calculated using a specified shear model, this value can be multiplied by the constant corrective factor of $g_{2_{desired}} / g_{2_{model}}$. This procedure assures that the calculations will at least start with the experimental value of dC_f/dRe_x at x_o.